UNIVERSITY OF CAPE TOWN
IYUNIVESITHI YASEKAPA • UNIVERSITEIT VAN KAAPSTAD

DYNAMIC PERFORMANCE OF PRE-CAST PRESTRESSED BEAMS – CAST IN-SITU SLAB COMPOSITE BRIDGES

By

EMMANUEL LEO

Submitted in partial fulfillment of the requirements for the degree of
Master of Science in Engineering

DEPARTMENT OF CIVIL ENGINEERING
FACULTY OF ENGINEERING AND BUILT ENVIRONMENT

Supervisor: Prof. P. Moyo

Co-supervisor: A/Prof. H. D. Beushausen

January 2013

DECLARATION

The research work presented herein was carried out by the author under the supervision of Professor Pilate Moyo in the Department of Civil Engineering at the University of Cape Town, in partial fulfillment of the requirements for the degree of Master of Science in Engineering.

To the best of my knowledge and belief, no part of this work has been submitted previously to any university, college or other institution or written by another person except where due reference is made. In addition, I certify that all information and literature used are cited within the text.

Signed by candidate

Signature:

Date: *31st January 2013*

ACKNOWLEDGEMENTS

This research work could not have been possible without the assistance, understanding and guidance given by numerous people throughout the project. The author would very much like to express his appreciation and sincere gratitude to his supervisors, Professor Pilate Moyo and Associate Professor Hans Beushausen, for their support, encouragement and guidance throughout this work. Furthermore, the author would like to thank all staff in the department of civil engineering and Concrete Materials and Structural Integrity Research Unit (CoMSIRU) for their extensive assistance throughout the experimental work.

The author would also like to thank his fellow students in the department of civil engineering at University of Cape Town (UCT) who shared their time and friendship with the author and rendered invaluable help throughout this work.

The authors wish to acknowledge with gratitude the following for supporting this research work. PPC and Afrisam for supplying Concrete materials and SCAW SA (Pty) Ltd; haggie-Wire & Strand Operations for donating the prestressing bars.

The author gratefully acknowledges the financial support provided by World Bank through University of Dar es Salaam (UDSM) for his master's studies at UCT.

Special thanks go to my family for their love, understanding and support they have given me during my stay in Cape Town.

Finally, I would not be grateful if I forget to thank almighty God for giving me strength, courage and ability to complete this research work.

ABSTRACT

Most bridge management systems still rely on visual inspections for condition assessment of bridges; this means that damage in inaccessible parts of the structure such as shear connectors in concrete composite bridges remain undetected until catastrophic failure occurs. Localized non-destructive techniques such as ultrasonic techniques, radar method, impact testing, magnetic based methods and proof load tests are limited to small areas, time consuming and require prior knowledge of the damaged zone. These limitations can be overcome by using dynamics-based techniques. The main objective of this work is to investigate experimentally the effectiveness of dynamics-based techniques in assessing the condition of shear connectors in concrete composite bridges consisting of pre-cast prestressed beams and a cast *in-situ* slab based on measurements taken from the surface of the accessible deck slab.

In this research, shear links of 8mm bars extended from beam to the slab are used to stimulate shear connectors in real bridges. The experimental work involved building five concrete composite beams each with different number of shear connectors. The testing procedure consisted of measuring the dynamic properties in both the undamaged and damaged beams. Damage was introduced by accelerating corrosion to a group of shear connectors near the supports in each composite beam. Push-off test was conducted in order to determine the shear capacity of the shear connectors in both undamaged and damaged state.

The modal tests were successfully executed and from the modal analysis results it was observed that a beam with large number of shear connectors produce high frequencies and high amplitudes of frequency response functions (FRFs) compared to the one with less number of shear connectors. After the shear connectors were damaged all beams showed similar results. In the FRFs, the frequency peaks shifted to the left and the peaks amplitudes changed, the natural frequencies generally dropped indicating the existence of damage. In an attempt to locate regions with damaged shear connectors, the Coordinate Modal Assurance Criteria (COMAC), change of flexibility, change of curvature and strain energy method were used. All methods showed positive and negative results. The

change of flexibility method showed minimum negative results compared to other methods in locating regions with damaged shear connectors. Generally, Results show that dynamics-based techniques can be used to detect and localize regions with damaged shear connectors in pre-cast prestressed beams - cast *in-situ* slab composite bridges by only taking vibration measurements from the surface of the accessible deck slab.

Table of Contents

LIST OF FIGURES

LIST OF TABLES

CHAPTER 1

INTRODUCTION

1.1 Background

Bridges are among the critical components of transportation systems and most expensive investment assets of any country's infrastructure. However, there is a growing number of deteriorated bridge structures due to ageing of these structures (Dilena & Morassi, 2008), extreme events such as earthquakes and impact loads or other problems such as corrosion of reinforcing steel, Increased loading, different types of loading and poor maintenance of expansion and contraction joints (Sibanda, *et al.*, 2008). The collapses of bridges around the world such as collapse of I-35 Bridge in Minneapolis in 2007 have raised many concerns regarding the current condition of bridges. In addition, there is a large number of bridges in South Africa and around the world which are in daily use without having enough information about their current condition.

Concrete composite bridges consisting of pre-cast prestressed beams and a cast *in-situ* slab are one of the most common types of bridges in service worldwide for short to medium spans (Nigel, 2003). In this construction, the slab is connected to the beams using shear connectors. Typical connection details for an I-section beam and the deck slab is shown in Figure 1.1.

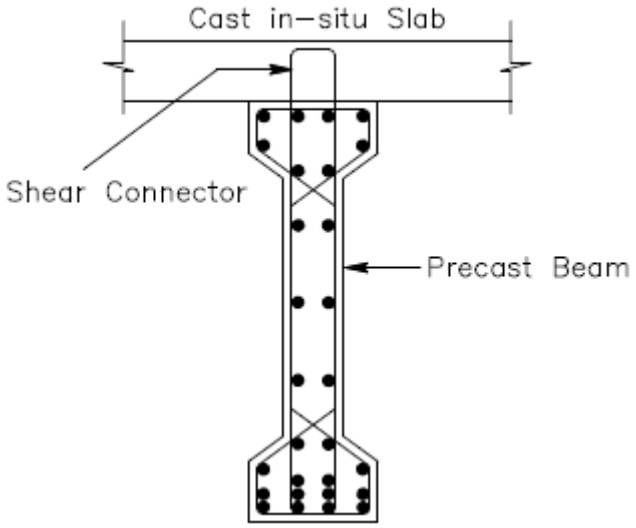

Figure 1.1: Typical beam-slab connection detail

This bridge is a composite structure because of difference in concrete properties between the pre-cast beams and cast in-situ slab (Ryall, *et al.*, 2003). Typical beam sections are I, T, M, U and box sections. The use of pre-cast beams results in cost saving as it reduces the need for formwork during construction and shorter construction period can be achieved (Nigel, 2003; Gajanan, 1979).

Generally, damage in structures can be defined as changes appearing in a structural system that may affect its current or future performance. In this case, damage is not meaningful without a comparison between an initial state of the structure and damaged state of the structure. Damage can also be limited to changes to the materials or geometrical properties of the system, including changes to the system connectivity, which adversely affect the performance of the system. In Figure 1.1, the shear connectors extend from the beam into the deck slab thus providing the connection between beam and slab. These connectors resist the horizontal and vertical flexural shear stresses that develop in the structure. Therefore, they are responsible for the composite action in the structure. The failure or even damage of these connectors will significantly compromise the composite action of the bridge beams and deck slab, thus reducing the load carrying capacity and horizontal shear resistance of the bridge. This therefore means that the composite action may be a potential weak area in these structures and need to be continuously assessed.

Most bridge management systems still rely on visual inspections for condition assessment. This technique has limited ability in detecting all possible damages in the bridges and depends mostly on the decisions of the bridge inspectors. Therefore, even for similar bridge conditions, a large variation in the results obtained can be expected and they may very well miss a damage that grows during the two year's time interval. Furthermore, damage in inaccessible parts of the structure such as shear connectors in concrete composite bridges will remain undetected until it is expensive to repair or catastrophic failure occurs. However, there are localized non-destructive techniques that can be applicable for detecting damaged shear connectors in bridges (Dilena & Morassi, 2008). These include ultrasonic techniques, radar method, impact testing, magnetic based

methods and proof load tests. Nevertheless, these techniques are limited to small area, time consuming, detect damage on or near the surface of the structure and require prior knowledge of the damaged location (Farrar & Jauregui, 1997).

In the last few decades, dynamics-based techniques have been proposed for damage identification and health monitoring in the areas of aerospace, automotive, civil and mechanical engineering (Doubling, *et al*., 1996). The techniques became promising tools in assessing and detecting damage in structures where prior knowledge of the damaged location is lacking (Humar, *et al.*, 2006). These techniques are generally classified as 'non-model-based' and 'model based' methods. Non-model-based damage identification methods employ response data obtained separately from the undamaged and the possibly damage state of the structure in order to detect and localize damage without involving a detailed analytical model of the structure. On the other hand, model-based damage identification use updating of an analytical model of the undamaged structure along with the response data from various possible condition state of the structure concerned to detect, localize and estimate damage severity (Wirtu, *et al.*, 2011). The basic idea of these techniques is that change in physical properties such as mass and stiffness of the structure due to damage results in the change of modal parameters i.e. natural frequencies, damping ratios, mode shapes and curvatures. The successful and comprehensive development of these techniques can reduce consequences of bridge failures and minimize maintenance and repair costs if internal structural damage such as damaged shear connectors in concrete composite bridges are detected at their earlier stages.

It should be noted that, despite the fact that much research work has been published on damage detection and localization methods, not much research work has been reported on concrete composite bridges consisting of reinforced concrete beam and concrete deck slab. The slow development is due to the fact that reinforced concrete, unlike metals, is a non homogeneous material with varying composition, raw materials and complex binding behaviors between different materials. Therefore, many damage detection and localization methods that appear to work well on other structures might perform poorly when being applied to reinforced concrete structures. Furthermore, in real field applications, there are many practical issues associated with the performance of damage

detection including environmental and operational influences, measurement noise, processing error and limited number of sensors. In particular, dynamics-based techniques rely on Experimental Modal Analysis (EMA) to produce modal parameters for damage detection and localization. The results of modal parameters estimation are heavily affected by measurements errors, environmental and operational conditions during the process. In addition, due to the limitation of the number of measurement points (sensors) the reconstruction of mode shapes is necessary for conducting damage detection and localization. Reconstruction of mode shape may produce errors especially under noise influence.

Sibanda, *et al.*, 2008 and Yong, *et al.*, 2006 used dynamics-based techniques to locate damaged shear connectors in a concrete composite bridge. Sibanda, *et al*., 2008 used 10mm bolts to stimulate shear connector in real bridge; Different damage scenarios were introduced by loosening some of the connectors. Yong, *et al*., 2006 used removable anchors to stimulate shear connectors in real bridge; simulation of shear connector damage at different locations was achieved by pulling out some of the connectors. In both cases the beams were made of reinforced concrete as opposed to pre-cast prestressed girders used in the prototype structure and the spacing of the shear connectors in the model is uniform whereas in reality the spacing of the connectors varies. In their work, some damaged connectors were located and false identification was also observed. It was found that the frequency change method is a good tool for detecting the change of stiffness in a structure resulting from the partial loss of shear connectors. The damping ratios were not consistent and therefore did not indicate whether the change is due to removal of the connectors or other parameters.

1.2 Objectives of the project

1.2.1 Main objective

The main objective of this project is to investigate experimentally the effectiveness of dynamics-based techniques in assessing the condition of shear connectors in concrete composite bridges consisting of pre-cast prestressed beams and a cast *in-situ* deck slab based on measurements taken from the surface of the deck slab. The research focus on

concrete composite bridges that are constructed using pre-cast prestressed I-beams section. I-beams sections are one of the more popular beam types used in many countries. Almost one-quarter of the more than one-half-million U.S. bridges make use of prestressed concrete beams in their designs, and I-beam is one of the more popular prestressed concrete beam type (Gene, *et al.*, 2005).

1.2.2 Specific objectives:

i) To investigate the effect of different spacing of shear connectors on dynamic performance of concrete composite bridges consisting of pre-cast prestressed beams and a cast *in-situ* deck slab.
ii) To investigate the effectiveness of dynamics-based techniques in detecting the existence of corrosion damage on shear connectors and locating regions with corrosion damaged shear connectors in concrete composite bridges consisting of pre-cast prestressed beams and a cast *in-situ* deck slab.

1.3 Key questions of the project

i) What is the behavior of composite action between structural elements in concrete composite structures?
ii) How dynamics-based techniques can be used to detect and locate damage in concrete composite structures?

1.4 Hypothesis statement

Dynamics-based techniques can be used to assess the condition of shear connectors in concrete composite bridges consisting of pre-cast prestressed beams and a cast *in-situ* deck slab with regard to the loss in composite action between beams and deck slab.

1.5 Scope of the project

This research is limited to condition assessment of shear connectors using dynamics-based techniques giving care to loss in composite action of bridge beams and slab. It does not include determining remaining service life and the effect of loss in composite action

on load carrying capacity of the structure. The research only considers pre-cast prestressed beams – cast *in-situ* slab composite bridges that are simply supported.

1.6 Thesis content

This work consists of six chapters, organized as follow:

Chapter 1 gives the background of this research project, the objectives of the study, key questions of the project and the scope of the work.

Chapter 2 provides a literature reviews on structure form of concrete composite bridges consisting of pre-cast prestressed beams and a cast *in-situ* deck slab. The behavior of composite action between beams and slab in this kind of bridges. Potential problems on these bridges and dynamics-based damage detection methods are also reviewed.

Chapter 3 discusses the fundamentals of Modal Testing (MT) and Experimental Modal Analysis (EMA). The basic structural dynamic theories including governing equations for structural systems and damping are described in this chapter.

Chapter 4 contains the methodology. This details the work done, which includes the construction of the experimental beams, description of instrumentation and dynamic testing for both undamaged and damaged beams, description of push-off test conducted in this study.

Chapter 5 presents the results from the experiment, reports the findings and observations of the study.

Chapter 6 summarizes the work of this report; draw conclusions and gives recommendations for future work.

CHAPTER 2

LITERATURE REVIEW

2.1 Introduction

Highway bridges constitute significant and critical components of transportation systems and are among the most expensive investment assets of any country's infrastructure. One of the most common types of bridges in service for short to medium spans worldwide is the concrete composite bridge consisting of pre-cast prestressed beams and a cast in-situ slab. According to the Federal Highway Administration (FHWA 2000), almost one-quarter of the more than one-half-million U.S. bridges make use of pre-stressed concrete beams in their designs. (Gene, *et al.*, 2005). This bridge is a composite structure because of difference in concrete properties between the pre-cast beams and cast in-situ slab (Ryall, *et al.*, 2003).

The use of prestressed concrete for beams has the advantage of overcoming concrete's natural weakness in tension. It can be used to produce beams with a longer span than is practical with ordinary reinforced concrete. Prestressing can reduce, or in some circumstances prevent the cracking of concrete under service condition, so decreasing deflection and improving the protection of reinforcements from corrosion. Other advantages of using pre-cast prestressed concrete beams includes minimized formwork and beams section can be smaller leading to considerable savings in materials, labor, and construction time.

The geometry and behavior of composite action between pre-cast prestressed beams and cast *in-situ* slab are the factors that need to be considered in order to understand these types of bridges.

2.2 The Geometry of the concrete composite bridge structure

The construction of these types of bridges involves the use of standardized sections for pre-cast pre-stressed beams. Typical beam sections are I, T, M, U and box sections. The

choice of the section to be used is determined by span of the bridge. The M, inverted T, and box section are used for short span (7 – 12 m) bridge deck, for medium span (12 – 36 m) Y and I beam sections are used, While U and T sections are suitable for long span (> 36 m) bridge decks (Somerville and Tiller, 1975). The development of these standard sections has primarily followed the industry's demand for increasing spans from the early inverted T- and I-sections of the 1950s, through the M-beam (introduced in the mid-1960s), to the modern Y-beam (introduced in 1990, designed to replace M-beam). The development of the Super-Y (SY) beam in 1992 allows the construction of bridges with spans of up to 40 m. (Stratford, *et al.*, 1999).

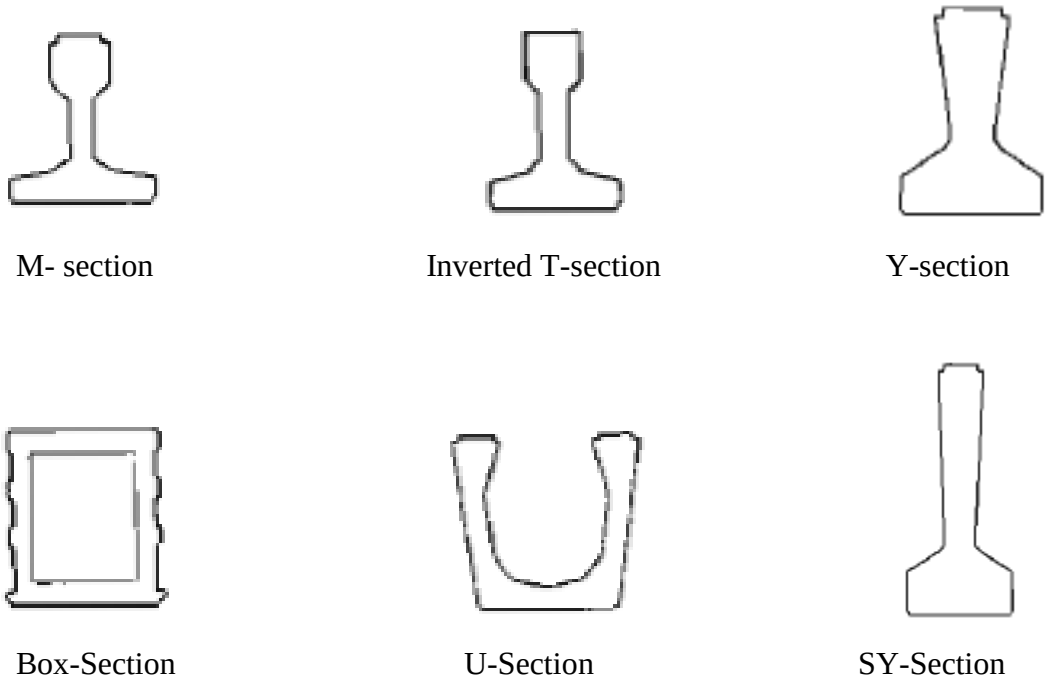

Figure 2.1: Typical concrete bridge beam sections

This research will focus on concrete composite bridges that are constructed using pre-cast prestressed I-beams section, a typical cross-section of the bridge with I-beams is shown in Figure 2.2. The connection between the pre-cast pre-stressed beams and cast in-situ slab in these types of bridges is by using shear connectors. These shear connectors are cast in pre-cast concrete beams during manufacturing. They resist the horizontal and vertical flexural shear stresses that develop in the structure. In this case these connectors

are responsible for the composite action and therefore the efficiency in the structure. The failure of these connectors would compromise the composite action of the structure, thus reducing the load carrying capacity and horizontal shear resistance of the bridge.

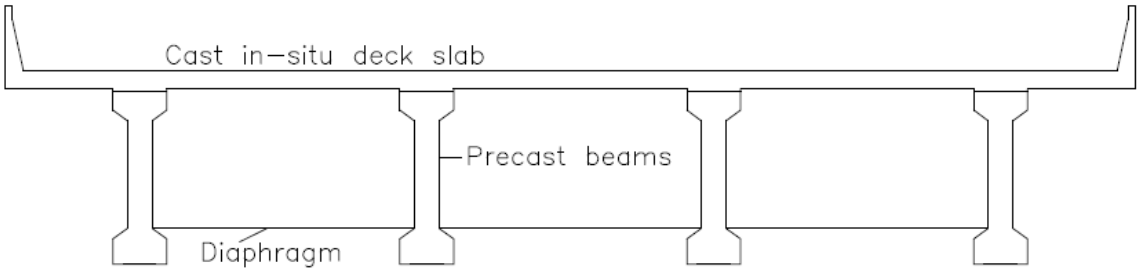

Figure 2.2: Typical cross-section of the concrete composite bridge

In concrete composite bridges, the arrangement of beams and slab has poor load distribution in the transverse direction. (Ryall, *et al.*, 2003). To improve the load distribution and resistance of lateral forces on the bridge, In-situ transverse diaphragms are cast through the holes left in precast prestressed beams. The diaphragms are cast directly at pier positions and within the span. Diaphragm contains normal reinforcement which passes through the web openings provided in the pre-cast beams. In some cases, the diaphragms are post-tensioned. During construction, intermediate diaphragms provide resistance against the accidental overturning of bridge girders, particularly for girders that have a large depth-to-bottom flange width ratio (Abendroth, *et al.*, 1995). The spacing and number of the diaphragms is a function of the overall span of the bridge and required load distribution factor (Sibanda, *et al.*, 2008). Cai & Avent, (2008) recommended that if intermediate diaphragms are to be provided to protect against lateral impact, they should be placed as close as possible to the locations of possible impact. Furthermore, concrete diaphragms are better for this purpose since they provide better impact protection than steel diaphragms. If the impact is not near the diaphragm location, diaphragms provide no direct protection. However, diaphragms located away from the impact point may help support the damaged girders.

Since this research aim at assessing the condition of shear connectors using dynamics-based techniques and also avoiding complex moulds, only a composite T-beam with a pre-cast prestressed web (representing beam in real bridges) and a flange (representing cast *in-situ* slab in real bridges) are constructed in the laboratory.

2.3 Mechanism of composite action of reinforcement and concrete

Maintaining composite action in reinforced concrete structures requires transfer of load between the concrete and steel. This load transfer is what is referred to as bond between steel and concrete. Therefore, the bond performance of reinforcing bars plays a major role in the behavior of reinforced concrete structures when subjected to static and dynamic loads (Chao, *et al*., 2009). Insufficient bond can lead to a significant decrease in the load-carrying capacity and stiffness of the structure when subjected to repeated loadings. In this case, reinforcement in reinforced concrete structure has to undergo the same strain or deformation as the surrounding concrete in order to prevent slip or separation of the two materials under load. The direct stress is transferred from the concrete to the bar interface so as to change the tensile stress in the reinforcing bar along its length. This load transfer is achieved by means of bond, idealized as a continuous stress field that develops in the vicinity of the steel-concrete interface. Corrosion of reinforcement is among the worst cause of concrete structures to deteriorate. Chloride attack and carbonation of concrete cover are the main causes of reinforcement corrosion. The damage mechanisms due to corrosion are mainly: cross-section reduction of the bars, induction of swelling stresses in the concrete around corroded bars and bond loss between concrete and steel (Carbone, *et al*., 2008). This research aim at assessing the condition of shear connectors in concrete composite bridges with regard to the degree of composite action between beams and slab.

2.4 The behavior of composite action between concrete composite bridge elements

The two primary effects to consider when looking at the basic behavior of a composite structure are (Ryall, *et al.*, 2003):

i) The difference between beam and slab in material properties.

ii) Shear connection between the beams and slab.

Differences between strength and stiffness of the materials acting compositely affect the load distribution in the structure (Ryall, *et al.*, 2003). The stiffer material resists proportionally more load than the less stiff material. In order to take such differences into account, the common practice is to transform the properties of one material into that of another by use of modular ratio (Nigel, 2003; Ryall *et al*, 2003). When the structure is at its elastic limit at service loads, the modular ratio is the ratio of the elastic modulus of the materials (Nigel, 2003; Ryall *et al*, 2003). However, at ultimate limit, the modular ratio is the ratio of the material strengths (Nigel, 2003; Ryall *et al*, 2003). This indicates that in the design of concrete composite bridges, the differences in material between beams and slab need to be considered to ensure a safe structure.

While composite construction is generally preferred because it results in cost saving it has also some drawbacks. One of the drawbacks is that it is more difficult to calculate the forces in the system due to time dependent effects, especially in the case of precast prestressed concrete beams with a cast-in place deck (Kosh and Roberts-wollmann, 2008). The time-dependent effects that occur in the beams and deck include creep, shrinkage and relaxation of prestressing steel. Forces and moments develop from differential shrinkage between the deck and beams because each component of the bridge has a different ultimate value and rate of creep and shrinkage. The younger concrete in the deck will shrink more than the older concrete in the beam. However, the entire cross-section must strain compatibly since the beams and the deck are made composite when the deck is poured. The beam restrains the deck shrinkage to some degree (Kosh and Roberts-wollmann, 2008). Since it is difficult or almost impossible in practice to obtain perfect composite action with shear connectors, there cannot be continuity in the strain through the cross-section of the beam and deck. The result is that compression develops in the top of the beam and tension develops in the bottom of the deck.

In the design of composite structures, components must be joined in such a manner that the overall structure retains its structural integrity while performing its intended functions subjected to load (static and dynamic) and environment conditions such as temperature and humidity. (Vinson and Sierakowski, 1990).

The strength and stiffness of concrete composite bridges depends largely on the degree of composite action between beams and slab. This composite action is provided by shear connectors through the interface between the pre-cast presstressed beams and cast *in-situ* slab. The degree of composite action is related to geometrical and mechanical properties of shear connectors. The mechanical properties can vary during loading history. Therefore, different sections of the structure may have different behaviors, ranging from that of a section with perfect connection to that with no connection. The failure of these connectors therefore results in poor load distribution and loss of stiffness of the structure. The load carrying capacity of the bridge will obviously be reduced (Yong, X. *et al.*, 2006). This is because loss in composite action may result in slip and the assembled structural members behave independently under load. On the other hand, when members act as a composite unit, the structure has an increased section for resisting loads. This results in lower deflections as compared to that of non-connected members or when the structure has lost its composite action (Queriroz, *et al.*, 2006; Ryall, *et al.*, 2003).

The shear connectors in these bridges transfer the horizontal shear stresses between the interfaces of the members. The connectors also resist both torsional and vertical shear stresses (Kumar, 1988). The ability of the shear connectors to transfer the longitudinal forces depends on their strength as well as the resistance of the concrete to longitudinal crushing induced by high concentration of shear force (Sibanda, *et al.*, 2008). The increase in allowable loads over bridges therefore means concrete composite bridges that are built long time ago might be under ultimate service conditions. This may compromise the composite action.

2.5 Composite action and interaction of composite elements

The strength and stiffness of composite action depends on the degree of shear connection between composite elements. The provision of adequate shear connection between tension and compression-resisting components of composite flexural members is essential to ensure the robust performance of such structural members under load (Al-Darzi and Chen, 2006). In concrete composite bridges the slab is cast over the precast beams and so a natural bond develops at the interface. However, this bond may be

destroyed by the effect of shrinkage and stresses due to variations of temperature, so it is necessary to provide shear connectors to give a reliable composite action. The purpose of the shear connectors is to transmit the horizontal shear and prevent uplift between beams and slab; to successfully do this, they must be strong enough to resist both horizontal and vertical forces and must also be of a shape that easily permits the concrete to surround them. For concrete beams with concrete slab, shear connectors used are usually either embedded reinforcing bars: dowels, half-buried spirals, or ends of stirrups (Gajanan, 1979).

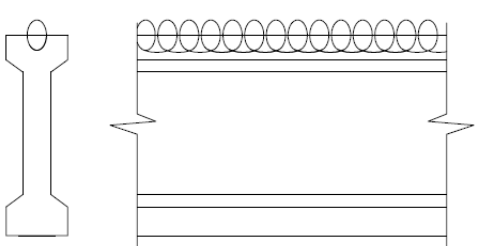

2.3(a): Half-buried spirals

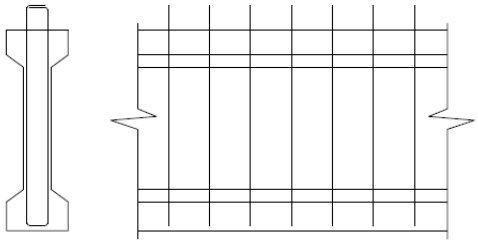

2.3(b): Ends of stirrups

Figure 2.3: Typical Shear connectors

The degree of shear connection deals with the equilibrium of forces within a composite structure. Consider a section of a simply supported concrete composite beam-slab with tension reinforcement in the beam as shown in Figure 2.4.

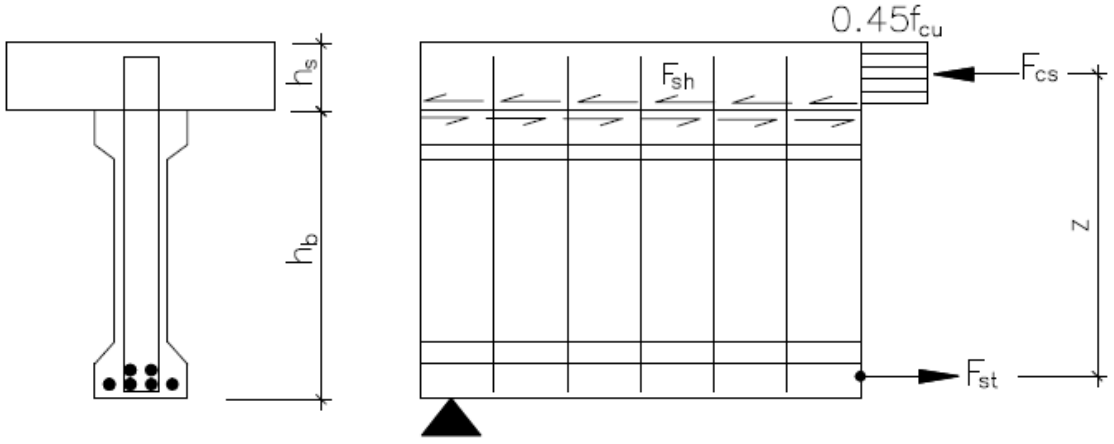

Figure 2.4: Equilibrium of forces of a composite beam in the longitudinal direction

In Figure 2.4, F_{cs} is the resultant axial compression force in the concrete slab, F_{st} is the resultant axial tensile force in the beam tension reinforcement and F_{shc} is the resultant shear force across beam/slab interface. In steel-concrete composite beam, Full shear connection flexural capacity of a composite member is determined by first ignoring the strength of the shear connection and only considering the axial strengths of the steel and concrete element, after which the minimum shear connection strength for full shear connection can be determined (Oehlers, *et al*., 1997). For a precast beam – cast in-situ slab composite structure, neglecting the effect of prestressing force and other reinforcement in the beam and slab, full shear connection flexural capacity of a composite member can be determined in a similar way but by considering the axial strengths of the beam tension reinforcement and compression concrete slab.

The maximum possible flexural capacity of a composite beam at the section in Figure 2.4 can be determined by comparing the shear strength of shear connection in the shear span (P_{shc}), axial strength of the concrete slab ($P_{cs} = 0.45f_{cu}A_{cs}$) and axial strength of the beam tension reinforcement ($P_{st} = f_yA_{st}$); where A_{cs} is the area of concrete slab, f_y is yield strength of beam tension reinforcement and A_{st} is the equivalent total area of all tension reinforcement in the beam. Assuming the strength of the shear connection $P_{shc} \geq F_{cs}$. Therefore, when $P_{cs} > P_{st}$, then the horizontal equilibrium is achieved when $F_{st} = P_{st}$ and hence $F_{cs} = P_{st}$. This is referred to as 'full shear connection' since the strength of the shear connection does not enter the calculation. In the case where the strength of the shear connection controls the flexural capacity of the composite section the horizontal equilibrium $F_{cs} = P_{shc}$ is achieved when $P_{shc} < F_{cs}$. This is referred as 'partial shear connection'. 'No shear connection' is when there are no shear connectors at the beam/slab interface, then $F_{cs} = P_{shc}$=0. If $(P_{shc})_f$ denote the minimum strength of shear connection required for full shear connection, then the degree of shear connection in term of the strength of the shear connection, η, is defined as (Oehlers, *et al*., 1997).

$$\eta = \frac{P_{shc}}{(P_{shc})_f} \tag{2.5a}$$

Similar, in term of compression force in the concrete, the degree of composite action η is defined as (EN1994-Eurocode 4),

$$\eta = \frac{N_c}{N_{c,f}} \tag{2.5b}$$

Where: N_c – Compression force in the concrete.

$N_{c,f}$ – Compression force in the concrete for full shear connection.

Considering deflection of composite beam, the degree of composite action (or efficiency) can be calculated by using the following formula (R. Gutkowski *et al*, 2008)

$$Efficiency = \frac{\delta_N - \delta_I}{\delta_N - \delta_C} \cdot 100\% \tag{2.5c}$$

Where δ_C is the theoretical fully composite deflection, δ_N the theoretical fully non-composite deflection (calculated as a layered beam without interlayer shear transfer), and δ_I is the measured deflection for incomplete (or partial) composite action of the specimen. In this case, sections with a high degree of composite action are much stiffer than the layered equivalents and will consequently deflect less as shown in Figure 2.5.

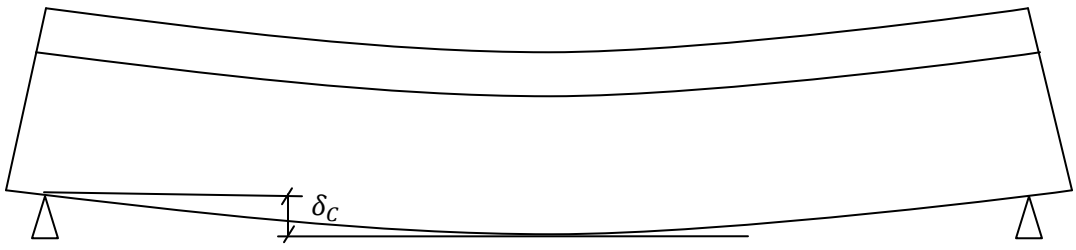

Figure 2.5(a): Full Composite Action (100%)

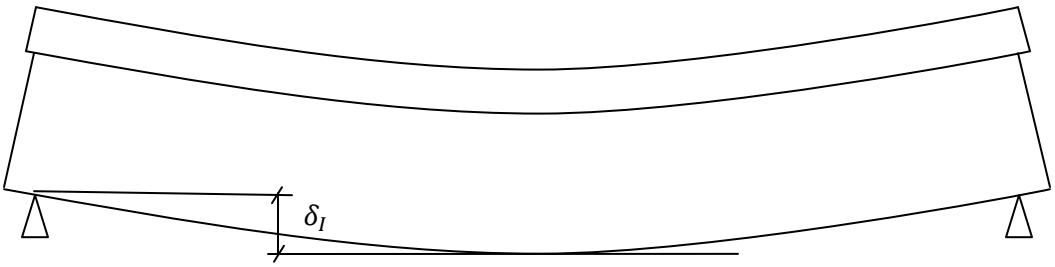

Figure 2.5(b): Intermediate Composite Action (between 0 % and 100%)

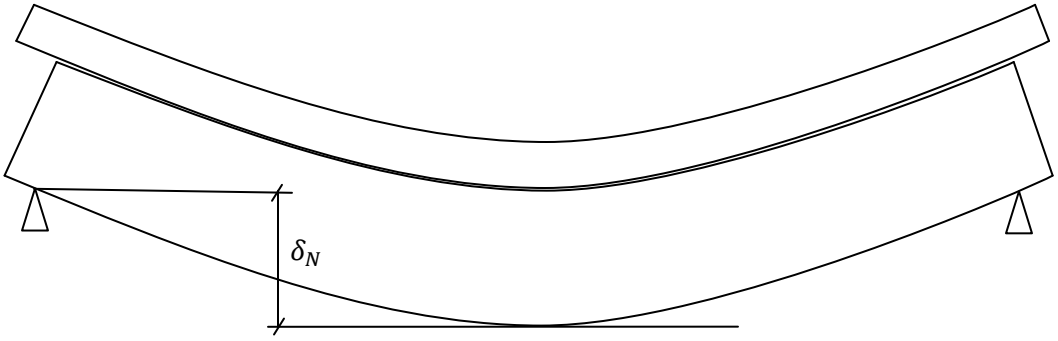

Figure 2.5(c): Full Non-Composite Action (0%)

$$i.e.\ \ \delta_C < \delta_I < \delta_N$$

Figure 2.5: Degree of composite action and deflection

The idea behind using shear connectors in concrete composite bridges is to reduce the amount of slip between beams and slab. The degree of interaction between composite elements deals with the compatibility of displacements (Oehlers, *et al*., 1997). For a concrete composite bridge with complete shear interaction between beams and slabs, there is no relative slip at the beam/slab interface. In practice, complete shear interaction is assumed to coincide with full shear connection (Wang, Y. C., 1998). The Shear Interaction factor S_{If} is given by,

$$S_{If} = \frac{N}{N_f} \tag{2.5d}$$

Where: N – Number of Shear connectors less than for full shear connection.

N_f – Number of shear connectors for full shear connection

The force transfer at the interface for composite sections is related to the rate of change of the force in the slab. The shear flow at service load conditions is given by (Gajanan, 1979 and Ryall, *et al.*, 2003):

$$q = \frac{VAy}{I} \tag{2.5e}$$

Where: q – Shear flow per unit length of beam at the interface.

V – Vertical shear force

A – Transformed area of concrete above the interface

Y – Distance between the center of area of A and the elastic neutral axis

I – Moment of inertia of transformed composite section about the neutral axis.

The shear flow is a function of vertical shear force as shown by above equation. The increase in vertical shear force resulting from an increase in service loads therefore increases the shear flow. Based on shear flow calculated above, the number of shear connectors per unit length at serviceability limit state is given by (Ryall, *et al.*, 2003):

$$N_O = \frac{q_n}{0.55P_u} \tag{2.5f}$$

Where: q_n – Shear flow at stage n

P_u – Nominal static strength of the connector

And at the ultimate limit state, the number of shear connectors required is given by;

$$N_O = \frac{\gamma q_n}{0.8P_u} \quad ; \quad \text{Where } \gamma \text{ is a constant} \tag{2.5g}$$

A perfect composite action can be obtained by prohibiting the relative displacement between beams and slab at their interface. The chemical and frictional bonds between the beams and slab are too weak to prevent slip. Therefore, shear connectors are usually added to provide a composite action. However, because of the deformability of the shear

connectors, a perfect composite action cannot be obtained in practice. In composite construction, the interaction between beams and slab can be classified as non composite (or the lower limit of composite action), partial composite action and full composite (or the upper limit of composite action). These three scenarios are described in more detail below.

2.5.1 Non-Composite Action ($\boldsymbol{\eta = 0}$)

A composite beam that has no means of positively connecting the two materials is commonly referred to as non-composite. The material layers have individual neutral axes and discontinuous flexural strains at the material interface (Gutkowski, *et al.*, 2008). An advantage of this type of construction is that a large amount of time and money could be saved by not designing, purchasing, and installing hundreds or thousands of shear connectors on the top of the beams. However, one of the most significant disadvantages is that the concrete slab must resist tension forces and the pre-cast prestressed concrete beam must resist compression forces, neither of which are ideal situations for each material individually. Because of this disadvantage, it is possible that a thicker concrete slab as well as a larger beam might have to be designed which increases the total weight of the structure. A typical strain diagram for non-composite beam is shown in Figure 2.6(a).

2.5.2 Partial Composite Action($\boldsymbol{0 < \eta < 1}$)

Partial composite action is achieved when the number of shear connectors used to connect the slab and beam is less than the number required to achieve full composite action. With this type of composite design, the horizontal relative motion (slip) between the two materials is not completely prevented, although the magnitude of that slip is not as large as that seen in non-composite construction. Slip reduces the efficiency below (strength and stiffness) to a level between a fully composite situation and a fully non-composite action (Gutkowski, *et al.*, 2008). A typical strain diagram for partial-composite beams can be seen in Figure 2.6(b).

2.5.3 Full Composite Action($\eta = 1$)

For full composite action, the cross-section has a single neutral axis and the two material flexural strains are identical at the material interface. For a section to be "fully composite" the shear connectors must provide strength that equals or exceeds the maximum shear force resulting from concrete crushing. In concrete composite bridges, Full shear connection is only related to beam strength and is reached when there is a sufficient number of shear connectors to prevent the concrete slab and beam from slipping relative to each other such that the addition of extra shear connectors do not affect the strength of the composite beam (Johnson, 1994). This results in the best situation for both elements where the majority of the slab is resisting compressive forces, and the majority of the beam is resisting the tension forces. Full composite action results in improved strength and stiffness over non-composite construction, and hence less weight structure. The strain diagram in Figure 2.6(c) shows that when full composite action is achieved, there is no discontinuity of strain at the interface between the beam and slab.

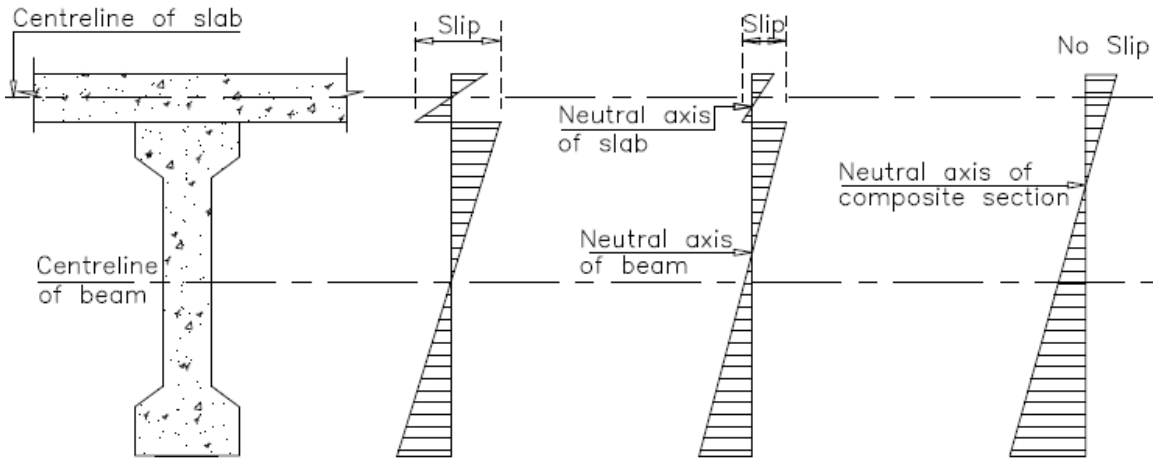

(a): Non-composite (b): Partial composite (c): Full composite

Figure 2.6: Strain diagrams for different composite action

2.6 Shear connectors stiffness

The load-slip characteristic is an important property of shear connectors. However, Gajanan (1979) and Seracino, *et al.*, (2004) noted that in design, the longitudinal slip between the members is neglected as the connection is treated as rigid. The assumption that the connection is rigid might be incorrect and may have adverse effect at ultimate loadings of the structure. Moreover, Queiroz, *et al.*, (2006) noted that in practice, slip between the members occurs. The shear connectors only come to effect when slip has occurs.

Though the behavior of shear connectors has been under investigation for more than 3 decades, most studies have focused on the shear connector strength. Of the publications available regarding the behavior of shear connectors, only a few provide descriptions of the shear connector load-slip curve to enable determination of the shear connector stiffness used in steel-concrete composite bridges.

The shear connector load-slip curve is generally nonlinear, and there is no unified definition of the shear connector stiffness. Johnson and May (1975) defined the shear connector stiffness as the secant stiffness at half the shear connector ultimate load. Studies by Johnson and May (1975) and Lloyd and Wright (1990) indicated that it was rather difficult to find any regression formula for the shear connector stiffness because of the extent of scatter in the value plotted against other parameters. However, as a rather simple suggestion, the writer observed that the shear connector stiffness may be conservatively estimated as the secant stiffness at the shear connector design strength with an equivalent slip of 0.8 mm. This concept is illustrated in Figure 2.7 and is based on the following observations confirmed by few available experimental results (Wang, Y. C., 1998).

- The shear connector design strength is taken as 80% of its maximum resistance *p.*
- The average working load in shear connectors is about *0.5P*.
- At this working load, suggested that the shear connector slip be lower than 0.5 mm.

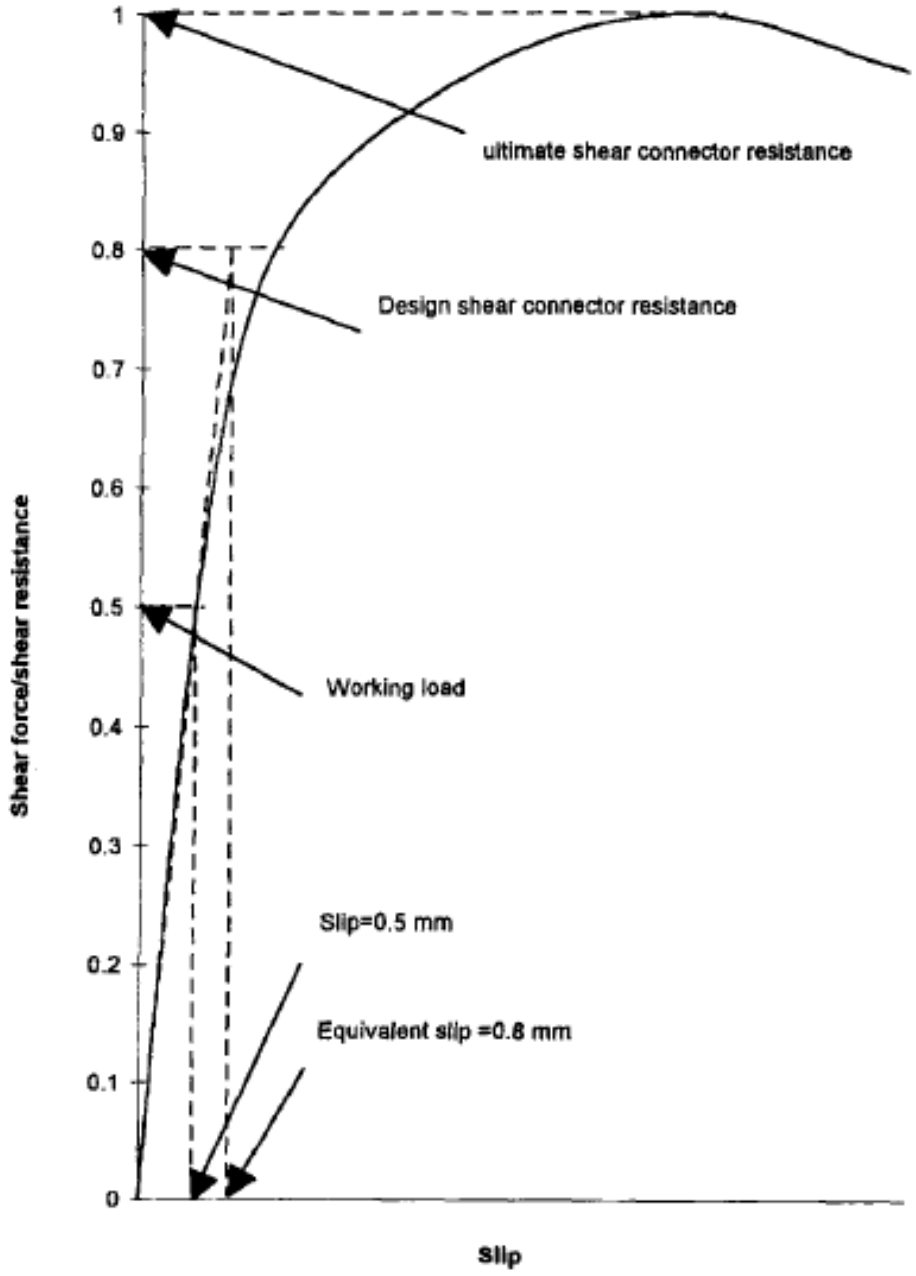

Figure 2.7: Determination of shear connector stiffness (Wang, Y. C., 1998)

Calculation example based on Figure 2.6: If the maximum resistance of the shear connector is 100kN, then the connector design strength is 80kN, with an equivalent slip of 0.8 mm, the secant stiffness of each shear connector is 100 kN/mm. This gives K equal to 500N/mm^2 for a shear connectors spacing of 200mm. Where, K is average density of shear connector's stiffness over the length of the beam.

2.7 Analytical model: Dynamic properties and composite action

Dynamic properties of a composite structure depend on the degree of composite action between the composite elements. Generally, the use shear connectors results to partial composite action between the composite elements. In this case, the analysis requires the consideration of interlayer slip between the composite elements. In dynamics, Hamilton's principle is normally used to solve these kinds of problem (Girhammar, *et al*., 2009 and Dilena & Morassi, 2003). The analysis is based on the same assumptions as for conventional Euler–Bernoulli beams without slip. The difference is referred only to the mechanism of slip between the layers. One of the simplifying assumptions is the approximation of the concentrated shearing forces from the discretely located connectors with a continuous shear flow per unit length along the interlayer. The connector load per unit length (V_{shc}) versus slip (Δu) relationship is linear elastic, i.e. $V_{shc} = K \cdot \Delta u$ where K is a constant slip modulus or average density of shear connector's stiffness over the length of the beam in N/m^2. For non-composite action or zero slip stiffness, $K \to 0$. For full composite action or infinite slip stiffness, $K \to \infty$. This means $K \to 0$ and $K \to \infty$ are the lower and upper bounds for the partial composite action.

Consider a cross-section of a typical composite pre-cast beam – cast in-situ slab as shown in Figure 2.8. M, V, N, p, r, c, V_{shc}, u, Δu, m_s, m_b and w representing moment, shear force, normal force, load intensity, distance between neutral axis of the two composite elements, centroid, slip force per unit length, axial displacement, interlayer slip, mass per unit length of the slab, mass per unit length of the beam and deflection respectively. The *x*-axis of the coordinate system is in the longitudinal direction and is located in the centroid of the full composite action (c_∞). The procedure used hereafter to formulate the relation between dynamic properties and degree of composite action is essentially the same as in Girhammar, *et al*., 2009. However, because in this research a simply supported one-dimensional composite beam is constructed, only pinned-pinned case is considered. It is important to note that the formulation does not include the effect of prestressing force while the experimental beams were fully prestressed to avoid cracking of concrete under self weight. And prestressing increases the natural frequency of the beam (Yaoting & Ruige, 2007).

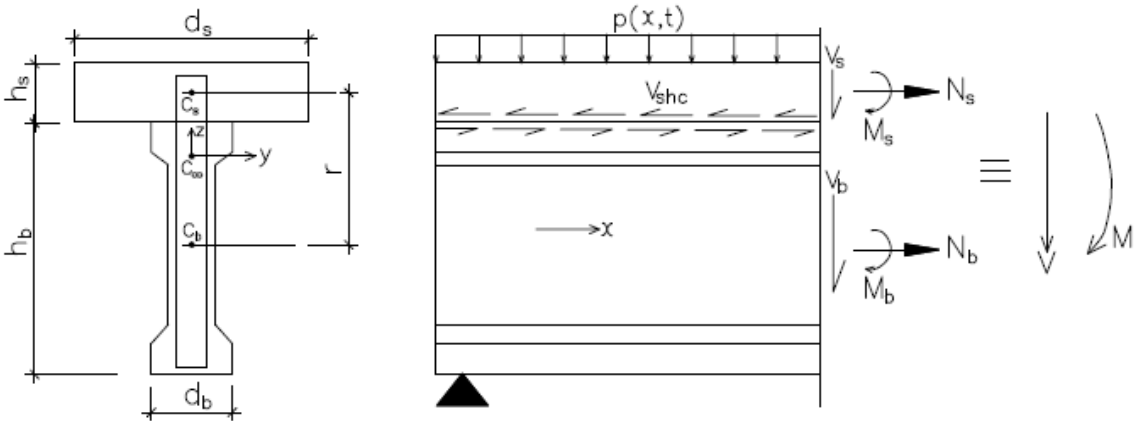

Figure 2.8: Geometrical parameters and forces on composite beam section

The differential equation that shows that relation between the axial displacement (u) and the lateral deflection(w) is defined as

$$E_s A_s \frac{\partial^3 u_s}{\partial x^3} - E_s A_s \cdot \alpha^2 \left(1 - \frac{\beta r}{\alpha^2}\right) \frac{\partial u_s}{\partial x} + \beta E I_0 \frac{\partial^2 w}{\partial x^2} = 0 \qquad (2.7a)$$

Where $E_i A_i =$ the axial stifness of the ith composite element

$E_i I_i =$ the bending stifness of the ith composite element

$$\alpha^2 = \left(\frac{1}{E_s A_s} + \frac{1}{E_b A_b} + \frac{r^2}{E I_0}\right) = \frac{K r^2}{E I_0 (1 - E I_0 / E I_\infty)}$$

$$\beta = \frac{K r}{E I_0}$$

$$E I_0 = E_s I_s + E_b I_b$$

$$E I_\infty = \frac{E I_0}{1 - \beta r / \alpha^2} = E I_0 + \frac{E A_p r^2}{E A_0}$$

$$E A_0 = E_s A_s + E_b A_b$$

$$E A_P = E_s A_s \cdot E_b A_b$$

Two non-dimensional parameters that depend on the slip modulus and the material, geometrical, axial and bending stiffness properties of the beam are αL and $E I_0 / E I_\infty$. where αL is the shear connector stiffness parameter and $E I_0 / E I_\infty$ is the relative bending stiffness parameter.

Subscripts b, s, 0 and ∞ refer to beam, slab, non-composite and full composite respectively. The axial and transverse displacements used as unknown variables are not independent, but subject to a constraint condition which is conveniently introduced into the variational procedure based on Hamilton's principle by use of a Lagrange multiplier. By introducing this new variable 'the Lagrange multiplier' two variables subject to a constraint may be treated as independent variables. This Lagrange multiplier can be interpreted as the added curvature of the composite beam due to the interlayer slip. Using the standard arguments from the calculus of variations, the Lagrange multiplier (λ) is given by

$$\lambda = \frac{E_s A_s}{K} \cdot \frac{\partial u_s}{\partial x} \tag{2.7b}$$

If the constraint condition according to equation (2.7a) is expressed in terms of moment by dividing them by β, then the Lagrange multiplier (λ) would be defined as

$$\lambda = \frac{N_s r}{EI_0} \tag{2.7c}$$

Then the coupled governing equations for the composite system are given by

$$EI_0 \frac{\partial^4 w}{\partial x^4} + rE_s A_s \frac{\partial^3 u_s}{\partial x^3} + m\frac{\partial^2 w}{\partial t^2} - p = 0 \tag{2.7d}$$

$$E_s A_s \frac{\partial^3 u_s}{\partial x^3} - E_s A_s \cdot \alpha^2 \left(1 - \frac{\beta r}{\alpha^2}\right) \frac{\partial u_s}{\partial x} + \beta EI_0 \frac{\partial^2 w}{\partial x^2} = 0 \tag{2.7e}$$

And the pertaining boundary conditions expressed as functions of deflection $w = w(x,t)$ and rotation $\partial w/\partial x = \partial w(x,t)/\partial x$ at the ends with $V_{B,x} = |V(w)|_{x=0,L}$ and $M_{B,x} = |M(\partial w/\partial x)|_{x=0,L}$ describing shears (V_B) and moments (M_B) at the boundary sections at $x = 0$ and $x = L$ respectively, are defined as

$$\left(EI_0\frac{\partial^2 w}{\partial x^2}+rE_sA_s\frac{\partial u_s}{\partial x}-M_{B,x}\right)\delta\frac{\partial w}{\partial x}\Big|_{x=o}^{L}=0 \tag{2.7f}$$

$$\left(-EI_0\frac{\partial^3 w}{\partial x^3}-rE_sA_s\frac{\partial^2 u_s}{\partial x^2}-V_{B,x}-V_{m_{B,x}}\right)\delta\frac{\partial w}{\partial x}\Big|_{x=0}^{L}=0 \tag{2.7g}$$

$$E_sA_s\frac{\partial u_s}{\partial x}\delta\left(\frac{E_sA_s}{K}\frac{\partial^2 u_s}{\partial x^2}\right)\Big|_{x=0}^{L}=0 \tag{2.7h}$$

For a pinned end $(w=M=N_s=M_{B,x}=0 \text{ at } x=0,L)$ the boundary conditions become

$$w=0 \tag{2.7i}$$

$$\frac{\partial^2 w}{\partial x^2}=0 \tag{2.7j}$$

$$\frac{\partial^4 w}{\partial x^4}=\frac{p}{EI_0} \tag{2.7k}$$

For the limit case of non-composite action

$$V_{shc}=0\,,\ \ \alpha L\to 0 \ \text{ and } \ \partial u_s/\partial x\to 0$$

For the limit case of full composite action

$$\Delta u=0\,,\ \ \alpha L\to\infty \ \text{ and } \ \partial^2 u_s/\partial x^2\to\infty$$

Equation (2.7d) then reduces to the conventional fourth-order differential equation valid for solid beams. Combining the coupled equations (2.7d) and (2.7e) we get equations (2.7l) and (2.7m) for the deflections and internal actions.

$$\frac{\partial^6 w}{\partial x^6}-\alpha^2\frac{\partial^4 w}{\partial x^4}+\frac{m}{EI_0}\frac{\partial^4 w}{\partial x^2\partial t^2}-\alpha^2\frac{m}{EI_\infty}\frac{\partial^2 w}{\partial t^2}=-\frac{\alpha^2}{EI_\infty}p+\frac{1}{EI_0}\frac{\partial^2 p}{\partial x^2} \tag{2.7l}$$

$$\frac{\partial u_s}{\partial x} = \frac{EI_\infty}{\alpha^2 r E_s A_s}\left[-\frac{\partial^4 w}{\partial x^4} + \alpha^2\left(1 - \frac{EI_0}{EI_\infty}\right)\frac{\partial^2 w}{\partial x^2} - \frac{m}{EI_0}\frac{\partial^2 w}{\partial t^2} + \frac{p}{EI_0}\right] \tag{2.7m}$$

For free vibration ($p = 0$), the solutions for equation (2.7l) are assumed to be in the following form:

$$w(x,t) = \phi(x) f(t) \tag{2.7n}$$

Where ϕ is an eigenmode which depends on the boundary conditions and f is the time function for natural vibrations that depends on the initial conditions. A standard separation of variables procedure applied on equation (2.7l) will then produce the following equations,

$$\frac{d^6\phi}{dx^6} - \alpha^2\frac{d^4\phi}{dx^4} + \omega^2\frac{m}{EI_0}\frac{d^4\phi}{dx^2} - \omega^2\alpha^2\frac{m}{EI_\infty}\phi = 0 \tag{2.7o}$$

$$\frac{d^2 f}{dt^2} + \omega^2 f = 0 \tag{2.7p}$$

Where ω is the eigenfrequency (real quantity).

Substituting equation (2.7n) into equation (2.7l) and using equation (2.7p) will result to

$$\frac{\partial u_s}{\partial x} = \left(\frac{1}{E_s A_s}\right)\cdot\frac{EI_\infty}{\alpha^2 r}\left[-\frac{d^4\phi}{dx^4} + \alpha^2\left(1 - \frac{EI_0}{EI_\infty}\right)\frac{d^2\phi}{dx^2} + \omega^2\frac{m}{EI_0}\phi\right] f(t)$$

$$= \frac{1}{E_s A_s}\varphi(x) f(t) \tag{2.7q}$$

The coupled differential equations (2.7d) and (2.7e) with ($p = 0$) can be written in terms of the eigenmodes as

$$EI_0\frac{d^4\phi}{dx^4} + r\frac{d^2\varphi}{dx^2} = \omega^2 m\phi \tag{2.7r}$$

$$\frac{d^2\varphi}{dx^2} - \alpha^2\left(1 - \frac{\beta r}{\alpha^2}\right)\varphi + \beta EI_0\frac{d^2\phi}{dx^2} = 0 \tag{2.7s}$$

The pertaining boundary conditions (2.7i), (2.7j) and (2.7k) for pinned ends in terms of eigenmode are,

$$\phi = 0 \tag{2.7t}$$

$$\frac{\partial^2\phi}{\partial x^2} = 0 \tag{2.7u}$$

$$\frac{\partial^4\phi}{\partial x^4} = 0 \tag{2.7v}$$

The general solution to equation (2.7o) will have the following form

$$\phi(x) = c_1 sin(|k_1|x) + c_2 cos(|k_1|x) + c_3 sinh(|k_2|x) + c_4 cosh(|k_2|x) + c_5 sinh(|k_3|x) + c_6 cosh(|k_3|x) \tag{2.7w}$$

Where $|k_1|$ is the absolute value of the imaginary is root k_1 and k_2, and k_3 are the two positive roots of the characteristic equation (2.7x),

$$k^6 - \alpha^2 k^4 - \omega^2\frac{m}{EI_0}k^2 + \alpha^2\omega^2\frac{m}{EI_\infty} = 0 \tag{2.7x}$$

The roots of equation (2.7x) are monotonically increasing functions of the non-dimensional composite action parameter αL. They also satisfy

$$\left(\omega^2\frac{m}{EI_\infty}\right)^{1/4} \leq |k_1| \leq \left(\omega^2\frac{m}{EI_0}\right)^{1/4} \tag{2.7y}$$

$$0 \leq |k_2| \leq \left(\omega^2\frac{m}{EI_\infty}\right)^{1/4} \tag{2.7z}$$

$$\left(\omega^2\frac{m}{EI_0}\right)^{1/4} \leq k_3 \tag{2.7.1a}$$

The roots and their intervals are based on the presumption that the eigenvalues $\omega^2 > 0$. Constants c_1 to c_6 are determined by the boundary conditions and the expression for φ implicitly defined in equation (2.7q).

For a countable infinite sequence of eigenfrequency (ω_n) with corresponding normalized eigenfunctions (ϕ_n) and corresponding frequency functions (f_n), and since the differential equations are linear. Superposition then gives the solution of the form

$$w(x,t) = \sum_{n=1}^{\infty} \phi(x) f(t) \tag{2.7.1b}$$

Where in view of equation (2.7p), $f_n(t) = a_n \sin(\omega t) + b_n \cos(\omega t)$ (2.7.1c)

Coefficients (a_n and b_n) are chosen in such a manner that the sum converges in some appropriate sense for free vibration.

The discrete eigenvalues (ω_n) are related through equation(2.7x) to $k_{1,n}$ as shown below,

$$\omega_n = \frac{k_{1,n}^2}{k_{1,n,\infty}^2}\left(1\Big/\sqrt{1+\frac{EI_\infty/EI_0-1}{1+\alpha^2/k_{1,n}^2}}\right)\omega_{n,\infty} = \sqrt{\frac{EI_{\text{eff}}}{EI_\infty}}\,\omega_{n,\infty} \tag{2.7.1d}$$

Where

$$k_{1,n} = \frac{\pi}{\mu_n L}$$

$$\frac{EI_{\text{eff}}}{EI_\infty} = \left(\frac{k_{1,n}}{k_{1,n,\infty}}\right)^4 \left(1+\frac{EI_\infty/EI_0-1}{1+\alpha^2/k_{1,n}^2}\right)^{-1} = \left(\frac{\mu_{1,n}}{\mu_{1,n,\infty}}\right)^4 \left(1+\frac{EI_\infty/EI_0-1}{1+(\mu/\pi)^2(\alpha L)^2}\right)^{-1}$$

$$\omega_{n,\infty} = k_{1,n,\infty}^2\sqrt{\frac{EI_\infty}{m}} = \left(\frac{\pi}{\mu_{n,\infty}L}\right)^2\sqrt{\frac{EI_\infty}{m}}$$

μ_n is the eigenmode length coefficient of eigen mode n

m is the mass per unit length of a composite section ($= m_s + m_b$)

E_{eff} is the effective composite bending stiffness for composite beam vibrations with partial interaction.

An approximate solution for composite beams with interlayer slip is proposed to be obtained by using eigenmode length coefficients given for solid sections. For beams with boundary conditions according to the four Euler cases, i.e. combinations of the three engineering admissible boundary conditions, we have

$$\mu_{n,0} = \mu_{n,\infty} = \mu_{n,solid} = \begin{cases} (n - 1/2)^{-1}\,(n \geq 2) & \mu_1 = 1.675 \text{ Euler case 1} \\ (n \pm 0)^{-1} & \mu_1 = 1 \text{ Euler case 2} \\ (n + 1/4)^{-1} & \mu_1 = 0.8 \text{ Euler case 3} \\ (n + 1/2)^{-1} & \mu_1 = 0.667 \text{ Euler case 4} \end{cases} \quad (2.7.1e)$$

For a composite beam of length L with both ends pinned, the boundary conditions (2.7i), (2.7j) and (2.7k) according to Euler case 2 (pnned-pinned) at $x = 0$ gives the following equations for determining three of the constants in equation (2.7w):

$$\begin{bmatrix} 1 & 1 & 1 \\ -k_{1,n}^2 & k_{2,n}^2 & k_{3,n}^2 \\ k_{1,n}^4 & k_{2,n}^4 & k_{3,n}^4 \end{bmatrix} \begin{bmatrix} c_2 \\ c_4 \\ c_6 \end{bmatrix} = \begin{bmatrix} 0 \\ 0 \\ 0 \end{bmatrix} \quad (2.7.1e)$$

The determinant of the coefficient matrix in equation (2.7w) is

$$\left(k_{1,n}^2 + k_{2,n}^2\right)\left(k_{1,n}^2 + k_{3,n}^2\right)\left(k_{3,n}^2 - k_{2,n}^2\right)$$

Since $k_{1,n}^2 < k_{2,n}^2 < k_{3,n}^2$ and in view of their respective intervals according to equations (2.7y), (2.7z) and (2.7.1a), no factor is zero and the determinant is not equal to zero. Therefore, the coefficients c_2, c_4 and c_6 must be equal to zero.

For other end $x = L$, the remaining equation can be written as

$$\begin{bmatrix} 1 & 1 & 1 \\ -k_{1,n}^2 & k_{2,n}^2 & k_{3,n}^2 \\ k_{1,n}^4 & k_{2,n}^4 & k_{3,n}^4 \end{bmatrix} \begin{bmatrix} c_1 sin\left(k_{1,n}L\right) \\ c_4 sinh\left(k_{2,n}L\right) \\ c_6 sinh\left(k_{3,n}L\right) \end{bmatrix} = \begin{bmatrix} 0 \\ 0 \\ 0 \end{bmatrix} \quad (2.7.1f)$$

Due to the similarities of equation (2.7.1f) with (2.7.1e), the coefficients $c_3 = c_5 = 0$ and non-trivial ($c_1 \neq 0$) solution

$$k_{1,n} = \frac{\pi}{\mu_n L} = \frac{n\pi}{L} \qquad (2.7.1g)$$

This exact solution for a partially composite beam with boundary conditions according to Euler case 2 is the same as the case in equation (2.7.1e) corresponding to the solid or full composite beam section ($n = 1$ and $\mu = 1$). Thus, the fundamental eigenmode length coefficient ($\mu = 1$) is independent of the composite action and relative bending stiffness.

2.8 Possible failure mechanism of the composite action between beams and slab

The strength and durability of concrete composite bridges depends on the type of the constituent materials, structural design, construction and maintenance. In spite of their relatively simple structural systems and well-defined supports, bridges suffers heavily from the effect of age, climate and traffic loads that often exceed the codified limits (Parkash, *et al.*, 2006). Reinforced concrete can fail due to inadequate strength, leading to mechanical failure, or due to a reduction in its durability. Corrosion and freeze/thaw cycles may damage a reinforced concrete bridge that is poorly designed or constructed. Cracking of the concrete section is nearly impossible to prevent; the concrete cracks either under excess loading or due to internal effects such as early thermal shrinkage when it cures. However, the size and location of cracks can be limited and controlled by appropriate reinforcement, control joints, curing methodology and concrete mix design. Cracking can allow moisture to penetrate and corrode the reinforcement including shear connectors.

The structural capacity of a composite bridge depends on resistance to the deformation of its components and connections; the component resistance is a function of material strength and dimensions, whereas the connection rigidity depends on shear connectors connecting the members together. The growth of traffic and increase in allowable axle loads means that bridges that are built many years ago are now heavily loaded (Dutta and Talukdar, 2002). Therefore, bridge components such as shear connectors in old concrete composite bridges might be overstressed leading to longitudinal shear failure. In this

case, it is important to monitor the composite action between beams and slab in this kind of bridges by assessing the condition of shear connectors.

2.8.1 Effect of failure in composite action on torsional stiffness of the system

Strength and stiffness of the system depend on the connection between structural members. The torsional stiffness is a function of the cross-section selected and the connection between the members of a composite structure. Torsion stiffness in concrete composite bridge elements is important to achieve proper distribution of live loads; it depends on the connection between the members and the shear modulus of elastic of the slab and beams. The connection between beams and slab in concrete composite bridges is by shear connectors. Damage of these shear connectors reduces the torsional stiffness of the system (Taberg, K.G., 1968).

2.8.2 Effect of loss in composite action on flexural stiffness of the system

Flexural stiffness of a composite structure is a function of the structure's material properties and geometry. In concrete composite structures, failure of shear connection leads to separation of members, the effective cross-sectional area reduces and thus its flexural stiffness. The transverse stiffness is provided by diaphragms. The effectiveness of the deck to distribute the loads in the transverse direction is a function of the ratio of the longitudinal to the transverse stiffness (Tamberg, K.G., 1968).

2.9 Classification of damage

The effects of damage on a structure can be classified as linear or nonlinear. (Doebling, *et al.*, 1996). A linear damage situation is defined as the case when the initially linear-elastic structure remains linear-elastic after damage. The changes in modal properties are a result of changes in the geometry and/or the material properties of the structure, but the structural response can still be modeled using linear equations of motion. Linear methods can be further classified as model-based and non-model based. Model-based methods assume that the monitored structure responds in some predetermined manner that can be accurately discretized by finite element analysis, such as the response described by Euler-Bernoulli beam theory, it involves updating certain parameters of the finite element

model using measured parameters. While response-based method utilizes change in experimental modal parameters to assess the performance of the structure. Nonlinear damage is defined as the case when the initially linear-elastic structure behaves in a nonlinear manner after the damage has been introduced.

A typical structural health monitoring (SHM) system includes three major components: a sensor system, a data processing system and a health evaluation system (Li, H., *et al*., 2004). As SHM is such a broad scope of the field, this research will focus on the third component of the SHM system, which is health evaluation system. Usually there are four different levels of damage evaluation in a structure (Doebling, *et al.*, 1996):

- Level 1: Determination that damage is present in the structure
- Level 2: Level 1 plus determination of the geometric location of the damage
- Level 3: Level 2 plus quantification of the severity of the damage
- Level 4: Level 3 plus prediction of the remaining service life of the structure.

The emphasis of this study will be on Level 1 and Level 2, using non-destructive dynamics-based damage detection methods i.e. change in frequency, damping ratios, mode shapes, curvature method, modal flexibility and modal strain energy to detect and locate regions with damaged shear connectors on concrete composite bridges.

Another category of classification for damage identification techniques makes the distinction between methods that are used for continuous monitoring of structural performance and methods that are applicable to the detection of damage caused by extreme events (Doebling, *et al.*, 1996). As an example, a system that uses continuous or intermittent accelerometer measurements from sensors mounted permanently to a bridge is different in terms of instrumentation and data acquisition requirements from a system that does not acquire data except during and immediately following an earthquake or a hurricane. It should be noted that the primary distinction between these situations has to do with the sensors and data acquisition system requirements.

2.10 Condition assessment for bridges

Two types of criteria are widely used to assess safety of existing bridges; these are load-carrying capacity and general condition (Frangopol, *et al*., 1997). These criteria are used routinely to determine if a bridge can remain operational in transportation network with or without special limitation. Safety of bridge structures is assured largely by maintaining these two aspects at acceptable levels, and they are important components of bridge management systems.

Bridge management system (BMS) is a means of managing bridge information to formulate maintenance programs within cost limitations. The objectives are to ensure that bridges achieve their design life and remain open to traffic continuously throughout their life; and also ensure that the risk of failure is always very low. The major task in bridge management includes activities such as inspection, assessment of condition and strength, repair, strengthening or replacement of components and various types of testing with the purpose of ensuring traffic safety and maintaining the bridge in a desired condition at the lowest possible cost. Confidence in BMSs is directly related to the degree to which evaluative standards are uniformly applicable across all bridges in the system to enable comprehensive and reliable ranking of maintenance and repair priorities (Gattulli & Chiaramonte, 2005).

Both destructive and non-destructive tests are used for assessment of bridge condition to establish the cause of deterioration, to locate defects and estimate their rate of development. The major tasks of non-destructive testing for condition assessment are to detect, verify, and quantify damage or deterioration in structural components. For the complete structure system, a global investigation should precede to locate possible damage or deterioration (Frangopol, *et al*., 1997). This global detection is currently performed mainly by visual inspection supported by professional experience. Using visual inspection anomalies are detected by recognizing changes from normal condition in color, shape, dimension, location, smoothness and reflection to light (Frangopol, *et al*., 1997).

There is a wide range of non-destructive techniques applicable to assessment of bridges condition but the suitability of each method depends on the precision required and accessibility of the structure. Before the application of the non-destructive technique, a desk study is important (McCann and Forde, 2001). The study seeks to provide the historical records of the bridge, i.e. the design loads used in the design of the structure, finite element model of the system, the contractor and type of construction. However, in most cases it is difficult to access all this information especially on bridges built a long time ago.

2.11 Damage detection techniques

There are different types of damage detection techniques using non-destructive testing, each based on different theoretical principles. These techniques produce different sets of information regarding the physical properties and state of the structure. Some of these techniques are ultrasonic techniques, radar method, impact testing, magnetic based methods and proof load tests. The disadvantage of these techniques is that they are limited to small area, detect a possible damage only near the surface of the structure, time consuming and require prior knowledge of the damaged zone (Farrar & Jauregui, 1997).

Visual inspection techniques are widely used for condition assessment of bridge structures. These techniques are however not applicable for assessing inner damaged parts of the structure such as shear connectors in concrete composite bridges. Localized non-destructive techniques such as ultrasonic techniques, radar method, impact testing, magnetic based methods and proof load tests can be used for detecting damaged shear connectors in concrete composite bridges. However, these techniques are limited to small areas, are time consuming, require prior knowledge of the vicinity of the damage and that the portion of the structure being inspected is readily accessible (Farrar & Jauregui, 1997). Moreover, experienced personnel are required to analyze and interpret the measured parameters.

To date there is little work in literature related to the use of these techniques in detecting damaged shear connectors in concrete composite bridges. This research focus on the use

of dynamics-based techniques in assessing the condition of shear connectors in concrete composite bridges based on measurements taken from the surface of the deck slab. The techniques are described in the next sections.

2.12 Dynamics-based techniques

For the past few decades, dynamics-based damage detection techniques have emerged as promising tools in assessing and detecting damage in structures (Sibanda, *et al*., 2008; Yong, *et al.*, 2006; Alvandi and Cremona, 2005; Wahab and De Roeck, 1999). The basic idea behind this techniques is that modal parameters i.e. natural frequencies, damping ratios, mode shapes and curvatures are functions of the physical properties of the structure (mass, damping, and stiffness). Therefore, changes in the physical properties due to damage will cause detectable changes in the modal properties. These techniques can therefore be used to detect internal structural damage such as damaged shear connectors when prior knowledge of the damage location is lacking.

The techniques include both global and local techniques.

2.12.1 Damage detection

The global dynamic parameters (Natural frequencies, damping ratios and mode shapes) of the structure provide the overall condition of the structure. These can only detect damage in a global sense.

2.12.1.1 Natural frequency based methods

The natural frequency is an important dynamic property of any elastic system and is mainly related to the equivalent modulus of elasticity or stiffness of system. Based on this point, shift in natural frequencies are considered as damage indicator in a global sense. The changes in resonant frequencies due to damage are compared and serve as an index for damage detection. The natural frequency of the structure shows the interrelation between its stiffness and its mass using the following expression;

$$\omega_n^2 = \frac{\Phi_n^T K \Phi_n}{\Phi_n^T M \Phi_n} \tag{2.12a}$$

Where: ω_n − natural frequency, $\Phi_n^T K \Phi_n$ − Modal stiffness and $\Phi_n^T M \Phi_n$ − Modal Mass. The assumption in damaged structures is that the mass of the system remains constant before and after damage and therefore any change in natural frequency is associated with change in stiffness. The natural frequencies of any structure can be monitored and any change due to damage can be detected.

An extensive research has been done using natural frequency as damage indicator. The main reason is that natural frequencies are easy to determine with a relatively high level of confidence. Also, Natural frequencies have much less statistical variation from random error sources than other modal parameters, which makes them a more robust means in the assessment of damage (Doubling, *et al*., 1998). However, the feasibility of using frequency changes for the purpose of damage localization is limited for at least two reasons (Kim, *et al.*, 2003). First, significant damage may cause very small changes in natural frequencies, particularly for larger structures, and these changes may go undetected due to measurement or processing errors. And also variations in the mass of the structure or environmental changes such as temperature or humidity fluctuations may introduce uncertainties in the measured frequency changes.

Although it is difficult in practice to use natural frequency to identify damage, some researchers have made great progress in this area. Morassi and Rocchetto (2003) presented the results of an experimental investigation into damage-induced changes in the modal parameters of steel-concrete composite beams subjected to small vibrations. The dynamic tests were performed on four composite beams, two having a partial connection and two having a total connection. The results of the tests revealed that, flexural frequencies show a rather high sensitivity to damage, and flexural frequencies can be considered as a reasonable indicator in damage detection. Sibanda *et al*, 2008 also noted that the frequency change method is a good tool for detecting the change of stiffness in a structure resulting from the partial loss of shear connector integrity but cannot localize damage.

2.12.1.2 Damping based methods

Damping on the other hand, represents the ability of a disturbed system to reduce vibrations to zero. The damping ratio is a measure of damping of the system. The damping ratio of any structure can also be measured and used to detect damage. Previous research has however shown that this parameter is difficult to measure and is also not sensitive to damage in most structures (Sibanda, *et al.*, 2008; Yong, *et al.*, 2006; Farrar, *et al.*, 1994).

Salone and Baldwin (1990) performed a dynamic test on a steel girder bridge with concrete decking to measure the steady-state response and the natural frequencies. The results showed that damping ratios were affected by deterioration but they were unreliable as damage indicator, because the trend was inconsistent with the severity of inflicted damage. This finding was confirmed by an experimental study by Farrar and Jauregui (1997), in their study the damping of a steel plate girder bridge did not consistently increase or decrease as damage severity increased.

The conclusion of many researchers is that damping is an unreliable indicator for damage identification due to inconsistency in changes of damping ratios. However, a different conclusion is obtained from Abdul Razak and Choi (2001). In their study, they tested three reinforced concrete beams; two subjected to different states of reinforcement corrosion and one remain undamaged. The results showed that the damping ratios for mode 2 and 3 increased considerably with increased damage severity. They concluded that the damping ratios of the second and third modes reflected a pattern consistent with the severity of the corrosion damage.

2.12.1.3 Mode Shapes

The mode shape is a unique characteristic of a structural system. It shows deformed shapes of the structure at a particular frequency and damping ratio. The mode shape of a system measured at different times can be superimposed to check for change in curvatures resulting from damage. If a structure is locally damaged, mode shape changes will occur in the vicinity of that damage. Therefore, a comparison between two sets of

mode shapes data either direct mode shapes or their derivatives can be used to identify damage. A large number of damage identification methods have been developed based on directly measured mode shapes or their derivatives.

Two commonly used methods to compare two sets of mode shapes are the Modal Assurance Criterion (MAC) and the Coordinate Modal Assurance Criterion (COMAC).

2.12.1.3.1 Modal Assurance Criteria (MAC) values

MAC values serve as reliable indexes to analyze and correlate mode shapes. The method makes uses of the orthogonal properties of the mode shape to correlate two modes (Frisswell and Mottershead, 1995). The modes extracted from a structure, at different times, can be analysed using MAC values to check for any notable changes and therefore damage. MAC values close to zero show that the mode shapes are orthogonal or dissimilar whereas values close to one show that the modes are similar. The MAC value that compare mode *i* and *j (*e.g. mode shape in the undamaged and damaged state) is calculated from (Frisswell and Mottershead, 1995):

$$MAC(i,j) = \frac{\left|\sum_{k=1}^{n}\left(\Phi_j\right)_k(\Phi_i)_k^*\right|^2}{\sum_{k=1}^{n}\left(\Phi_j\right)_k(\Phi_i)_k^*} \qquad (2.12b)$$

Where: $(\Phi)_k$ denotes an element of mode shape vector and the asterisk denotes complex conjugate with *n* being the modal degree of freedom.

The technique however has some limitations. Frisswell and Mottershead (1995) noted that it is difficult to compare modes that are close in frequency or that are measured at insufficient transducer locations using MAC values. Also (Sibanda, *et al.*, 2008) noted that MAC is a good tool for detecting the change of stiffness in a structure but cannot localize damage.

2.12.1.3.2 Coordinate Modal Assurance Criteria (COMAC) values

COMAC values, unlike MAC values, compute the correlation between two similar locations of the modes. This algorithm can therefore localize damage within a structure. These values are estimated from the following algorithm suggested by Pandey, *et al.*, 1991.

$$COMAC(i,j) = \frac{\sum_{l=1}^{L}\left|\varphi_{il}^{u} \cdot \varphi_{il}^{d}\right|^{2}}{\sum_{l=1}^{L}(\varphi_{il}^{u})^{2} \cdot \sum_{l=1}^{L}\left(\varphi_{il}^{d}\right)^{2}} \qquad (2.12c)$$

Where: $\varphi^{u}\ and\ \varphi^{d}$ - Unit mass normalized mode shape vectors for the undamaged and damaged structure respectively.

l – Represents an individual correlated pair of which a total of L pairs are available.

COMAC values greater than 0.9 show correlation between the two points on the modes whereas a value less than 0.9 means that the points are not related. This can be the case when the structure has been damaged. This technique thus can be used to localize damage in the structure. However, some authors (Yong, *et al.*, 2006) noted that COMAC can detect some damage locations but can also make some false identification.

Both MAC and COMAC are considered as Direct Mode shape methods. Next bullet describes Mode shape curvature based methods.

2.12.1.3.3 Mode shape curvature based methods.

These methods have been used in damage identification due to the fact that curvature changes are highly localized to the region of damage. They are more pronounced than changes in the displacement of mode shapes themselves and are therefore more sensitive to damage (Dutta & Talukdar, 2004). However, the quality of damage detection achieved in practice depends upon determining a proper sampling interval for discretization of the displacement mode shapes (sazonov & klinkhachorn, 2004). Change in curvatures increases with reduction in flexural stiffness of the structure, therefore, the amount of damage can be obtained from the amplitude of curvature's change. Using the relationship

between the flexural stiffness (*EI*) of a simply supported beam and the frequency (ω_n) of the n^{th} vibration mode

$$\omega_n = \frac{n^2\pi^2}{L^2}\sqrt{\frac{EI}{m}} \tag{2.12d}$$

Where *L* is the length of the beam and *m* the mass for unit length, *E* – Modulus of elasticity and *I* – Moment of inertia of the section. From the theory of structure the relation between the curvature '*k*' of beam's axis and the bending moment '*M*' at location *x* along the length of the beam is given by

$$k = \frac{M_x}{EI} \tag{2.12e}$$

Substitution of equation (2.12d) in (2.12e) gives equation (2.12f) which shows the relationship between curvature and natural frequencies.

$$k = \frac{1}{\omega^2}\cdot\frac{n^4\pi^4 M_x}{mL^4} \tag{2.12f}$$

The relationship between curvature and beam deflection is then expressed by

$$k = \left[\frac{\partial^2\phi}{\partial x^2}\right]\left[1+\left[\frac{\partial\phi}{\partial x}\right]^2\right]^{-3/2} \tag{2.12g}$$

Where ϕ is the vertical displacement at the selected cross-section along the length of the beam. For very small deflections and slope, equation (2.12g) can be approximated to

$$k = \frac{\partial^2\phi}{\partial x^2} \tag{2.12h}$$

The partial derivative in the second member can be computed through an approximation formula called central difference formula equation (2.12i).

$$\phi''_{ji} = \frac{\phi_{(j+d)i} - 2\phi_{ji} + \phi_{(j-d)i}}{d^2} \quad (2.12i)$$

With *i* being the mode shape number, *j* the node number, and *d* the distance between the nodes.

The use of mode shape curvature to predict the location of damage has shown reasonably good results. A comparative research study confirmed that the mode shape curvature is a far more sensitive indicator than the MAC and COMAC values of the mode shapes themselves (Pandey, *et al.*, 1991). However, most successful results were obtained from numerical data, and a big challenge is still to determine an accurate way to obtain mode shape curvature from experimental data (Ractiffe, 1997).

The global techniques described above, except mode shapes, only satisfy the first level of damage detection i.e. identify that damage has occurred in the structure but cannot localize it. Location of the damage may be possible using one of the dynamics-based algorithms described in the next section.

2.12.2 Damage localization

Localization of damaged regions in structure can be done using modal-based algorithms. These are usually referred to as mode shape derivatives because they use mode shape data to localize damage within the structure (Pandey, *et al.*, 1991). The following section describes these algorithms.

2.12.2.1 Change in curvature method

Pandey, *et al.*, (1991) assumed that structural damage only affects the structure's stiffness matrix and its mass distribution. The pre and post-damage mode shapes are first extracted from an experimental analysis. Curvature of the mode shapes for the beams in its undamaged and damaged conditions are estimated numerically from the displacement mode shapes using any differentiation schemes such as the forward difference method, central difference and backward difference methods.

The curvature values which can be obtained from equation (2.12i) are used to calculate Curvature Damage Indicators (CDI). This index computes a damage factor for all points of interest and thus can be used to localize damage in the structure. Wahab and De Roeck (1999) used the following expression to calculate CDI values for a damaged beam structure:

$$CDI = \frac{1}{N}\sum_{n=1}^{N}\left|v_{oi}^{II} - v_{di}^{II}\right| \qquad (2.12j)$$

Where: N – Number of modes

$v_{oi}^{II}\ and\ v_{di}^{II}$ – Curvature values for the undamaged and damaged structure at node *i*.

In their study, Wahab and Roeck (1999) observed that damage in some location of the structure could be located whilst damage in other locations could not be located. False damage was also detected.

2.12.2.2 Change in Flexibility method

Damage increases the flexibility of the structure. The modal flexibility matrix includes the influence of both the mode shapes and natural frequencies. Huth, *et al.,* (2005) defined modal flexibility matrix as the accumulation of the contributions from all available mode shapes and corresponding natural frequencies. The undamaged regions are expected to have higher amplitude of vibrating than the damaged sections. This phenomenon can be used to locate damage in a structure.

The modal flexibility matrix is derived as follows:

$$[M]\{\ddot{u}\} + [K]\{\dot{u}\} = 0 \qquad (2.12k)$$

$$where\ \{u\} = \{\emptyset\}cos\omega t \qquad (2.12l)$$

Substituting equation (2.12k) into equation (2.12l), it becomes

$$[K][\Phi] - [\omega^2][M][\Phi] = 0 \qquad (2.12m)$$

Pre-multiplying equation (2.12m) by the transpose of the modal vector $[\emptyset]^T$

$$[\Phi]^T[K][\Phi] - [\omega^2][\Phi]^T[M][\Phi] = 0 \tag{2.12n}$$

For normalized eigenvectors, the orthogonal condition is given by

$$[\Phi]^T[M][\Phi] = [I] \tag{2.12o}$$

Substituting equation (2.12o) into equation (2.12n), it becomes

$$[\Phi]^T[K][\Phi] - [\omega^2][I] = 0 \tag{2.12p}$$

$$[\Phi]^{-1}[K]^{-1}[\Phi]^{-T} = \left[\frac{1}{\omega^2}\right][I] \tag{2.12q}$$

$$[K]^{-1} = \left[\frac{1}{\omega^2}\right][\Phi][\Phi]^T = \sum_{i=1}^{n} \frac{1}{\omega_i^2}\{\Phi_i\}\{\Phi_i\}^T = [F] \tag{2.12r}$$

The change of nodal flexibility matrix is given as follow:

$$\Delta[F] = [F^d] - [F^u] \tag{2.12s}$$

Where $[F]$ is the modal flexibility, $[K]$ is the stiffness matrix, M is the mass matrix, $[\Phi]$ is the mass normalize matrix, $\left[\frac{1}{\omega^2}\right]$ is a diagonal matrix containing the reciprocal of the squire of natural frequencies in ascending order, ω_i is the i^{th} natural frequency of the structure and Φ_i is the i^{th} unit mass normalized modal vector. Index '*u* and *d*' refer to the undamaged and damaged state respectively (Huth, *et al.*, 2005, Paz and Leigh 2004).

For each column of $[\Delta F]$ matrix, the damaged locations are defined as the absolute maximum, δj_{max}, at each measurement *j*. Because of the inverse relationship with square of the natural frequencies, the measured flexibility matrix converges rapidly with increasing values of frequency. Hence, the flexibility matrix can be easily and accurately estimated from a few of the lower frequency modes of vibration of the structure, which can be easily measured (Pandey and Biswas 1994).

Yong, *et al.*, (2006) used this method to locate damaged shear connectors in a concrete composite bridge. Some damaged connectors were located and false identification was also observed. Farrar and Jauregui (1997) also used this technique to localize damage in a bridge structure. This technique was only efficient when severe damage was inflicted in the structure. Likewise some false damage was observed.

2.12.2.3 Change in stiffness method

Damage reduces the stiffness of the structure. This algorithm uses the eigen-value problem of a structure to compare eigen-vectors of damaged and undamaged structure. The general eigen-value problem for an undamped structure is given by:

$$(\lambda_i[M] + [K]\{\psi_i\}) = 0 \tag{2.12t}$$

Where: λ_i - The ith eigen-value

[M], [K] - Mass and the stiffness matrix respectively

$\{\psi_i\}$ – Displacement vector

The eigen-value problem of the damaged structure is formulated from first replacing the pre-damaged eigenvectors and eigen-values with a set of post-damaged modal parameters (Farrar and Jauregui, 1997).

$$\left(\lambda_i^d[M - \Delta M_d] + [K - \Delta K_d]\{\psi_i\}^d\right) \tag{2.12u}$$

Where: ΔM_d and ΔK_d – change in mass and stiffness due to damage respectively.

The damaged vector $\{D_i\}$ for the i^{th} mode is given by:

$$\{D_i\} = \left(\lambda_i^d[M] + [K]\{\psi_i\}^d\right) = \left(\lambda_i^d[\Delta M_d] + [\Delta K_d]\{\psi_i\}^d\right) \tag{2.12v}$$

Damage is assumed to change only the stiffness of the structure i.e. $[\Delta M_d] = 0$. Therefore the damage vector reduces to:

$$\{D_i\} = ([\Delta K_d]\{\psi_i\}^d) \tag{2.12w}$$

$$[K]^u \cong \sum_{i=1}^{n} (\omega_i^u)^2 \{\Phi_i^u\}\{\Phi_i^u\}^T \ \ and \ \ [K]^d \approx \sum_{i=1}^{n} (\omega_i^d)^2 \{\Phi_i^d\}\{\Phi_i^d\}^T \qquad (2.12x)$$

Where: $[K]^u$ and $[K]^d$ are stiffness matrices for undamaged and damaged structure respectively.

$$[\Delta K] = [K]^u - [K]^d \qquad (2.12y)$$

As in the flexibility method, the modal stiffness can be calculated for all measured locations on the structure. The resulting damage vectors can be used to localize damaged sections in the structure.

2.12.2.4 Change in strain energy method

This damage indicator method was developed by Stubbs and Kim (1994) to detect the existence and location of damage in a structure and is based on the assumption that strain energy stored in damaged regions will decrease after the occurrence of damage. This method has been extensively used in previous damage detection studies and it shows better performance over other existing damage detection methods (Li, 2010; Rivelos, *et al.*, 2010; Alvandi & Cremona, 2006; Barroso & Rodriguez, 2004 and Farrar & Jauregui, 1997). When damage occurs, the modal strain energy in that load path alters due to high sensitivity of the frequency and shape of that mode. By using changes in modal strain energy as damage indicator, not only the damaged location but also the magnitude of the damage can be determined.

Considering a general Euler-Bernoulli beam, the strain energy stored in a system is expressed by,

$$U_i = \frac{1}{2}\int_0^L EI(w''(x))^2 dx \qquad (2.12z)$$

Where *EI* is the flexural rigidity of the beam and *w* is the beam deflection. Similarly, the energy in modal space associated with a particular mode shape Φ_i for undamaged case is given as (Alvandi and Cremona, 2006):

$$U_i^u = \frac{1}{2}\int_0^L EI^u(\Phi_i^{u''}(x))^2 dx \qquad (2.12.1a)$$

Where $\Phi_i^{u''}(x)$ is the second derivative or curvature of mode shape *i* with respect to *x*.

For a beam with N elements, the modal strain energy associated with the j^{th} element for the i^{th} mode is expressed as: (Alvandi and Cremona, 2006; Zhang and Aktan, 1995):

$$U_{ij}^u = \frac{1}{2}\int_{a_j}^{a_{j+1}} (EI^u)_j(\Phi_i^{u''}(x))^2 dx \qquad (2.12.1b)$$

Where: a_j and a_{j+1} – Bounds for element *j*.

The fractional strain energy of the j^{th} element is calculated from:

$$F_{ij} = \frac{U_{ij}^u}{U_i^u} = \frac{\frac{1}{2}\int_{a_j}^{a_{j+1}}(EI^u)_j(\Phi_i^{u''}(x))^2 dx}{\frac{1}{2}\int_0^L EI^u(\Phi_i^{u''}(x))^2 dx} \qquad (2.12.1c)$$

:

Similar expressions can be derived for a damaged case:

$$U_i^d = \frac{1}{2}\int_0^L EI^d\left(\Phi_i^{d''}(x)\right)^2 dx \qquad (2.12.1d)$$

For j^{th} element:

$$U_{ij}^d = \frac{1}{2}\int_{a_j}^{a_{j+1}} (EI^d)_j\left(\Phi_i^{d''}(x)\right)^2 dx \qquad (2.12.1e)$$

By assuming that the fraction of modal energy is the same for damaged and undamaged structures, it is found that,

$$\frac{\frac{1}{2}\int_{a_j}^{a_{j+1}}(EI^u)_j(\Phi_i^{u\prime\prime}(x))^2dx}{\frac{1}{2}\int_0^L EI^u(\Phi_i^{u\prime\prime}(x))^2dx}=\frac{\frac{1}{2}\int_{a_j}^{a_{j+1}}(EI^d)_j\left(\Phi_i^{d\prime\prime}(x)\right)^2dx}{\frac{1}{2}\int_0^L EI^d\left(\Phi_i^{d\prime\prime}(x)\right)^2dx} \tag{2.12.1f}$$

When rearranging equation (2.12.1f), the damage indicator (β_{ij}) of mode *i* and member *j* is obtained from:

$$\beta_{ij}=\frac{(EI)_j}{(EI^*)_j}=\frac{\int_{a_j}^{a_{j+1}}\left(\Phi_i^{d\prime\prime}(x)\right)^2dx\int_0^L(\Phi_i^{u\prime\prime}(x))^2dx}{\int_{a_j}^{a_{j+1}}(\Phi_i^{u\prime\prime}(x))^2dx\int_0^L\left(\Phi_i^{d\prime\prime}(x)\right)^2dx} \tag{2.12.1g}$$

Here it is assumed that the flexural rigidity $(EI)_j$ of the damaged and undamaged modes is constant over the entire length of the element *j*. To establish a comparative basis for different modes, the β_{ij} is transformed into the standard normal space, and the normalized damage indicator Z_{ij} is given by:

$$Z_{ij}=\frac{\beta_{ij}-\mu_{\beta ij}}{\sigma_{\beta ij}} \tag{2.12.1h}$$

Where $\mu_{\beta ij}$ being the mean and $\sigma_{\beta ij}$ the standard deviation of the values for all *j* elements. The estimation of the damage severity for element j is expressed by:

$$\alpha_{ij}=1-\frac{1}{\beta_{ij}} \tag{2.12.1i}$$

Alvandi and Cremona (2006) studied the performance of both flexibility method and strain energy method on a simply supported beam. Measured modal parameters which use only few mode shapes and modal frequencies of the structure obtained by random force excitation were used. The authors assess the performance of these techniques by introducing different noise levels to the response signals of a simulated beam which was excited by random force. They concluded that both methods are capable of detecting and localizing damaged elements but in the case of complex and simultaneous damages, the flexibility method is less efficient. Moreover, the strain energy method demonstrates stability in presence of noisy signal.

2.13 Summary of Literature review

Most bridge management systems still rely on visual inspections for condition assessment; this means that damage in inaccessible parts of the structure such as shear connectors in concrete composite bridges will remain undetected until it is expensive to repair or catastrophic failure occurs. However, there are localized non-destructive techniques that can be applied for detecting damaged shear connectors in bridges (Sibanda, *et al.*, 2008 and Dilena & Morassi, 2008). These include ultrasonic techniques, radar method, impact testing, magnetic based methods and proof load tests. Nevertheless, these techniques are limited to small areas, time consuming and require prior knowledge of the damaged location.

For the last few decades, dynamics-based techniques became promising tools in assessing and detecting damage in structures where prior knowledge of the damaged location is lacking. The basic idea of these techniques is that change in physical properties i.e. mass, damping and stiffness of the structure due to damage results in the change of modal parameters i.e. natural frequencies, damping ratios, mode shapes and curvatures. These techniques can therefore be used to detect internal structural damage such as damaged shear connectors in concrete composite bridges.

Important literature findings related to damage detection and localization are summarized as follows:

Modal frequencies can be measured easily and accurately. Change of natural frequency can be used for detecting the existence of damage but cannot localize damage. This is because frequencies are not spatially specific and are not very sensitive to damage, such that its application is limited to simple structures. Mode shapes can be described as a vibration form in which a structure oscillates with the corresponding natural frequencies. The mode shapes have the advantage of being spatially specific. Both approaches generate extra errors and make damage detection more difficult. It is often very difficult or impracticable to measure the response along all of the degree of freedom necessary for the complete definition of a given mode shape. A dense array of sensors would be needed in order to capture an accurate mode shapes.

If a structure is locally damaged, mode shape changes will occur in the vicinity of that damage. Therefore, a comparison between two sets of direct mode shape data or their derivative can be used to identify damage. Two commonly used methods to compare two sets of mode shapes are the MAC and COMAC. The MAC values measure the similarity of two modes. A MAC value of 1 means perfect match and a value of 0 means they are completely dissimilar. Thus a reduction of MAC value may be an indication of damage. The COMAC differs from MAC in the way that it gives a point-wise measure of the difference between two sets mode shapes. A low COMAC value would indicate discordance at a point and thus is a possible damage location indicator. Research that utilized these two techniques gave somewhat good results in the identification of damage.

Damage localization methods reviewed are change of curvatures method, change of flexibility method, change of stiffness and strain energy method. The advantage of using the modal flexibility method over stiffness method is that the flexibility matrix is most sensitive to changes in the lower-frequency modes of the structures due to the inverse relationship to the square of the natural frequencies. Therefore, a good estimation of the modal flexibility can be made with the inclusion of the first few natural frequencies and their associated mode shapes. The advantage of using the curvature and modal strain energy method is that only measured mode shapes are required in the damage identification without knowledge of the complete stiffness and mass matrices of the structure. Only the mode shapes of the first few modes and their corresponding derivatives are required to locate damage. Therefore, the change of modal flexibility method, change of curvature and modal strain energy methods are chosen in this study as their corresponding algorithm can be applied to beams and can be implemented using the first few vibration modes. In addition both methods are able to locate damage regions based on the magnitude of the damage index (peaks) in the plots diagrams.

Next chapter describes the basis of structural dynamics, the procedures for modal testing and experimental modal analysis to characterize the dynamic properties of a structure.

CHAPTER 3

MODAL TESTING (MT) AND EXPERIMENTAL MODAL ANALYSIS (EMA)

3.1 Introduction

MT and EMA are the process of characterizing the dynamic properties of a structure by exciting the structure and identifying its modes of vibration. While experimental modal analysis is the process of determining the modal parameters from the acquired data, modal testing describes the performance of the testing and the acquisition of the modal data from the test structure. The main aim of this chapter is to understand procedures involved in MT and EMA. It provides an overview of the dynamic testing for modal analysis which includes measurement mechanisms and signal processing. As the input and output relation of the linear system can be written in the frequency domain, the general frequency response transfer function used for modal analysis is also reviewed. Modal extraction methods, validation of measurements are also reviewed.

This chapter begins by presenting basic concepts of structural dynamic theories, which includes; governing equations for structural systems and damping, Linear differential equations relate the effects of the mass, stiffness and damping in a way that leads to determination of natural frequencies, mode shapes and damping ratios of the idealized system. Two common methods i.e. logarithmic decrement and bandwidth method are introduced for determining the damping ratio in a system experimentally. In addition, an alternative method of considering the dynamic equilibrium of the system, Rayleigh's method, is reviewed.

3.2 Basic dynamic equations

The structure shown in Figure 3.1 is called a lumped parameter system of a single degree-of-freedom because it's physical properties are "lumped" into the mass, spring, and damper elements (Clough and Penzien, 1993). When the elastic structure is excited by a force or displacement motion, the forced linear vibration of the structure can be described by a homogeneous dynamic equilibrium equation given as follows:

$$m\ddot{u} + c\dot{u} + ku = F(t) \tag{3.2a}$$

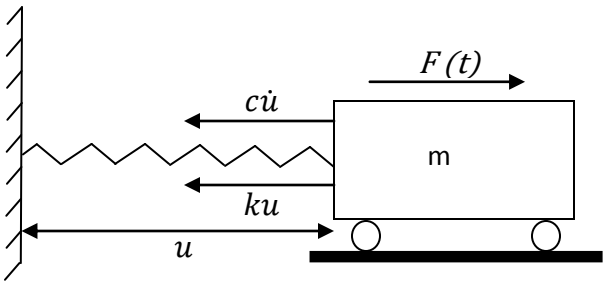

Figure 3.1: Dynamic equilibrium of a single degree-of-freedom system

Where *m* and *k* are the mass and spring constant of the oscillator respectively and *c* is the viscous damping coefficient. *F(t*) is the time dependent excitation force applied to the system. $\ddot{u}, \dot{u}\ and\ u$ are the corresponding response of acceleration, velocity and displacement respectively.

Equation (3.2*a*) is a statement of Newton's second law of motion; a force balance among three types of internal forces in any structure made of elastic materials. These internal forces are inertial (mass), dissipative (damping), and restoring (stiffness) forces. Some forms of damping (e.g. viscous) are always present in all real structures. The free vibration without damping of the linear multiple degree-of-freedom system requires that the force vector $\{F\}$ and damping matrix $[C]$ equal zero in equation (3.2*a*). The general form of this equation is given as follows:

$$[M]\{\ddot{u}\} + [K]\{\dot{u}\} = 0 \tag{3.2b}$$

The solution of equation (3.2b) is in the form as

$$u_i = a_i \sin(\omega t - \alpha) \qquad\qquad i = 1,2 \ldots\ldots, n \tag{3.2c}$$

Or in vector notation

$$\{u\}\{a\}sin(\omega t - \alpha) \tag{3.2d}$$

Where a_i is the amplitude of motion of the i^{th} coordinate and *n* is the number of degrees of freedom, *t* is the time of motion, ω is the circular frequency and α is the phase angle.

After substituting equation (3.2d) into equation (3.2b), and rearranging the terms, it forms equation (3.2e), which is an important mathematical problem known as Eigen problem.

$$|[K] - \omega^2[M]|\{a\} = \{0\} \tag{3.2e}$$

This eigenproblem is then used to find the nontrivial solution which yields

$$|[K] - \omega^2[M]| = 0 \tag{3.2f}$$

By using equation (3.2*f*), the circular frequency (ω), natural frequency (*f*), and the period of motion (*T*) are then determined as follows:

$$\omega = \sqrt{\frac{k}{m}} \tag{3.2g}$$

$$\omega = 2\pi f \tag{3.2h}$$

$$f = \frac{1}{T} \tag{3.2i}$$

$$T = \frac{2\pi}{\omega} \tag{3.2j}$$

For each of these values of ω^2 satisfying the characteristics equation (3.2*f*), they are used to solve equation (3.2*e*) for $a_1, a_2, \ldots\ldots a_n$ in terms of an arbitrary constant.

3.3 Damping ratio

3.3.1 Logarithmic decrement

In order to determine the damping coefficient of a system experimentally, a free vibration is carried out on the structure to obtain a record of its oscillatory motion, such as the one shown in Figure 3.2, and measure the rate of decay of the amplitude of motion.

The decay may be conveniently expressed by the logarithmic decrement δ which is defined as the natural logarithm of the ratio of any two successive peak amplitudes for the displacement or acceleration in the free vibration as shown in equation (3.3a) and (3.3b) respectively.

$$\delta = ln\frac{u_1}{u_2} \quad or \quad \delta = ln\frac{\ddot{u}_1}{\ddot{u}_2} \tag{3.3a, 3.3b}$$

Where $u\ and\ \ddot{u}$ are the corresponding response of displacement and acceleration respectively, subscript 1 and 2 denote two consecutive peaks.

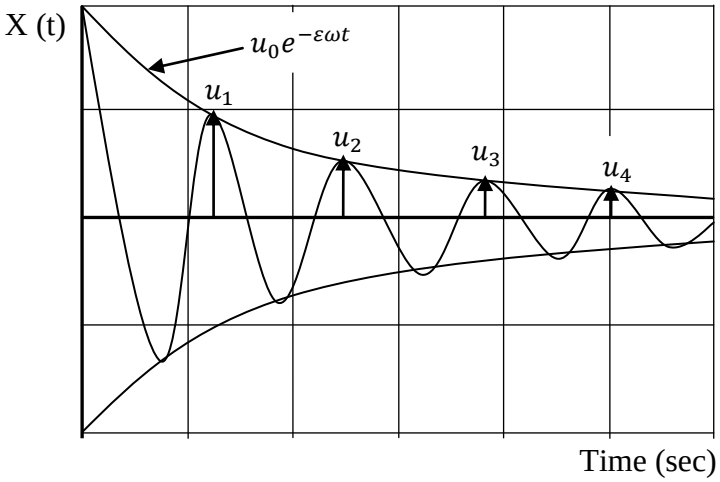

Figure 3.2: Free-vibration response of an under damped system.

After determining the amplitudes of two successive peaks of the system in free vibration experimentally, the damping ratio ξ can be calculated as follows:

$$\delta = \frac{2\pi\xi}{\sqrt{1-\xi^2}} \tag{3.3c}$$

3.3.2 Bandwidth method

The bandwidth method, also known as the half-power method, is an alternative way to estimate the damping ratio (Clough and Penzien, 1993). A typical frequency amplitude curve obtained experimentally for a moderately damped structure is shown in Figure 3.3.

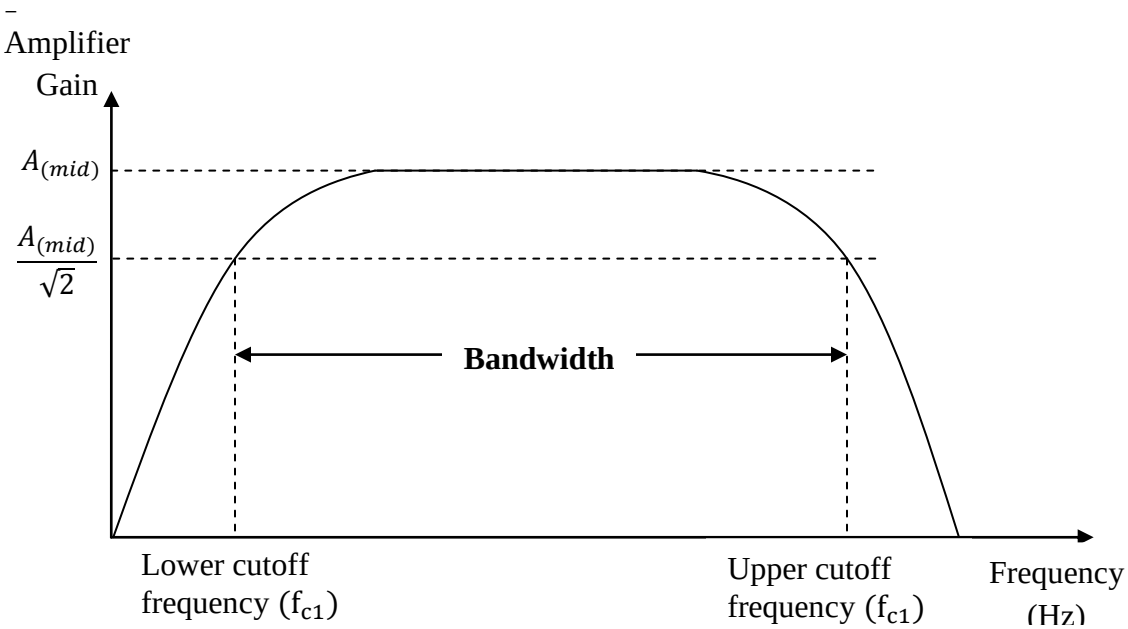

Figure 3.3: Typical frequency response curve.

The shape of the curve is controlled by an amount of damping presented in the system; in particular, the bandwidth, that is the difference between two frequencies corresponding to the same response amplitude, is related to the damping in the system. In the evaluation of damping it is convenient to measure the bandwidth at $1/\sqrt{2}$ of the peak amplitude. The frequencies corresponding to this bandwidth, f_1 and f_2 are referred to as half-power points. The damping ratio ξ is then calculated as follows:

$$\xi = \frac{f_2 - f_1}{f_2 + f_1} \tag{3.3d}$$

3.4 Rayleigh's method

Rayleigh's method is used to find the approximate value of the fundamental natural frequency of a discrete system. Rayleigh's principle can be stated as follows: "The frequency of vibration of a conservative system vibrating about an equilibrium position has a stationary value in the neighborhood of a natural mode. This stationary value, in fact, is a minimum in the neighborhood of the fundamental natural mode. This method, in which the natural frequency is obtained by equating maximum kinetic energy with maximum potential energy, is known as Reyleigh's method." (Chopra, 1995).

By considering the principle of conservation of energy, if no external forces are acting on the system and there is no dissipation of energy due to damping, maximum strain energy (SE_{max}) equals maximum kinetic energy (KE_{max}).

$$SE_{max} = KE_{max} \tag{3.4a}$$

$$Strain\ Energy\ in\ spring\ (SE) = \frac{1}{2}ku^2 \tag{3.4b}$$

$$Kinetic\ Energy\ of\ body\ (KE) = \frac{1}{2}m\dot{u}^2 \tag{3.4c}$$

$$u = \phi sin\omega t \tag{3.4d}$$

Where *m* and *k* are the mass and spring constant of the oscillator respectively, $u\ and\ \dot{u}$ are response of displacement and velocity respectively, ϕ denotes the vector of amplitudes (mode shape), ω represents the natural frequency of vibration, and t is the time of motion. Substituting equation (3.4b) and (3.4c) into equation (3.4a), the fundamental natural frequency of a discrete system is given as follows:

$$\frac{1}{2}\phi^T K\phi = \frac{1}{2}\omega^2\phi^T M\phi \tag{3.4e}$$

$$\omega^2 = \frac{\phi^T K\phi}{\phi^T M\phi} \tag{3.4f}$$

3.5 Modal Analysis

Modal analysis is an important tool in the analysis, diagnosis, design and control of vibration. The experimental determination of modal parameters i.e. natural frequencies, modal damping, damping mass, mode shapes is called experimental modal analysis and is based on vibration measurements that fall within the general designation of modal testing. The objective of this form of vibration testing is to acquire sets of frequency response functions (FRFs) that are sufficiently accurate and extensive in both the frequency and spatial domains to enable analysis and extractions of the dynamic properties for all the required modes of vibration of the structure.

Experimental modal analysis (EMA) comprises a set of experimentally-based procedures which lead to the construction of a mathematical model that can be used to describe the dynamic behavior of the test object. The mathematical models are almost always finite element models (FEM). This model can be used on a variety of useful applications including (Ewins, 2000).

i. Visualization of the modes of vibration of the test structure for the purpose of gaining physical insight and an understanding of the often complex dynamic properties of real structures;
ii. Comparison of the actual (measured) vibration behavior of a real structure with corresponding parameters predicted from a theoretical model;
iii. Correcting or refining that theoretical model;
iv. Predicting the effects of making modifications, or predicting what modifications to introduce to change the structure's behavior;
v. Predicting the behavior of structures formed by coupling two or more components together;
vi. Detecting damage or other changes in the integrity of a structure during its service life;
vii. Identification of 'unpredictable' parameters such as damping, dynamic friction effects, excitation forces from unknown sources, etc.

Parameters that must be carefully defined before performing modal analysis test include, among others, the frequency range of interest, the selection of the transducer (response and excitation) locations, the selection of the suspension locations (when adequate), and the type of excitation to be used.

Common problems that may be overlooked are related to broken leads, badly connected cables, badly attached transducers. Careful checks will avoid most of these problems.

3.6 Modal testing

Vibration testing for experimental modal analysis is commonly known as modal testing. Prior knowledge of areas such as vibration analysis, instrumentation, signal processing, and modal identification is required to understand modal testing. The basic aim of modal testing is to obtain FRFs relating output vibrations responses at a number of coordinates of interest, usually under the form of accelerations (or velocities, or displacements), to input vibration excitations, usually under the form of driving forces, applied at a given coordinate.

Ewins (2001) pointed out the basic procedures that must be executed to conduct a model test (having first thoroughly familiarized with the associated theory so that one can detect and explain any deviations of actual behavior from the expected and assumed characteristics of a linear, multi-degree-of-freedom system (MDOF)) are as follows:

i. Set up the test structure in a mounting configuration which has been carefully selected and which can be controlled.

ii. Provide a means of exciting the structure into vibration in a controllable and measured way. This may be by means of a non-attached device, such as an impact hammer or similar, or by an exciter which is connected firmly to the test structure. These exciters can generate the required excitation forces by several means: mechanical, electromagnetic, electro-hydraulic, etc.

iii. Provide a means of (transducers for) measuring the resulting response of the test structure, and to do so with the minimum of interference to the test object (often difficult to achieve).

iv. Provide signal processing and analysis facilities so that the required information can be extracted from the individual measured time histories yielded by the transducers. Here, it is usually necessary to convert raw measured data in the time domain into equivalent spectra in the frequency domain, as frequency domain parameters are more commonly used to describe most vibration phenomena.

v. Subject the measured response function data to a subsequent analysis stage, often employing curve fitting techniques, in order to construct a mathematical model of standard form (linear, MDOF system) whose dynamic properties most closely resemble those observed on the test structure.

vi. Check that the resulting model is adequate for the intended application (before releasing the test structure).

In order to perform modal testing a number of hardware components must be available. These components may be interfaced with a host computer allowing for coordination of the operation of the overall system and enhancing the data-processing capabilities, if adequate software is available. The hardware components are schematically represented in Figure 3.4.

3.7 Measurement mechanisms

An experimental vibration system generally consists of three main measurement mechanisms (Silva, 2001):

(i) The excitation mechanism;
(ii) The sensing mechanism;
(iii) The Data acquisition and processing mechanism.

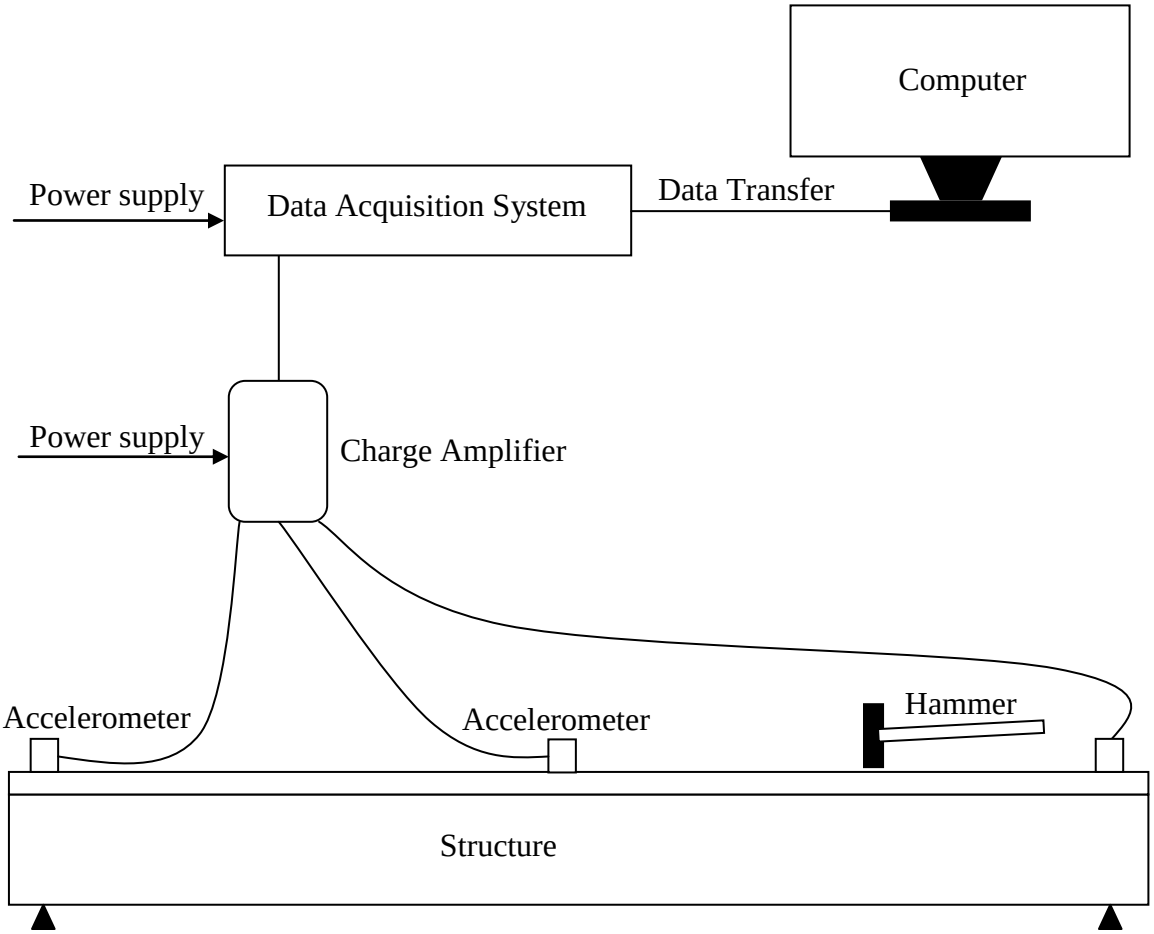

Figure 3.4: Dynamic measurement system

3.7.1 The excitation mechanism

This mechanism is constituted by a system which provides the input motion to the structure under analysis, generally under the form of a driving force applied at a given coordinate. Shakers and impact hammer are commonly used structural exciters in modal testing.

Impact or impulse hammer (Figure 3.5), which consists of a hammer with a force transducer attached to its head. This device does not need a signal generator and a power amplifier and nothing is attached to the structure. Hence, the excitation system does not affect the dynamics of the test structure. The hammer, by itself, is the excitation mechanism and is used to impact the structure and thus excite a broad range of

frequencies. The type of impulse force from the hammer is varied by changing hammer/tip heads. The amount of force applied is varied by changing drop heights.

The Shaker also known as fixed exciter (Figure 3.6), is usually an electromagnetic or electro-hydraulic vibrator, driven by a power amplifier. Unlike impact hammer this device need a signal generator and can be chosen from a variety of different possibilities (stepped-sine, swept sine, impulse, random, etc) to match the requirements of the structure under test. Shakers can be positioned on top of the structure and allowed to vibrate freely. This type of excitation mechanism may be easily controlled both in frequency and amplitude and therefore offers the best overall accuracy. However, it also has some disadvantages, such as the need for the exciter to be connected to the test structure. Despite the use of connecting devices (named push rods, drive rods, or stringers) designed to reduce the attachment consequences, there are always some constraining effects and mass loading of the structure. These exciters vary in size and their choice depends on the structure under test. The main characteristics to take into consideration are force level, displacement level, and frequency range. The objective is for the exciter to provide inputs large enough to result in easily measured responses. The applied excitation force is commonly measured by means of a loaded cell (known as force transducer) which is located at the end of the stringer and is rigidly connected to the test structure.

Figure 3.5: Impulse hammer

Figure 3.6: Electromagnetic shaker

3.7.1.1 Types of excitation

Structural dynamic testing can be performed based on different types of test, including (Ren and Zong, 2003):

(i) Forced vibration.

(ii) Ambient vibration test.

(iii) Free vibration.

These three types of excitation are briefly discussed as follows:

3.7.1.1.1 Forced vibration excitation

In this method, the structure is excited by artificial means such as impact hammer or shakers. A condition of vibration is induced by suddenly dropping a load on the structure. By utilizing a known forcing function, many of the uncertainties in the data collection and processing can be avoided. The weight of the impact hammer can be adjusted to produce different force levels to the structure. These hammers can be hand held, suspended by chain, or dropped. The advantage of using impact hammers are that they are fast to use and the test can be repeated numerous times. On the other hand, linear variable mass shakers can be used for both vertical and horizontal excitation and can be used for various types of excitation. They can generate and maintain a steady state sinusoidal forcing, or other wave forms which may include combinations of steady state or transient waves. The disadvantage of artificial excitation in real structures is that it requires the temporary closing of the structure while tests are performed, this could be a serious problem for the infrastructures that are intensively used.

3.7.1.1.2 Ambient vibration excitation

In this method, the structure is excited naturally by the disturbances caused by wind, traffic, waves, seismic activity or tidal fluctuation as environmental excitation. It represents a real operating condition of the structure during its daily use. The advantage of using ambient excitation includes low cost, does not require temporary closing of the structure during testing, long term excitation, and in some cases the frequency content is appropriate for the structure. However, the disadvantage of using ambient excitation

includes the variability in amplitude, duration, direction, frequency content, and difficulty in accurately measuring excitation. Once the excitation source is collected, the data analysis is critical as noise in the data makes determination of the vibration characteristics more difficult. As a result, reliance must be placed on the measurement of vibrations induced by ambient excitation sources.

3.7.1.1.3 Free vibration

In the free vibration test, the structure is subjected to an initial condition of velocity or movement displacement**.** No external force acts on the system after release the structure to vibrate thus allowing it to vibrate freely and thereby enabling the recording of its resulting movement. Free vibration can be induced by impacting. In real structures, energy is lost as a result of friction or heat generation, resulting in the free vibration decay.

In the event of an initial condition of velocity applied to the structure, a compulsive force must be applied to the structure so that the time frame is shorter than that of the period of the system. In order to do so, several techniques are applied: strike the structure with heavy weights, produce small explosions, and launch rockets from the structure, among others. This type of dynamic testing has an advantage of being inexpensive since no equipment is needed to excite the structure.

In this research, type of excitation used is free vibration using impact hammer.

The response of the structure under these excitation forces is recorded using response transducers. This is described in the following sections.

3.7.2 The sensing mechanism

Sensing mechanism is basically constituted by sensing devices known as transducers. When a structure is excited, the transducers capture the physical motion of the structure and convert it to electrical signals. The electric signals generated are proportional to the physical parameter of measuring target. There is a large variety of such devices and the most commonly used in experimental modal analysis are the piezoelectric transducers

either for measuring force excitation (force transducers) or for measuring acceleration response (accelerometers). A typical example of an accelerometer is shown in Figure 3.7.

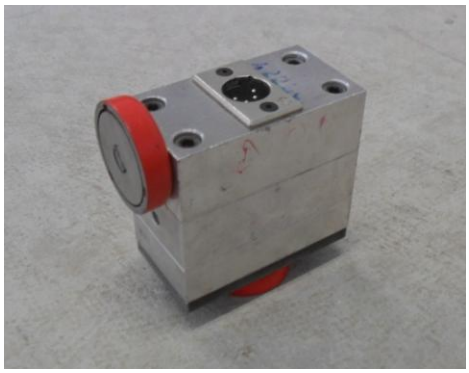

Figure 3.7: Accelerometer

Piezoelectric sensors are commonly comprised of materials such as quartz or ceramic. When a piezoelectric sensor experiences a change in load, such as compressive force, an electrical charge is generated; this is usually a function of frequency. Piezoelectric sensors can measure the generated charge by pre-loading the internal frictional forces. These types of sensors usually operate within a wide range of frequency. The electrical signals acquired by the transducers are analogue signals, which require conditioning and amplifying. A signal conditioner is used to condition the analogue signals from the transducers into voltage proportional to the measured physical quantities. Signal amplification increases the resolution of the input signal and increases its signal-to-noise ratio.

3.7.3 The data acquisition and processing mechanism

This mechanism measure the signals developed by the sensing mechanism and ascertain the magnitudes and phase of the excitation forces and responses. Analyzers are used to extract and derive the modal characteristics (i.e. natural frequencies, damping ratios and mode shapes) of structures. The most common analyzers are based on the Fast Fourier Transform (FFT) algorithm and provide direct measurement of the FRFs. They are

known as spectrum analyzers or FFT analyzers. There are two main subsets of analysis procedures developed, time-domain and frequency-domain methods. Time-domain methods produce modal characteristics directly from the response records in the time domain. Frequency-domain methods accomplish the same tasks by converting the response signals into the frequency domain.

Generally, MT and EMA can be divided into three major steps (Dackermann U, 2010): Signal processing, frequency response function (FRF) and modal parameter estimation. These are described in the next section.

3.8 Major Steps for MT & EMA

3.8.1 Signal processing

Signal processing deals with operations on or analysis of signals. In MT and EMA, the concern is the conversion of analogue signals into a corresponding sequence of digital values and the other concern is the transformation of the digital data from the time domain to the frequency domain by using the Discrete Fourier transform (DFT) algorithm.

Time-domain data is very difficult to interpret, which makes it necessary to work in the frequency-domain. The process of converting the analogue time-domain signal into a digital frequency-domain signal is carried out inside a spectrum analyzer, where the energy of a signal is separated into various frequency bands through a set of filters, and the method used is called Fourier transform. For the application of transient response prediction of structures, the Fourier transform is widely used. More specifically, a version known as the discrete Fourier transform (DFT) is often used, as this can very readily be implemented by using an efficient set of algorithms on computers, known as the ‘fast Fourier transform’ (FFT).

As the Fourier transform algorithm involves discrete data over a limited time period, digital signal processing errors such as aliasing and leakage may be introduced. Further,

noise interference due to electrical noise on the transducer signals (e.g. power supply noise, calibration motion, rattles) may also create errors.

Aliasing is a phenomenon that occurs when the sampling rate is less than twice the highest frequency in the data. It is a result of the inability of the Fourier transform to decide which frequencies are within and which ones are outside the analysis band. Aliasing produces a distorted representation of data, which could result in significant erroneous frequency interpretation in the vibration analysis. Aliasing also occurs when converting analogue (continuous) data to digital (discrete) data. Aliasing example is shown in Figure 3.8.

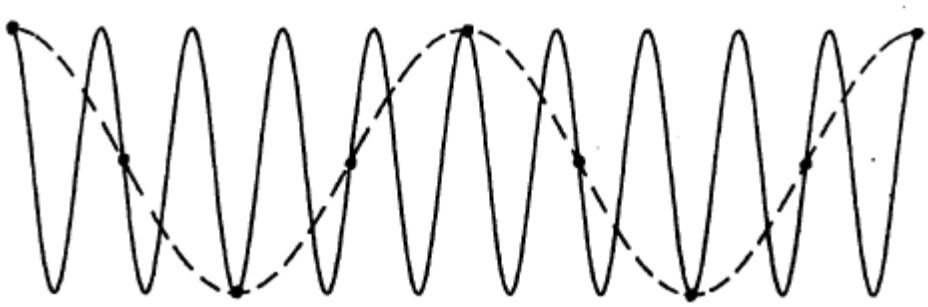

Figure 3.8: Aliasing example (Allemang, 1999)

Aliasing can be minimized by using a sampling rate of at least twice the highest frequency present in the data, which is formulated by Shannon's sampling Theorem:

$$F_{Samp} = \frac{1}{\Delta t} = F_{Nq}\text{x } 2\ ; \tag{3.8a}$$

$$F_{Nyq} =\geq F_{Max} \tag{3.8b}$$

The Nyquist frequency (F_{Nyq}) is the theoretical limit for the maximum frequency (F_{max}). Signals above F_{Nyq} will appear after being digitized as a frequency below F_{Nyq}. This serious error is controlled by using anti-aliasing or analogue filters, this filters

automatically cut-off frequencies at or above half the sampling frequency F_{Samp}. Filters that are used include low pass, high pass, broadband, narrow band and notch filter.

A Signal analyzer or analogue – to – digital converter, on the other hand, measure specific parameters of interest i.e. force and response levels. These analyzers mainly convert the analogue input signal to digital signal to produce strings of discrete values. The acquired continuous signal is first sampled and then converted into a discrete-time series digital signal. The time interval between two samples is equal to the inverse of the sampling frequency. The resolution of digital signal samples is equal to 2^B, where B is the number of bits used in signal analyzer. For example, a 16-bit signal analyzer will discretise the amplitude range of the signal to a resolution of 65536 grids. Two types of analyzers that are commonly used include Frequency Response Analyzers (FRA) and Spectrum Analyzers (SA). The main difference between the FRA and the SA is that the SA simultaneously measures all the frequency components in the time signal whereas the FRA extracts a single frequency at a time. Analyzers estimate the Fourier Transforms (FT) or Spectral Densities (SD) of signals which are supplied as inputs for analysis. (Ewins, 2000).

After the digitizing process, the continuous time signals are discretised into a sequence of values commonly known as discrete time series. A discrete time series has values that are defined only at discrete values time. Discrete time signals, also known as signals in the time domain, usually consist of many frequency components that are superimposed. The conversion of a time signal into its various frequency components is, for example, performed by Fast Fourier Transform (FFT). The FFT algorithm is given as:

$$x(k) = \sum_{j=0}^{N-1} X(j) W_N^{-jk} \tag{3.8c}$$

Which represents the discrete series $x(k)$ at the time instant k of a sampled data N, with k=0,1,2,…., N-1 and j=0,1,2….,N-1 where $W_N^{-i2\pi N}$.

During the process of FFT, some problems may occur, one problem with the analysis of vibration data is that the signal is assumed to be periodic over the sampling interval

chosen. In general, this will not be true and leads to a problem known "Leakage". Leakage is the unwanted distortion caused by artificial truncation of sampled data (Maia *et al.* 1997). A common tool used to overcome the leakage problem is windowing. This function consists of a process of 'weighting' the original time history data to reduce the noise distortion and the effect of leakage.

Some of the developed window function includes uniform or rectangular, flat top, hanning, force and exponential windows. The force and exponential windows are typically used when performing impact excitation for acquiring FRFs. A Force window is usually applied to the impact excitation to remove noise from the impulse signal. Ideally, the impulse signal is non-zero for the small time period of the excitation (e.g. hammer hit) and zero for remaining time. Therefore, any non-zero data following the impulse signal is assumed to be noise and thus is considered to be zero. Exponential windows are commonly used for response signals, to ensure that the transient signal decay sufficiently at the end of the sampling period. This decay is employed by introducing artificial damping into the measurement data (Schwarz & Richardson, 1999).

3.8.2 Frequency response function

The frequency response function (FRF) is the most important measurement that is needed for experimental modal analysis. The FRF describes the input-output relationship between two points on a structure as a function of frequency. That is, the FRF is a measure of how much displacement, velocity, or acceleration response a structure has at an output point per unit of excitation force at an input point. The general procedure for utilizing FRFs for system identification is shown in Figure 3.9.

To obtain FRF data, transducers (e.g. accelerometers) record an electric output signal from the test structure, while the input signal is obtained from the source of excitation. For example, when the impulse force $F(\omega)$ with respect to frequency (ω) and the resulting output signal (or response motion) $X(\omega)$ of the vibration system are measured using accelerometers attached to the system, the resulting data are used to generate the FRF $H(\omega)$ for the system using equation 3.1*d* and 3.1*e* (Maia and Silva 1997).

$$X(\omega) = H(\omega)F(\omega) \quad or \quad H(\omega) = \frac{X(\omega)}{F(\omega)} \tag{3.8d}$$

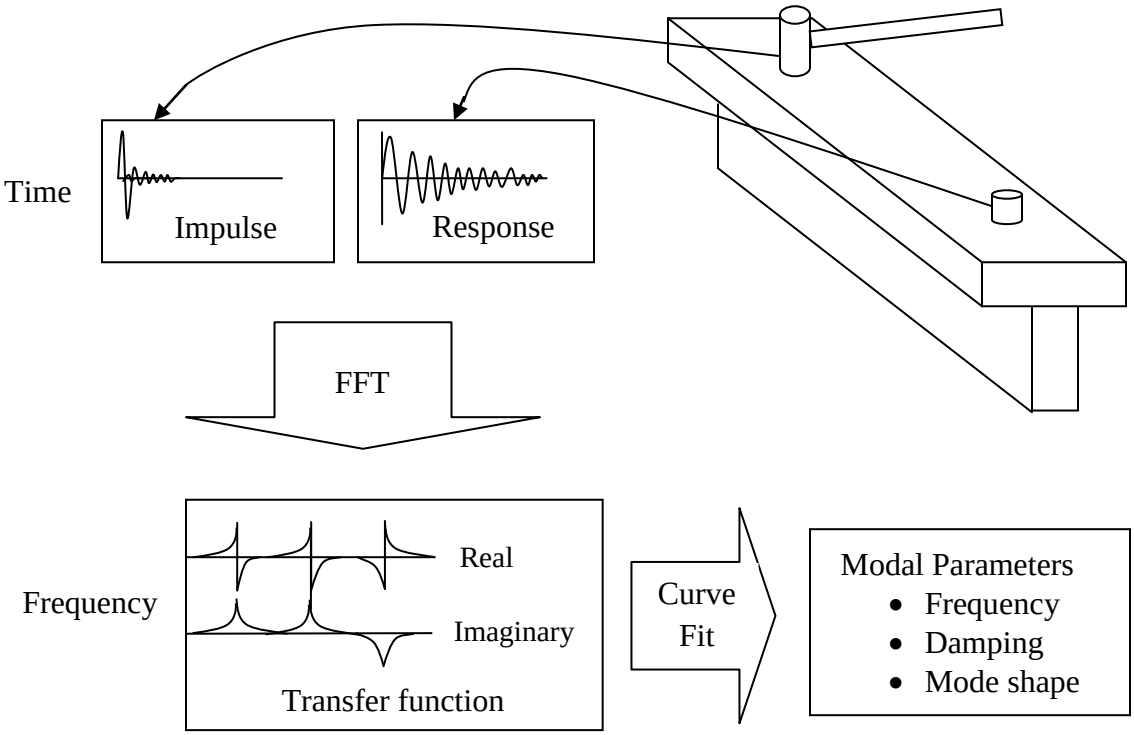

Figure 3.9: Transfer function method (Schwarz & Richardson; 1999)

FRF can be presented in rectangular coordinates (real part vs. frequency, and imaginary part vs. frequency) or in polar coordinates (amplitude or magnitude vs. frequency, and phase vs. frequency). At resonance, in the polar system, the magnitude reaches a maximum at resonance, while the phase lag approaches 90° (Figure 3.10). In rectangular presentation, the imaginary part is a maximum and the real part is zero. This is shown for a single-degree-of-freedom (SDOF) system in Figure 3.11. These characteristics enable the identification of the modal parameters of a structure from the FRF.

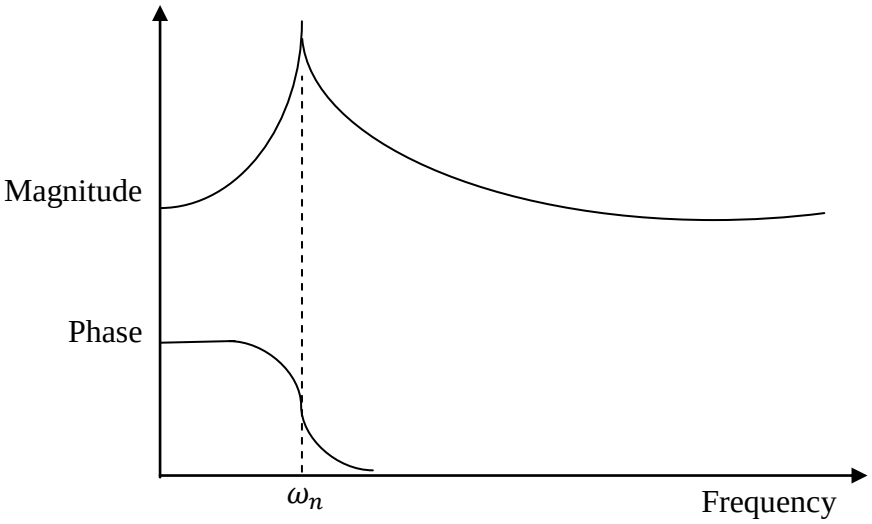

Figure 3.10: FRF graph in polar coordinate for SDOF

.

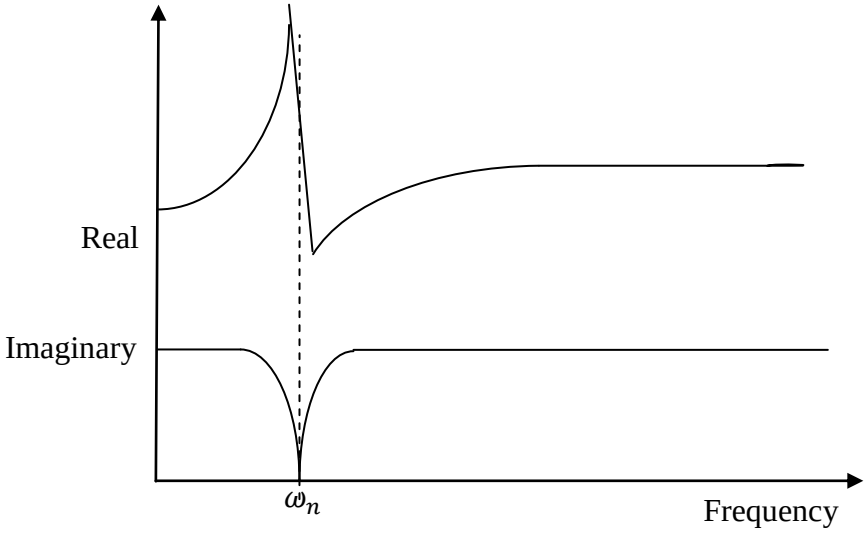

Figure 3.11: FRF graph in rectangular for SDOF

3.8.3 Modal parameter extraction

Modal extraction is a process of extracting modal parameters of the structure from the response data. These parameters can be extracted from time domain or measured FRFs. Before these methods are described, the next section deals with preliminary checks that

need to be done on FRF so as to check validity of the measured data and therefore the accuracy of modal parameters of the structure.

3.8.3.1 Preliminary checks on FRF data

The response data is usually affected by noise, resistance of lead wires and their capacitance. For this reason, preliminary checks are necessary to avoid analyzing poor data resulting in incorrect modal parameters. The following checks are done on measured FRF (Ewins, 2000).

i) Low frequency asymptotes
ii) Anti-resonances
iii) High frequency asymptotes
iv) Shape of FRF skeleton
v) Nyquist plot

The characteristic of FRF's at low frequencies i.e. below the first resonance indicates the degree of reliability of the data. This is the region that gives the behavior of the support conditions of the test. For grounded system, stiffness characteristics that appear as an asymptotic to the stiffness line at the lowest frequency is expected (Ewins, 2000). The magnitude of this stiffness should be equal to the static stiffness at that point.

The incidence of anti-resonances also indicates the quality of the measured data. Anti-resonances are expected to occur between two adjacent resonances, instead of minima for a point FRF. Conversely, for a transfer FRF's between two points separated on the structure, a minima is expected (Ewins, 2000). The anti-resonance troughs for point FRF should have the same sharpness as the resonance peaks. These problems are chiefly due to inadequate vibration or limitation of the spectrum analyzer resolution.

A check on the upper end frequency range that reveals an asymptotic curve to mass or stiffness line of mobility measurements indicates a high probability of unreliable data (Ewins, 2000). The author suggests that this reflects a situation where the excitation is applied at a point of very high mass or flexibility. Such a tendency results in considerable difficulties for modal analysis process. This problem may be minimized using different excitation points.

The shape of FRF's is also used for checking reliability of measured data. In this case, relative positions of resonances, anti-resonances and the ambient levels of FRF curve are used to check validity of measured data. A mass and stiffness lines through the FRF curve should pass through the middle of the FRF plot for consistence resonance and anti-resonances frequencies.

If all checks on measured FRFs are satisfied, modal parameters of the system can be extracted, otherwise re-testing will be necessary.

3.8.3.2 Modal extraction methods

The modal parameters i.e. natural frequency, damping and mode shapes can be estimated through three different approaches illustrated in Figure 3.12. In analytical system, the modal parameters are determined from the system matrices by formulating the eigensolution of the system. In experimental modal analysis (EMA), the modal parameters are extracted either from the FRF in the frequency domain, or from the impulse response function (IRF) in the time domain.

In EMA, the modal parameters are mainly estimated in the frequency domain by means of FRFs and curve fitting techniques. Generally, curve fitting is a process of matching mathematical model to a set of experimentally measured data points; this is done by minimizing the squared error or squared difference between the analytical function and the measured input-output data.

The time domain methods are suitable for large frequency range, whereas the frequency techniques give the best results for limited frequency range where the number of modes is relatively few (Maia, *et al.*, 1998). The time-domain based methods are further split into direct and indirect techniques. The indirect methods means that the identification of FRFs is based on modal parameters (i.e. natural frequency, damping ratios and modal constants) where the direct techniques refer to the identification based on the general matrix equation of dynamic equilibrium (Maia, *et al.*, 1997).

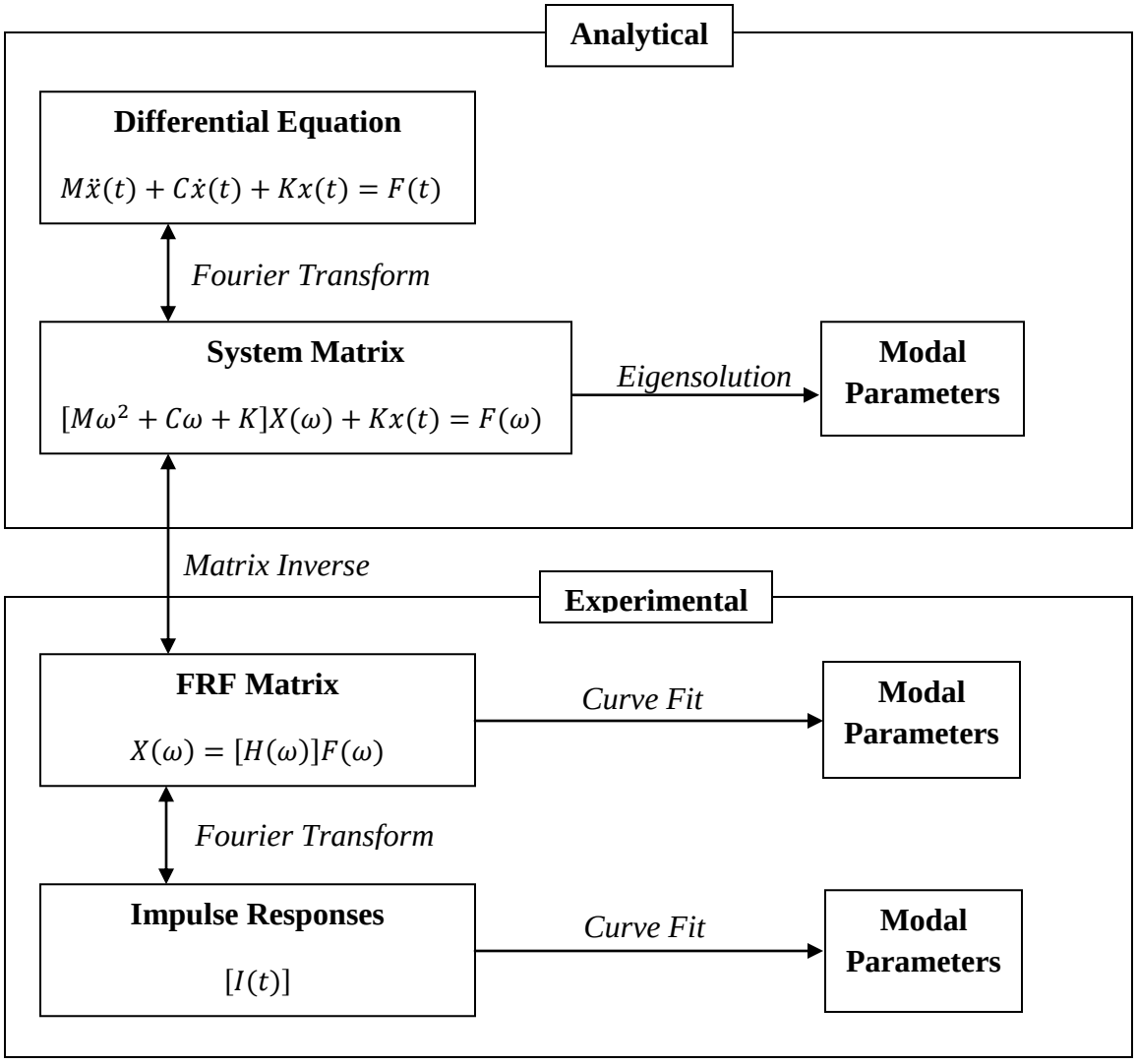

Figure 3.12: Modal parameters extraction methods (Schwarz & Richardson, 1999)

Both time and frequency techniques are further classified into Single-Input-Single-Output based (SISO), Single-Input-Multiple-Output methods (SIMO) and Multiple-Input-Multiple-Output (MIMO) methods. The Single-Input-Single-Output (SISO) methods use a single FRF at a time from a single excitation point to compute modal parameters. On the other hand, Single-Input-Multiple-Output (SIMO) methods analyze multiple FRFs simultaneously with responses taken from different positions but using one excitation point. The Multiple-Input-Multiple-Output (MIMO) processes all the available FRFs from multiple excitation points.

These methods are well described in Ewins, 2000 and Maia, *et al.*, 1997. Next bullet Rational Fractional Polynomial method (RFP) is presented which is mostly used by many commercial packages of modal analysis software.

3.8.3.3 Rational Fractional Polynomial method (RFP)

The RFP method is a curve fitting technique and widely used MDOF frequency domain method. Curve fitting is a process of matching a parametric model of an FRF to experimental data. The unknown parameters of the model are the natural frequencies, damping ratios and residues for each mode. Using the RFP method, the formulation of the FRF is expressed in rational fractional form and the error function to be minimized is established in such a way that the system of equations is linear, without requiring initial estimates for the modal parameters (Maia, *et al.*, 1997).

In this method, the FRF is expressed in terms of ratio of two polynomials (in place of the summation of simple fractions) as:

$$H(\omega) = \frac{\sum_{k=0}^{2N-1} a_k (i\omega)^k}{\sum_{k=0}^{2N} b_k (i\omega)^k} \qquad (3.8e)$$

Defining a linearized error function between the measured FRF values and the model, and minimizing it, a linear system of equations is obtained, from which the coefficients a_k and b_k are evaluated. As such a system is usually ill-conditioned; the problem is reformulated in terms of orthogonal polynomials. Knowing the resulting coefficients, the modal parameters are retrieved. In checking the quality of the extracted parameters in this method it is usual to make calculations taking each time a different set of data points and checking for the repeatability and variation of the results (Maia, *et al.*, 1997).

3.9 Validation of measurements

Throughout the complete modal test, checks should be made to assess the quality of the measured data. There are several techniques in general that can be used to provide an indication of the quality of the measured data, e.g. repeatability, reciprocity, and coherence (Silva, 2001).

Almost always, repeatability and reciprocity checks are done by comparing sets of FRF curves to see if there are any major differences. The comparisons are made significantly easier if difference function curves are plotted for the sets of data.

Repeatability checks are performed by repeating some measurements and comparing the results with previously measured curves. These checks assess the stability of the structural characteristics over a period of time. It is usually assumed that a structure does not change with time or as a result of the excitation itself but there are a number of practical effects, such as bolt slackening, fretting, change of temperature and humidity, etc., that can alter the characteristics of a structure.

Reciprocity checks are based on Maxwell's rule of reciprocity. The FRF matrix is symmetric and this property can be used as a check on the quality of the measured data. In fact, for a linear conservative system, the FRF measured for a force at location *j* and a response at location *i* should correspond directly to the FRF measured for a force at location *i* and response at location *j*.

Almost all spectrum analyzers incorporate the calculation of the coherence, which is nothing but a correlation coefficient that measures the degree of consistency of all averages of the FRF evaluated by the analyzer. A coherent equal to 1 indicates that each average is exactly the same. Low coherence value indicate a significant variance on the averages and, therefore, poor data quality. Usually, low-frequency regions and regions close to resonances and ant-resonances yield low coherence values. The reason for this is poor performance of many transducers at low frequencies and low signal-to-noise ratios close to resonances and ant-resonances.

3.10 Summary

MT and EMA serves as a tool to extract the dynamic properties of a given structure. The aim of this chapter is to review the basics of structural dynamics and understand procedures for MT and EMA. The testing equipments used in modal testing, type of excitations and necessary checks on measured FRFs to ensure the reliability of measurements are reviewed.

CHAPTER 4

METHODOLOGY

4.1 Introduction

For the last few decades, dynamics-based techniques became promising tools in assessing and detecting damage in structures where prior knowledge of the damaged location is lacking. Researchers like Sibanda, *et al.*, 2008; Yong, *et al.*, 2006; Farrar & Jauregui, 1995 and others investigated how these techniques can be used to detect and locate damages in concrete composite bridges. Both positive and negative results were observed using these techniques. However, to date, these techniques have not been used for detecting and locating damage on concrete composite bridges based on vibration data measured on top of the accessible deck slab.

The main objective of this research is to investigate the effectiveness of dynamics-based techniques in assessing the condition of shear connectors in concrete composite bridges consisting of pre-cast prestressed beams and a cast *in-situ* deck slab based on measurements taken from the surface of the deck slab. The work consists of experimental study which involved building five concrete composite beam models each with different number of shear connectors and hence spacing between shear connectors. Number of the shear connectors range from spacing that provides nearly full composite action of the composite beam to different four other cases of spacing that provides partial composite action of the concrete composite beam. Then artificial damage (i.e. corrosion) was introduced to a group of shear connectors in each model. It was decided to introduce damage by corrosion because it was the easiest way of damaging the shear connectors without damaging the concrete. Dynamic testing was then conducted for each model in an attempt to detect the degree of composite action between prestressed concrete beam and slab in both undamaged and damaged case. In addition push-off test was conducted in order to determine the capacity of the shear connectors or load slip behavior of the shear connectors in undamaged and damaged state.

4.2 Research approach

The research was conducted using experimental study. It involved model construction, experimental testing to detect the degree of composite action between the prestressed beam and slab (Figure 4.2) and application of damage identification methods to detect artificial damage on a concrete composite beam models. The experimental work involved building five concrete composite beam models each with different number of shear connectors ranging from number of shear connectors which provide nearly full composite action (CASE A) to other four case which provide partial composite action (CASE B1 to B4). The number of shear connectors obtained in the design for full composite action (CASE A) was 21 spaced at 92mm apart. For partial composite action, the number of shear connectors was 17 spaced at 115mm (CASE B4), 13 spaced at 155mm (CASE B3), 9 spaced at 230mm (CASE B2) and 7 spaced at 310mm (CASE B1). The flow-chart Figure 4.1 describes in detail the approach and scope of the work that was carried out in this investigation.

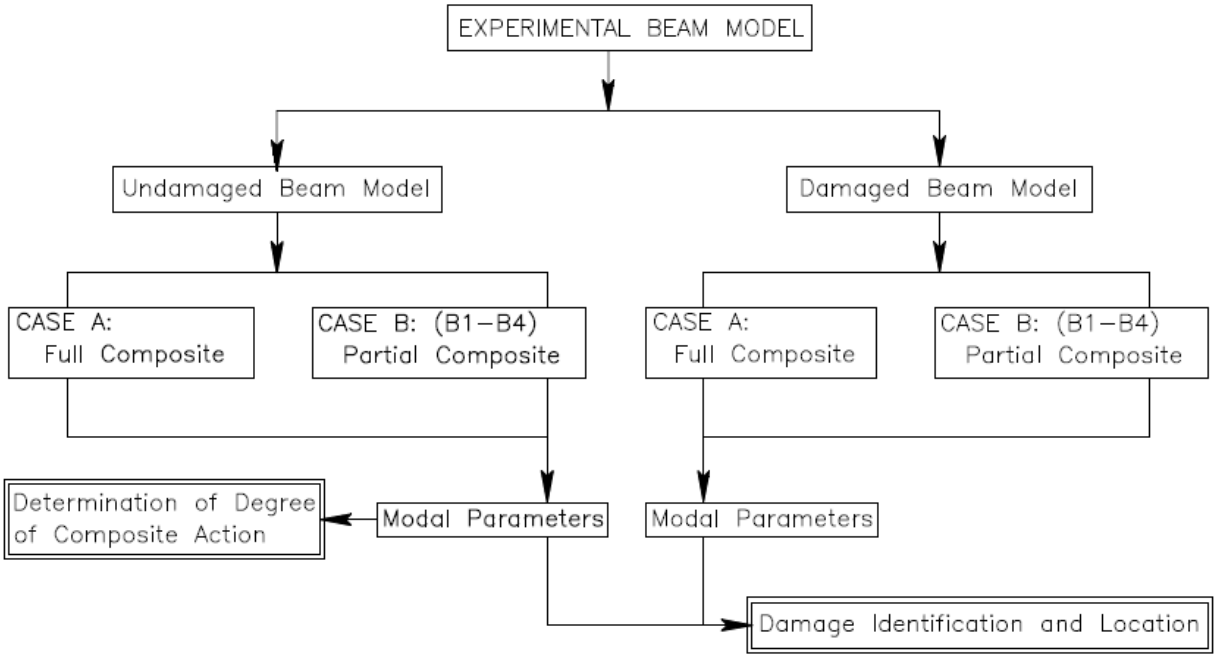

Figure 4.1: Research flow chart

4.3 Model construction

The objective of the research is to investigate the effectiveness of dynamics-based techniques in assessing the condition of shear connectors. To avoid use of complex moulds, a model of concrete composite beam consisting of rectangular beam (stimulating precast pre-stressed beams) and a concrete flange (stimulating a cast *in-situ* slab) was constructed for the research.

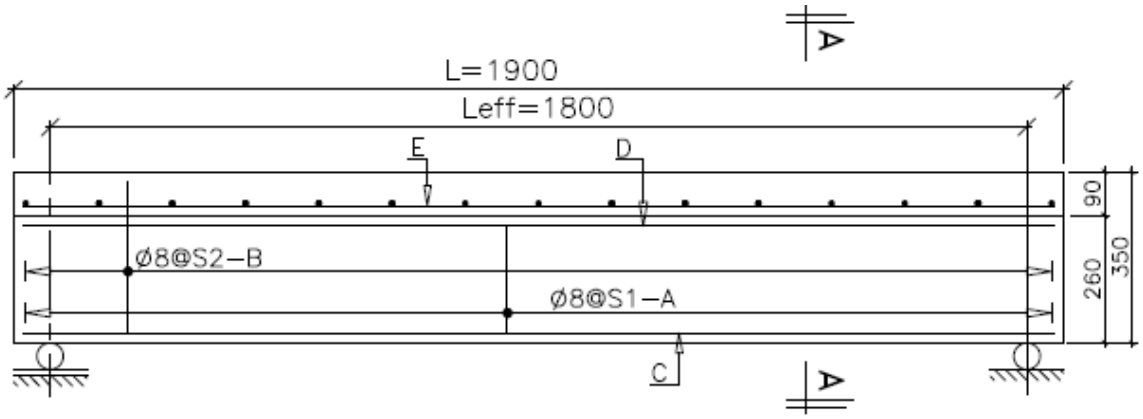

4.2(a): Longitudinal section of the beam

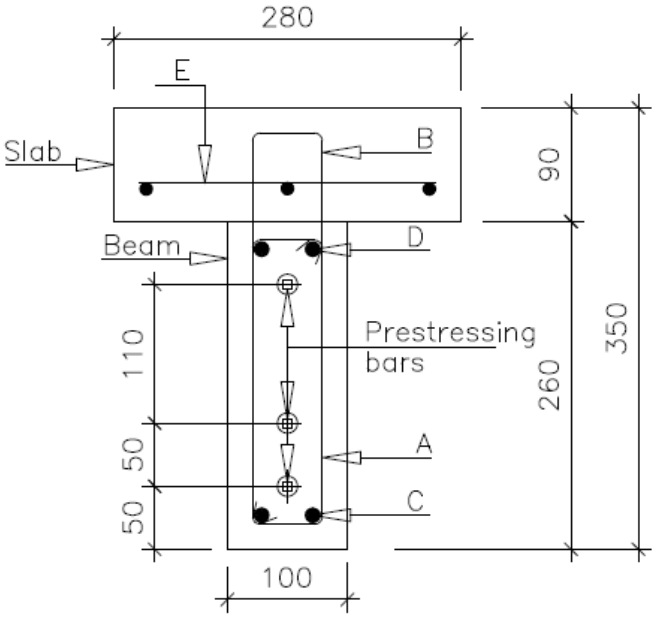

4.2(b): Section A-A

Figure 4.2: Experimental beam - reinforcement detail

Figure 4.2 shows a connection details between beam and slab that was used in each experimental model. Shear links of 8mm bars ‘A’ for vertical shear resistance of the beam, Shear links of 8mm bars ‘B’ extended from beam to the slab to stimulate shear connectors in real bridges. 10mm diameter bars ‘C’ and ‘D’ as beam reinforcements and a mesh of 10mm diameter ‘E’ as slab reinforcement. The anchors were placed such that the composite action in the model is similar to that in real bridges

In prototype bridges, diaphragms are cast across girders on piers and also between supports. The reinforcement for diaphragms passes through holes provided in the web of the girders for monolithic construction. This diaphragms help to distribute the loads and also act as a bracers in transverse direction (Nigel, 2003). In this research, no transverse stability that was provided to beams hence only flexural modes of vibration were considered.

4.4 Concrete strength and material used

In prototype bridges, the beams are made stronger than the deck slab because they support imposed load and weight of the slab in addition to their self weight. In this research the target concrete compressive strength for the slab was 30MPa and that of the beams was 50MPa. The concrete cover used is 20mm. The mix design consists of 0.45 water to binder ratio for the beam and 0.7 water to binder ratio for the slab. 19mm Greywacke stones and Klipheuwel sand were used for both beam and slab. Beams were pres-stressed using 7mm diameter prestressing bars with a braking load of 64.3kN.

4.5 Construction process for experimental composite beams

Firstly, the tendons were positioned as shown in Figure 4.2b and then tensioned to sixty percent of the braking load and held between anchorages as shown on Figure 4.3(a and b). The force and location of the prestressing bars were designed such that when there is no load the entire web section is under compression. That is, the tension produced in the bottom fibers of the web under self weight is not enough to cancel out the compression. The beams were then cast with shear connectors extended above the beam surface as shown in Figure 4.3(c). Anchorages were released when concrete has hardened to enough

strength in three days so that the prestress force is transferred to the concrete through bond. To help acceleration of corrosion on some shear connectors, wires were connected to shear connectors before cast of slab, other reinforcement were insulated at the joints where they meet with the shear connectors. A mesh of 10mm reinforcement bars were used for the slabs as shown in Figure 4.3(d) then the slabs were cast to form a T- beam as shown in Figure 4.3(e). Figure 4.3(f) shows striping of the beam using a small crane. The complete models are shown in Figure 4.3(g and h).

4.3(a)

4.3(b)

4.3(c)

4.3(d)

4.3(e)

4.3(f)

4.3(g)

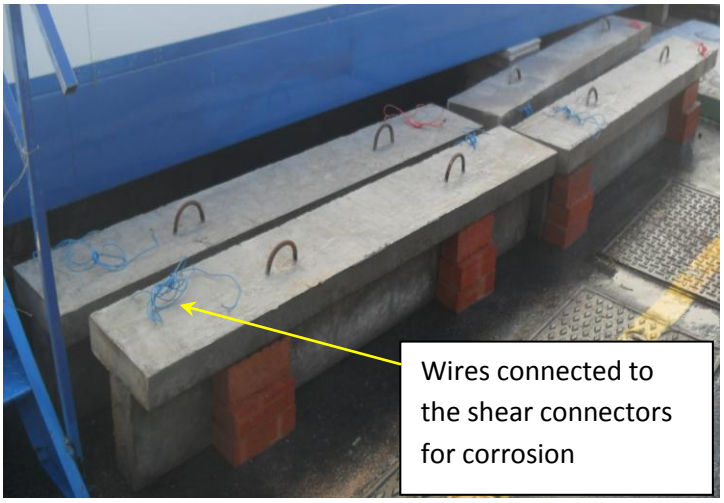

4.3(h)

Figure 4.3: Construction process for beams

4.6 Push-off test

In concrete composite bridges, the purpose of the shear connectors is to transmit the horizontal shear between beams and slab; to successfully do this, they must be strong enough to resist both horizontal and vertical forces. In this research, it was decided to conduct push-off test in order to determine the shear capacity of the shear connectors in both undamaged and damaged state. The specimen used to apply shear stresses to the connection is shown in Figure 4.4 and 4.5. It composes of a central piece (simulating the precast beam) and two lateral pieces (simulating the cast *in-situ* slab). The connector

consisted of a steel bar bent in a hoop shape and placed in precast beam during its molding. The bond at slab/beam interface was prevented by greasing the precast beam before casting of slab.

The dimensions of the specimens used in these tests are also shown in Figure 4.4. These dimensions were chosen taking into account both the recommendations given in BS 5400 part 5 (1979) and the dimensions of the concrete composite beam used for dynamic test.

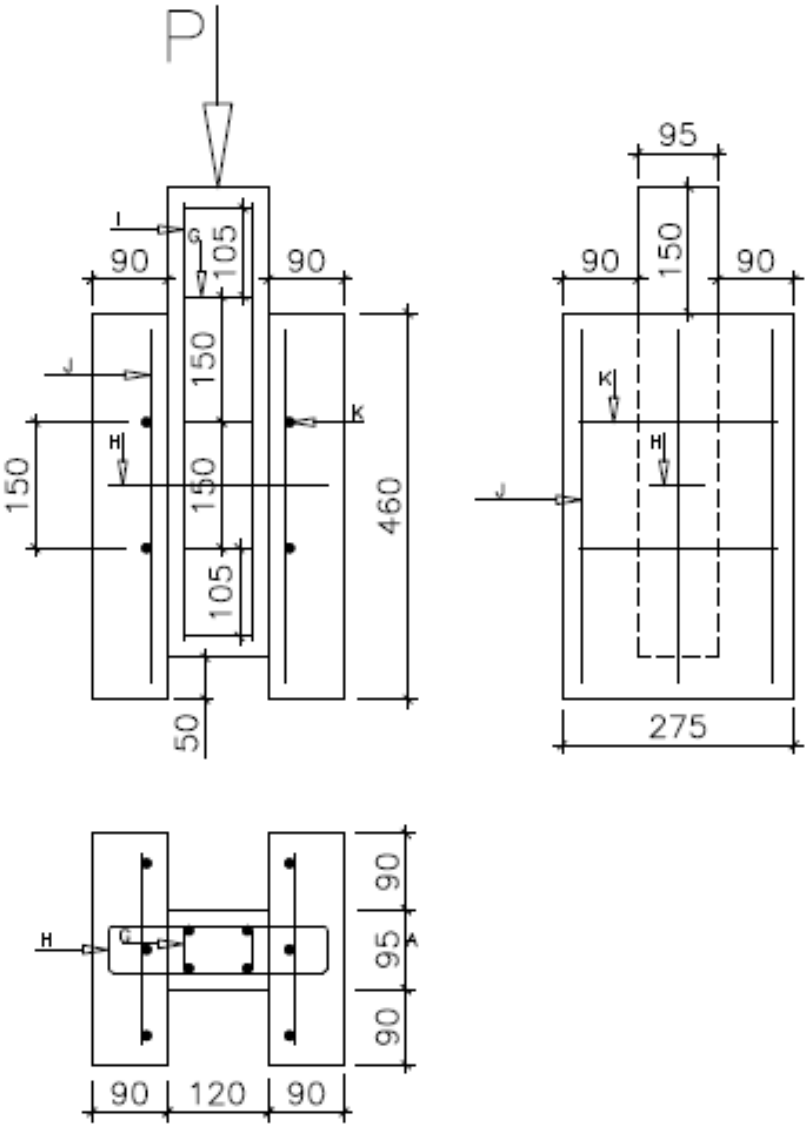

Figure 4.4: Specimen for push-off test (RC detail)

4.5(a) 4.5(b)

Figure 4.5: Specimen for push-off test

4.7 Damaging of shear connectors

The testing procedure consisted of measuring the dynamic properties in both the undamaged and damaged model. Damage was introduced by accelerating corrosion to a group of shear connectors near the supports in each composite beam model. The specimens were damaged by accelerating corrosion to 15% mass loss of the shear connectors using Faraday's formula, equation (4.1). Dynamic test was then repeated for each beam to detect the artificial damage of shear connectors by investigating changes of the dynamic properties such as frequencies, mode shapes, damping ratios and frequency response functions.

The location 'near the supports' was chosen because shear connectors in these locations are vulnerable to corrosion in real bridges. In this research near the supports means 25% of the whole distance of the beam from the supports, all shear connectors in this distance from each support were damaged in each beam. Number of shear connectors damaged depended on the number and spacing of shear connectors in the beam. A total of 12 shear connectors were damaged in beam 'A', 8 in beam 'B4', 6 in beam 'B3' and 4 in beam 'B2' and 'B1'.

Corrosion of steel in concrete is a slow process. Due to the protective nature of concrete, it takes a reasonably long time for initiation and progress of reinforcement corrosion even in the case of severe corrosive exposure conditions. It is difficult to achieve a significant degree of reinforcement corrosion in a limited duration available for performing research studies. For this reason, various techniques for inducing accelerated corrosion of steel in concrete are used by the researchers. In this research the impressed current technique also called galvanostatic method was used to accelerate corrosion on shear connectors. This method consists of applying a constant current from a DC source to the steel embedded in concrete to induce significant corrosion in a short period of time. The degree of induced corrosion or the percentage of actual amount of steel lost in corrosion can be determined theoretically using Faraday's law. Using the actual amount of steel to be lost in corrosion, an equivalent corrosion current density to be used can be determined.

Set-ups used for inducing reinforcement corrosion through impressed current consist of a DC power source, a counter electrode and an electrolyte. The positive terminal of the DC power source is connected to the steel bars (anode) and the negative terminal is connected to the counter electrode (cathode). The current is impressed from counter electrode to the reinforcement bars through concrete with the help of the electrolyte (sodium chloride solution). Figure 4.6 and 4.7 shows the set up used to accelerate corrosion on shear connectors in experimental composite beams and push-off test specimens respectively.

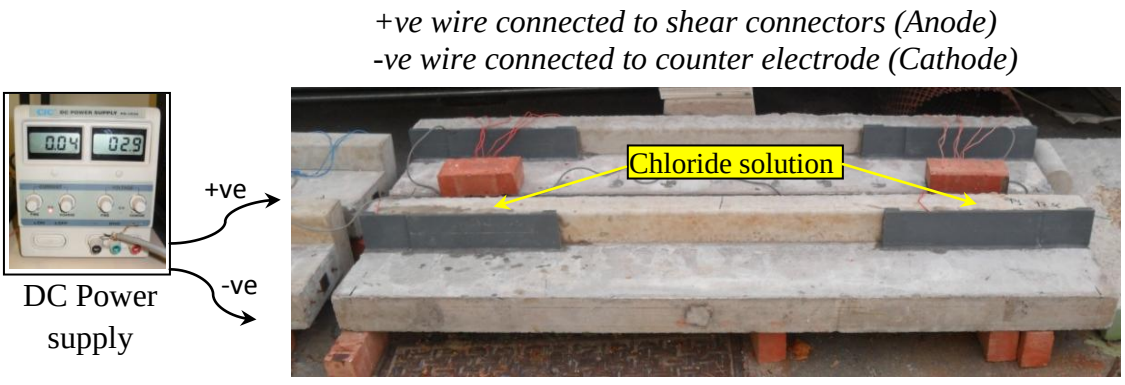

Figure 4.6: Set up for accelerating corrosion on shear connectors in composite beams

+ve wire connected to shear connectors (Anode)
-ve wire connected to counter electrode (Cathode)

Figure 4.7: Set up for accelerating corrosion on shear connectors in push-off specimens

The mass of rust produced per unit surface area of the bar due to applied current over a given time was determined theoretically using the following expression based on Faraday's law.

$$m_{th} = \frac{W \cdot I_{app} \cdot t}{F} \tag{4.1}$$

Where m_{th}= Theoretical mass of rust per unit surface area of the bar (g/cm^2);

W = equivalent weight of steel which is taken as the ratio of atomic weight of Iron to the valency of iron (27.925g).

I_{app} = Applied current density (Amp/cm^2);

t = Duration of induced corrosion (sec) and

F = Faraday's constant (96487 Amp-sec).

4.8 Experimental testing

As discussed in section 2.5, when the slab is cast over the precast beams, a natural bond develops at the interface. In real bridges this effect may be destroyed by the effect of shrinkage, stresses due to variations of temperature or vehicle loadings as the vehicle pass over the bridge; the shear connectors come to effect to transfer effectively the longitudinal shear from the slab concrete to the precast beam member when this bond is destroyed. To stimulate this in the laboratory before conducting modal testing, each experimental composite beam was loaded three times to 30kN so as to destroy the natural bond and making them active for dynamic testing.

Modal testing was performed on each model using dynamic testing equipments which includes the hammer, accelerometers, charge amplifier and data acquisition system. All these instruments were carefully inspected and calibrated to ensure that they work effectively as intended. A hammer for providing a source of excitation to the test specimens and the responses of the beams were measured by accelerometers. In EMA, the converted signals from the accelerometers were analyzed and the modal parameters of the beams were determined. Each of the five beams was tested in its undamaged and damaged state. The set up of the test is shown in Figure 4.8.

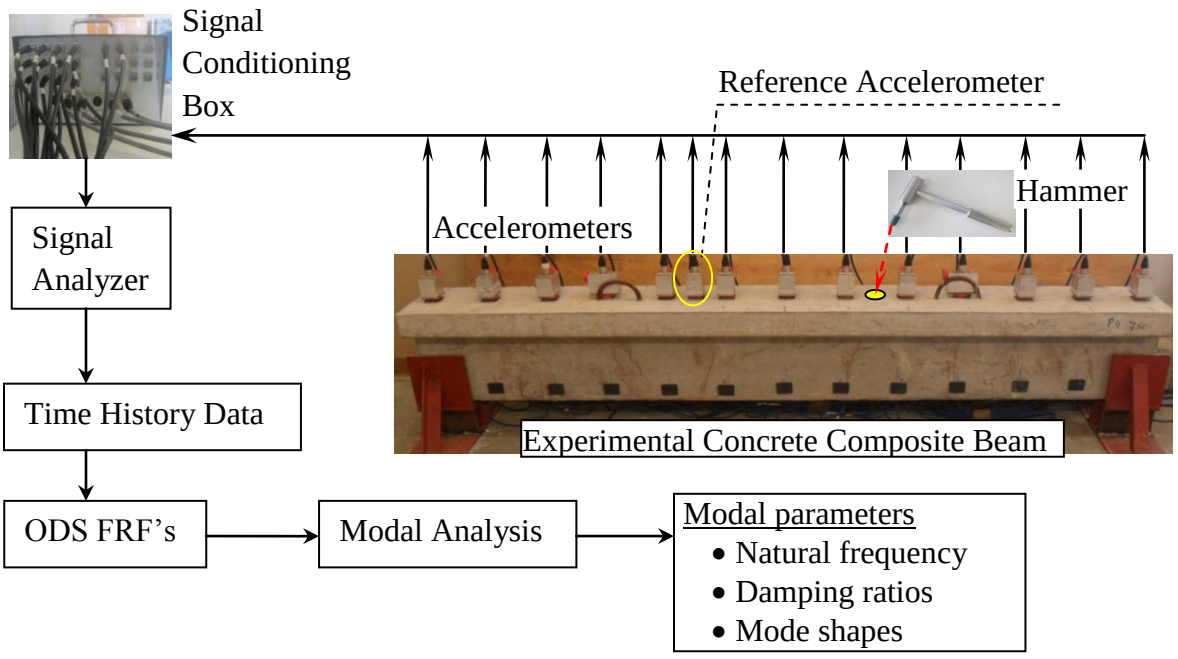

Figure 4.8: Schematic diagram for the experimental dynamic test

The position of the excitation force is of importance in dynamic testing. The optimum location of an exciter should be such that all modes of interest are excited. The beams were first excited at a certain reference point situated at location 'C' (Figure 4.9) which is at 3/8 of the total distance (1.8m) between the supports. This position was chosen based on the reasons that none of the first seven flexural mode shapes has a node point at at this location on fact that if a node point of a mode is located at the reference point then this mode is not excited and hence cannot be identified and also this location is further away

from the supports and hence provide better excitation and less interference from the supports. The impact hammer that was first used to excite the beams was a Dytran Model 5803A (5.4Kg), which is shown in Figure 3.5. With this hammer it was only possible to get frequency up to 500Hz. It was then decided to excite a beam using a small hammer without measuring force and use one accelerometer as reference paced at the same location 'C' as shown in Figure 4.9. With this set up it was possible to get frequency up to 1500Hz. The mode shapes of the first seven flexural modes and their node points along the beam are illustrated in Figure 4.9.

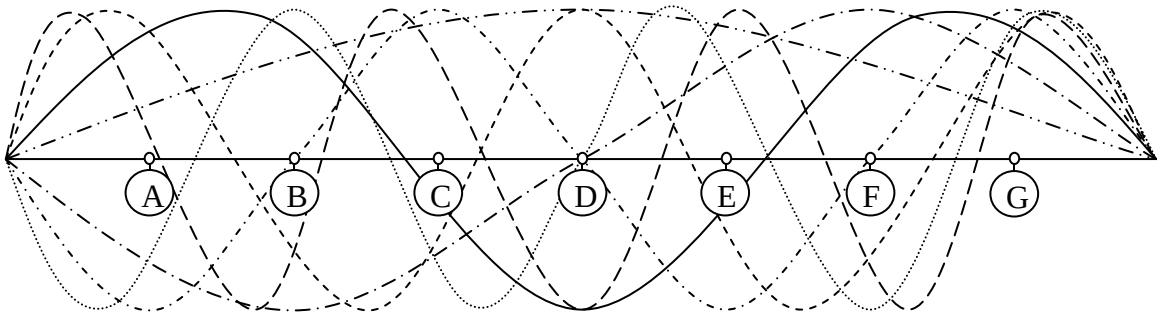

–·· Mode 1; –·– Mode 2; —— Mode 3; –·– Mode 4; - - - - Mode 5; ····· Mode 6; – – Mode 7.

Figure 4.9: First seven bending mode shapes of a simply supported beam

The responses were measured by thirteen equally spaced force balanced accelerometers mounted on the top surface of the composite beam as shown in Figure 4.6. Forced balanced accelerometers (QA 700) shown in Figure 3.7 with sensivity betweeen 3.4V/g and 3.5V/g were used to measure response of the structure**.** Each accelerometer was attached onto a small piece of steel plate and glued to the top of the concrete beam to provide firm and solid contact between accelerometers and the specimens. The dimensions of the small square steel plate were 40 mm × 40 mm × 1 mm. The accelerometers were located at each end of the composite beam in line with the supports and at the locations spaced 150mm from one another as shown in Figure 4.8. The time history signals of the accelerometers were amplified and conditioned by signal conditioner.

LabVIEW SignalExpress software from NATIONAL INSTRUMENT was used for acquiring data from two data acquisition devices each with 8 channels installed in a computer. The data obtained were imported into ME'scopeVES (Visual Engineering Serees) software from VIBRANT TECHNOLOGY for experimental modal analysis. In ME'scopeVES, the modal analysis is performed using transfer functions which have been recorded with the signal analysis.

For each test, the sampling rate was set to 5,000Hz with 65,536 time domain data points being recorded. In the frequency domain, this corresponds to a frequency range of 2,500Hz with 32,768 FRF data points, thus giving a frequency resolution of 0.0763Hz per data point. To reduce interference of noise , averaging of three excitation per test was employed. To further improve the quality of the time history measurements, the following signal processsing techniques were applied: a pre-trigger delay was used to ensure that the entire impact excitation signal was captured and a rectangular window was applied for the response channel (accelerometer measurements) to ensure that the transient signals showed sufficient decay at the end of the sampling period.

The acquired response time history signals (amplitude versus time) were then converted into frequency spectra (amplitude versus frequency) using the Fourier transform as described in section 3.8.2. Since no forces were measured, a different set of measurements called operating deflecting shapes (ODS) FRFs were calculated in this case. The ODS FRF is a complex valued frequency domain function like an FRF, but it is calculated differently (Schwarz and Richardson, 2001). *An ODS FRF is formed by combining the auto power spectra (APS) of a roving response with the phase of the cross power spectra (XPS) between the roving response and a reference response.* The XPS contains the relative phase between two responses, and the APS of each response contains the correct magnitude of the response. More importantly, an ODS FRF has *peaks at resonances*, so it is easier to display ODS's from a set of ODS FRFs and observe mode shapes at resonant frequencies. For each undamaged and damaged state of the beam, averaged ODS FRFs from three different hammer hit were recorded for each beam in undamaged and damaged case and repeated five to ten times to check the repeatability

of the results. Thereby an average of five measurements test were obtained from each composite beam and a total of 30 measurements from the entire dynamic test series.

With frequency response function (FRF) being computed, modal parameter estimation technique was then performed to estimate the modal parameters. The modal parameter estimation is often referred to as curve fitting and was carried out using commercial software ME'scopeVES.

4.9 Summary

This chapter presented the methodology used in this research. Firstly, the details of five reinforced concrete composite beams cast in the laboratory were presented, this include materials used, reinforcement detail and construction process. Then, the detail of the Push-off test specimen to determine the capacity of the shear connectors was described. The procedure used to introduce artificial damage by accelerating corrosion on shear connectors and the number of shear connectors corroded in each beam was described. The procedures for modal testing and experimental modal analysis used in this research is also discussed, this include equipments used and the set up of the test. Next chapter present and discuss the results obtained from the experimental investigations.

CHAPTER 5

RESULTS AND DISCUSSIONS

5.1 Introduction

This chapter reports the findings and observations of the investigation which incorporates the results for push-off test to understand the capacity of shear connectors used in this research before and after damage, the global modal parameters extracted from the undamaged and damaged experimental composite beams and results on various dynamics-based damage detection algorithms for locating damage introduced in the beams. The global modal parameters identified were natural frequencies, damping ratios, mode shapes and Modal assurance criterion (MAC) values. The localized damage detection techniques investigated are the co-ordinate modal assurance criterion (COMAC), flexibility change method, two dimensional mode shape curvature changes and change in strain energy method.

As stated in the first chapter, the main aim of this study is to investigate the effectiveness of dynamics based techniques in assessing the conditions of shear connectors in concrete composite bridges giving care to the loss of composite action between pre-cast prestressed beam and slab by just taking measurements from the surface of the slab. First stage of the work was to excise the composite beams by just loading three times to 30kN so as to destroy or reduce the natural bond between the beam and the slab and making them active for dynamic test as explained in section 2.5. Second stage of the work was extraction of global modal parameters (modal signature) of the undamaged composite beams from response measurements. The third stage was extraction of modal parameters of the damaged composite beams from response measurements after artificially damaged the beams by accelerating corrosion on some shear connectors. Lastly, different damage localizing algorithms were then applied on modal data extracted to try localizing the region of the damaged shear connectors in all experimental beams. The results obtained are discussed in the subsequent sections of this chapter.

5.2 Frequency response function (FRFs)

The responses of the structure were measured at support locations and at an interval of 150mm along the length of the structure. A typical response signal from one of the accelerometers is shown in Figure 5.1. This figure shows the response (acceleration) of the beam caused by the force applied to the structure (three force excitations).

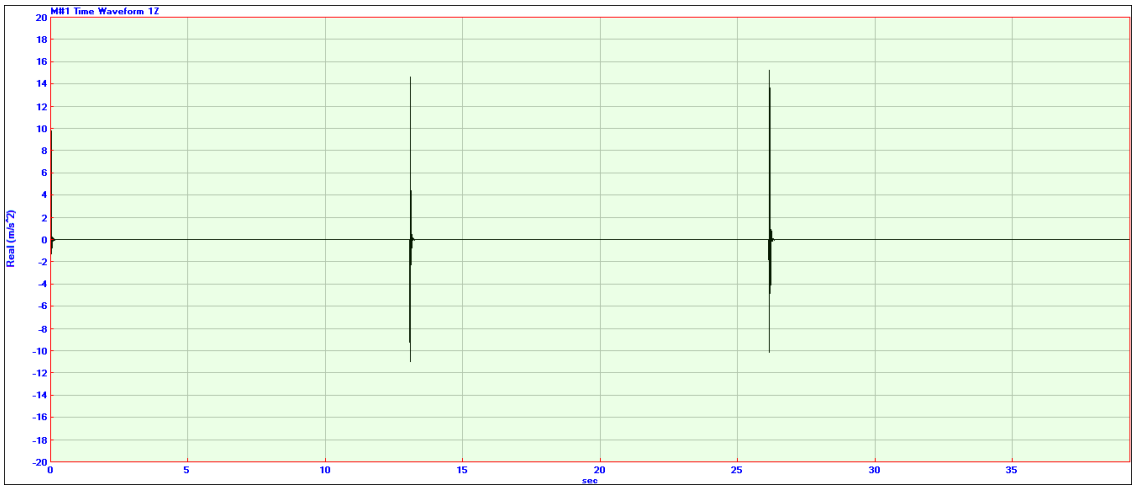

5.1(a): Impact response (three hits)

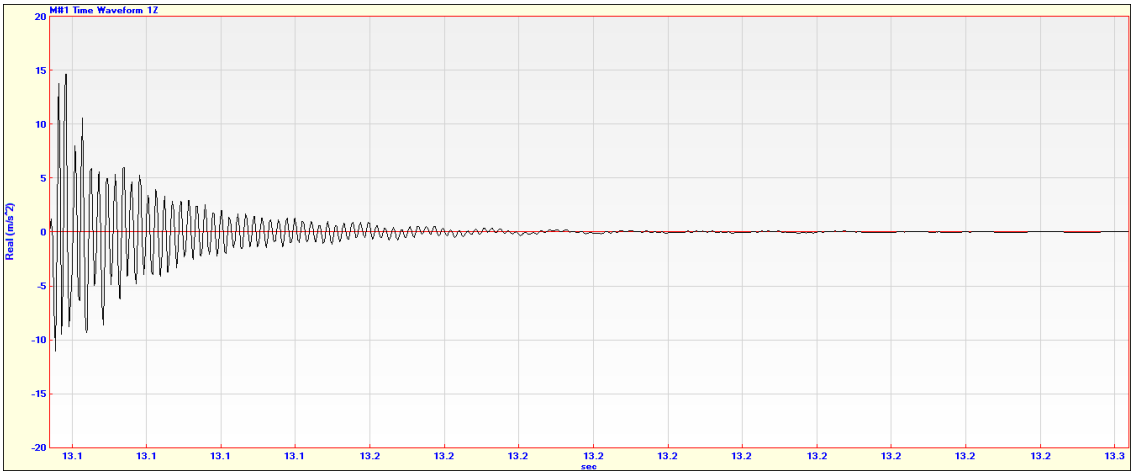

5.1(b): Magnified signal for one hit

Figure 5.1: Typical time wave signal

Response measurements shown in Figure 5.1 were used to compute FRFs of the system. The FRFs for one of the systems is shown in Figure 5.2. The peaks of this graph indicate mode of vibrations characterized by the modal frequency and damping ratio which are the modal signatures of the structure. In the FRFs graph distinct frequency peaks are visible, which describe the natural frequency of the structure. With the equipments available in our laboratory, it was only possible to obtain natural frequencies of the first three bending modes. Peaks labeled 1, 2 and 3 are the first, second and third flexural or bending modes of the system. These signatures were used to assess the degree of composite action between beam and slab and the condition of shear connectors after damage.

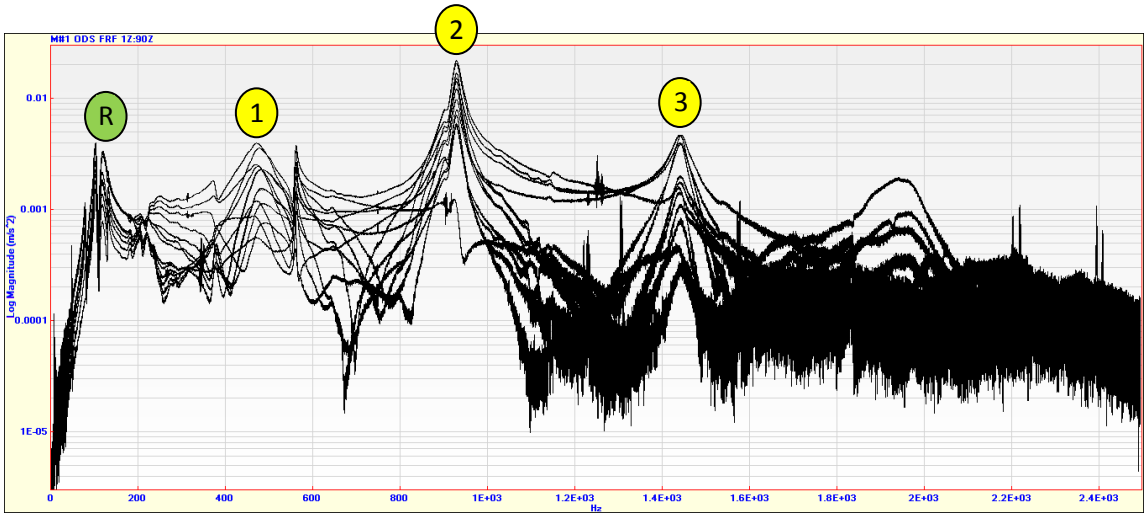

Figure 5.2: FRFs graph

As can be seen from the FRFs graph, the effect of prestressing caused the natural frequency of the first three bending modes to range between 400Hz and 1500Hz which is very high compared to normal reinforced concrete beam. Additional peaks are observed; these peaks indicate other modes and the effect caused by the nonlinearity of the structure. Peaks labeled ‘R’ are rigid modes of the beams caused by disturbance at supports because of short beams (1.8m) and hence stiffer beams.

5.3 Extraction of Modal parameters

The modal parameters (natural frequency, damping ratios and mode shapes) were extracted from the FRFs by means of experimental modal analysis procedures, which were described in chapter three. The Rational Fractional Polynomial (RFP) method, described in chapter three, was used to curve-fit the calculated FRFs to extract the modal parameters. The curve fitting technique requires three steps:

- Determine the number of modes in a frequency span of the FRF measurement data.
- Estimate modal frequency and damping for the modes in the frequency span.
- Estimate modal residues (mode shape components) for each mode that has frequency and damping estimates.

The Complex Mode Indicator Function (CMIF) was used to determine the number of modes present in the calculated FRFs. The concept of CMIF is developed by performing singular value decomposition (SVD) of the Frequency Response Function (FRF) matrix at each spectral line. The CMIF is defined as the eigenvalues, which are the square of the singular values, solved from the normal matrix formed from the FRF matrix at each spectral line. The normal matrix is obtained by pre-multiplying the FRF matrix by its Hermitian matrix as $[H(j\omega)]^H[H(j\omega)]$. The CMIF is the plot of these eigenvalues on a log magnitude scale as a function of frequency as shown in Figure 5.3.

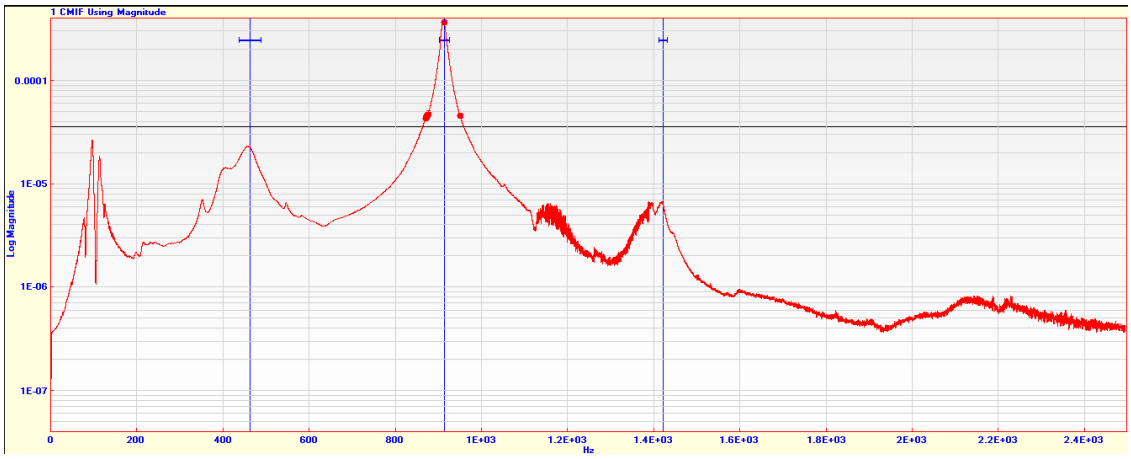

Figure 5.3: Modal Indicator graph

The peaks detected in the CMIF plot indicate the existence of modes, and the corresponding located frequencies of these peaks give the damped natural frequencies for each mode. It must be noted that not all peaks in CMIF indicate modes. Errors such as noise, leakage, nonlinearity and a cross Eigen-value effect can also make a peak (Shih, *et al.*, 1989). Typical first three bending mode shapes extracted from each composite beam are shown in Figure 5.4.

(a): 1st bending mode

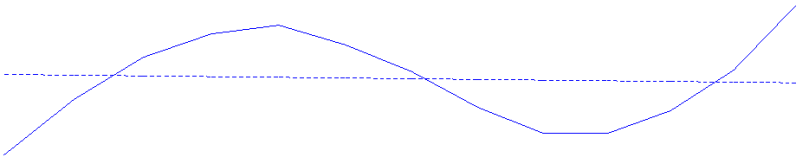

(b): 2nd bending mode

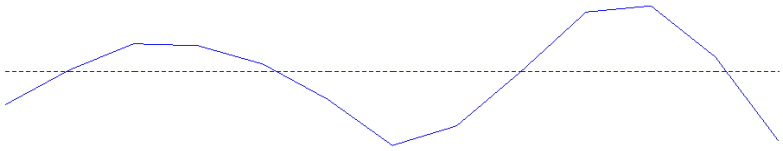

(c): 3rd bending mode

Figure 5.4: Typical Mode shapes

5.4 EXPERIMENTAL RESULTS

5.4.1 Static bending test of the composite beams

It was decided to conduct static bending test before dynamic test as an excise to beams so as to destroy or reduce a natural bond that was possible to be formed at beam/slab interface during casting of slab. Each beam was loaded to 30kN and repeated three times.

5.4.2 Push-off test

Push-off test was conducted in order to determine the shear capacity of the shear connectors used in the experimental composite beams as described in section 4.6. Six specimens were prepared for the test; three of them were damaged by accelerating corrosion to 15% mass loss of the shear connectors as in experimental composite beams using Faraday's formula, equation (4.1). Push-off test was then conducted for both undamaged and damaged specimens as shown in Figure 5.5 and best result was selected.

Figure 5.5: Push-off test set up

The relative displacement between the central piece and two lateral pieces was measured using Linear Variable Differential Transformer (LVDT) with sensitivity 34.14 and 34.18mV/V/mm placed on both sides of the specimen and average was taken. The change in heights of the lateral pieces due to applied load was also measured at intervals of 4kN using dial gauges. These readings were subtracted from the LVDT measurements to reduce the effect of height change of the specimens due to applied load. Figure 5.6 present load-slip curve for both undamaged and damaged specimen. From the experiment all undamaged specimens failed at average of 68kN while damaged specimens failed at average of 62kN; this is equivalent to 1.5kN shear capacity loss at each shear connector cross-section.

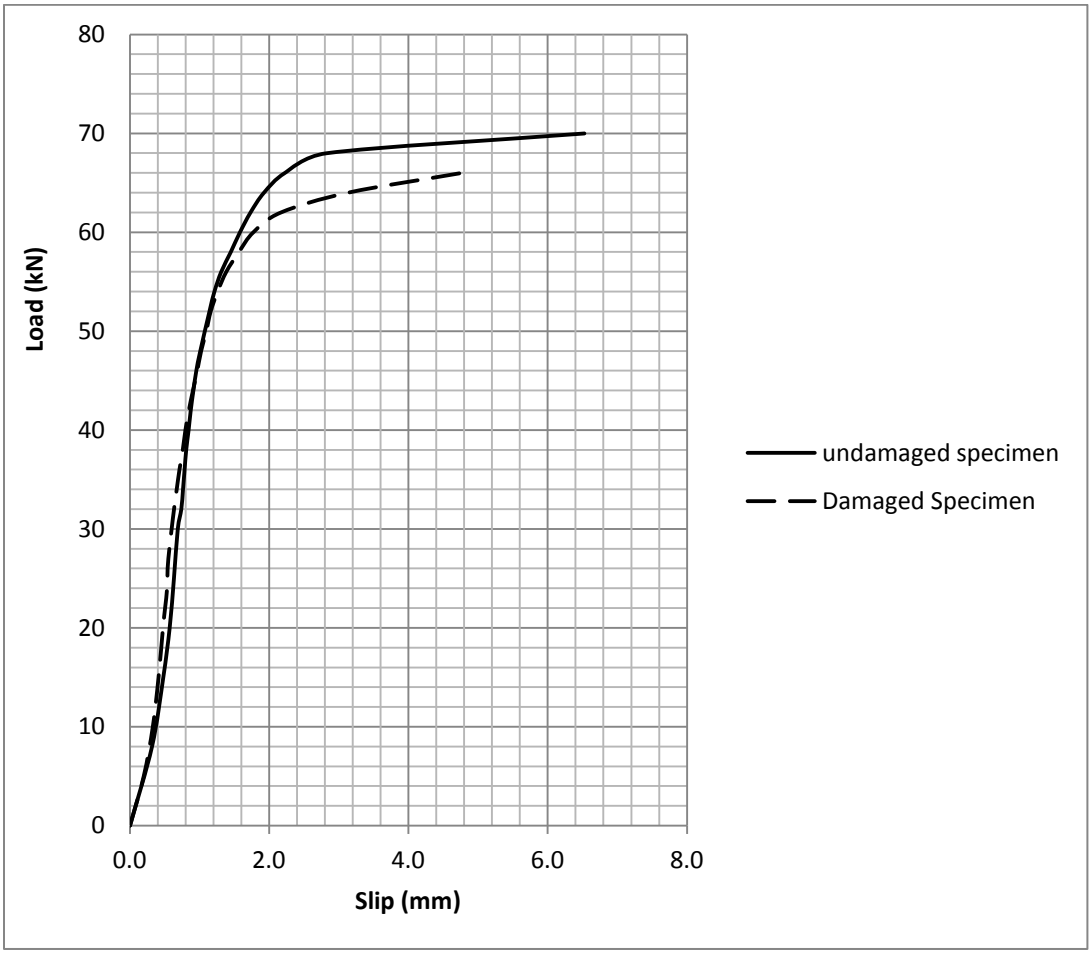

Figure 5.6: load-slip curve

5.4.3 Degree of Composite action or fixity between beam and slab

In concrete composite construction, the degree of composite action between beams and slab is achieved by means of shear connectors as discussed in section 2.4 and 2.5. In this research, as described in chapter 4, five concrete composite beam models each with different number of shear connectors ranging from number of shear connectors which provide nearly full composite action (CASE A) to other four case which provide partial composite action (CASE B1 to B4) were constructed in the laboratory.

All beams were identical, but with different number and spacing of shear connectors. The number and spacing of shear connectors in each beam are as shown in Table 5.1. Before damage was introduced to some of the shear connectors in the beams, each beam was tested in its intact state to determine the difference in dynamic characteristics based on the difference in number and spacing of shear connectors in each beam. Difference in FRFs, natural frequency, damping ratio and mode shapes were observed and are discussed in the next sections.

5.4.3.1 Difference in FRFs

Measured FRFs have advantage over modal data as they contain information about all the modes the structure possesses and not only that for the frequency range measurement. Figure 5.7 illustrate a difference in FRFs using the first trace of each beam. Blue trace is for a beam with ‘21’ shear connectors; Red is for ‘17’ shear connectors; Black is for ‘13’ shear connectors; Pink is for ‘9’ shear connectors and Green for ‘7’ shear connectors. As it can be seen from the Figure, it is evident that the frequency peak of the FRFs has high amplitude and shift towards right for a beam with large number of shear connectors (or less space between shear connectors). This proves that FRFs graph is sensitive to degree of composite action provided by shear connectors between beams and slab in real bridges.

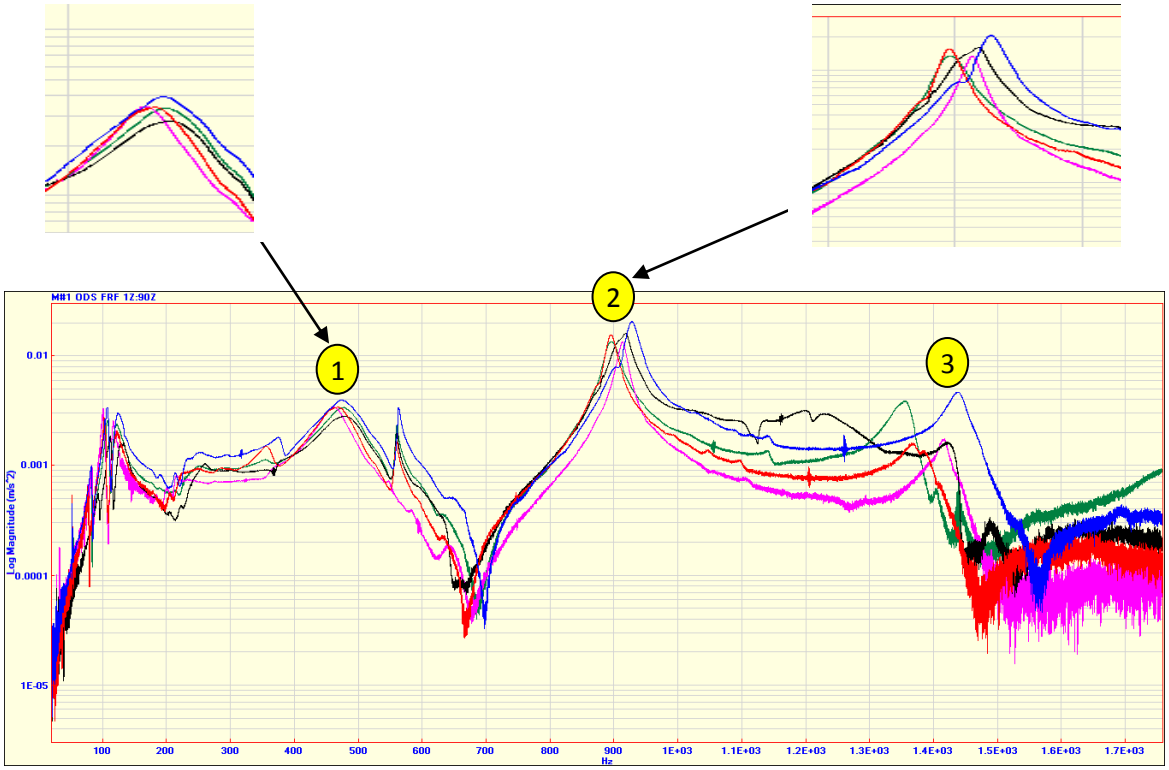

Figure 5.7: Overlaid FRF for all beams (only one trace)

5.4.3.2 Natural frequencies

Table 5.1 present the results of the natural frequencies of the first three bending modes of vibration for each beam in an undamaged state obtained from the experiment. As can be seen from the FRF graphs (Figure 5.4), the signals after the peak of the second mode are a bit rough compared to signals before the second peak. Considering that the third mode is on the rough side, it was not possible to estimate accurately the natural frequencies of the third mode by curve-fitting. The natural frequencies for the 3rd mode were roughly estimated from the FRFs graphs.

From the results, the general trend shows that the natural frequency is increasing as the number of shear connectors are increasing. This is very clear on the 2nd and 3rd mode. Frequencies of the 2nd mode seem to be more sensitive to number of shear connectors. The results of beam 'A' and beam 'B4' and the general trend on the results of 1st mode

might be caused by construction problems as these beams were not cast on the same day and also beam 'A' and beam 'B4' might have not been compacted properly because of small spacing between shear connectors.

Table 5.1: Experimental natural frequencies.

Beam	Number of shear connectors	Spacing	Bending Modes		
			1st	2nd	3rd
A	21	92	480	929	1440
B4	17	115	467	895	1390
B3	13	155	483	920	1430
B2	9	230	464	914	1420
B1	7	310	460	898	1360

5.4.3.3 Damping of the system

Damping is the ability of a disturbed system to dissipate energy. The damping ratio is a dimensionless measure of damping of the system describing how oscillations in a system decay after a disturbance. As explained in section 5.4.3.2 that the signals for 3rd mode were not good enough for curve fitting. Table 5.2 present the results of the damping ratios of the first and second bending modes of vibration for each beam in an undamaged state obtained from the experiment. From the results, the general trend for the values of damping ratio is not consistent as the numbers of shear connectors are increasing although theoretically the damping ratio should decrease as the number shear connectors are increasing. The reason for such inconsistency is that damping is difficult to evaluate accurately due to measurement errors and uncertainties.

Table 5.2: Experimental damping ratio.

Beam	Number of shear connectors	Spacing	Bending Modes	
			1st	2nd
A	21	92	8.16	1.25
B4	17	115	6.60	1.16
B3	13	155	9.72	1.96
B2	9	230	7.45	1.47
B1	7	310	12.2	1.83

5.4.3.4 Mode shapes

The mode shape is a unique characteristic of a structural system. It shows deformed shapes of the structure at a particular frequency and damping ratio. Figure 5.8 shows comparison of scaled mode shapes plotted in one graph for all beams in undamaged state. Scaling was necessary for effective comparisons of the modes on the fact that when mode shapes are obtained experimentally from operating data, they are not properly scaled to preserve the mass and elastic properties of the structure. Operating data means measuring structure responses without excitation force (Schwarz and Richardson, 2003). The mode data are normalized by dividing the values recorded at each data point by the maximum value, so that the peak value becomes +/-1. Generally, it was expected to have less deflection of mode shape values for beam with large number of shear connectors. However, from the results of 1st mode, a beam with 13 shear connectors deflected less than the beam with 21 shear connectors. This correlate well with the results of natural frequencies, the only reason might be because of construction problems. Same trend can also be seen for the case of 2nd mode at sagging region but at the support a beam with 21 shear connectors show small movement than all beams.

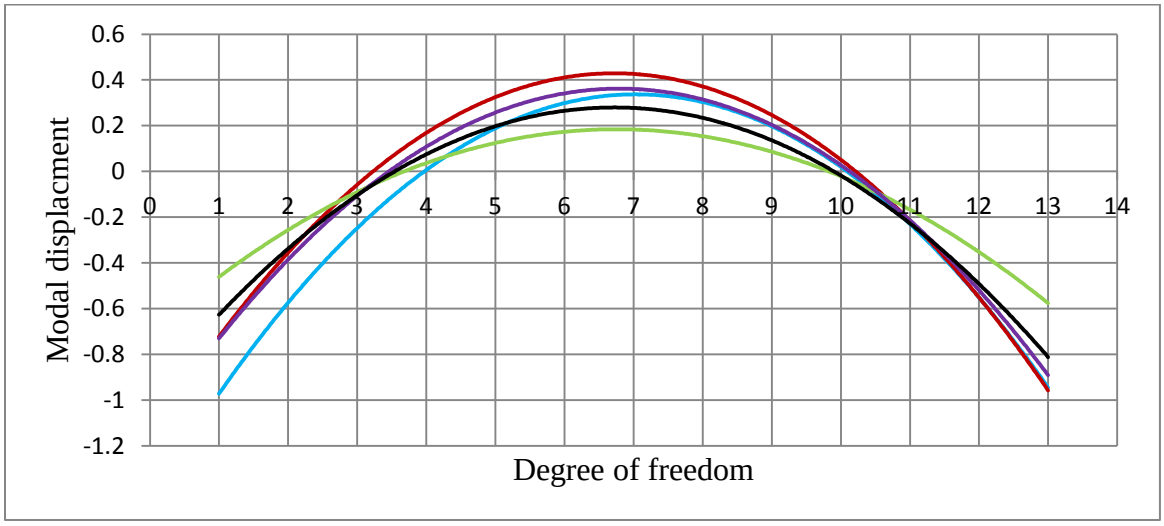

5.8(a):1st Mode Shapes

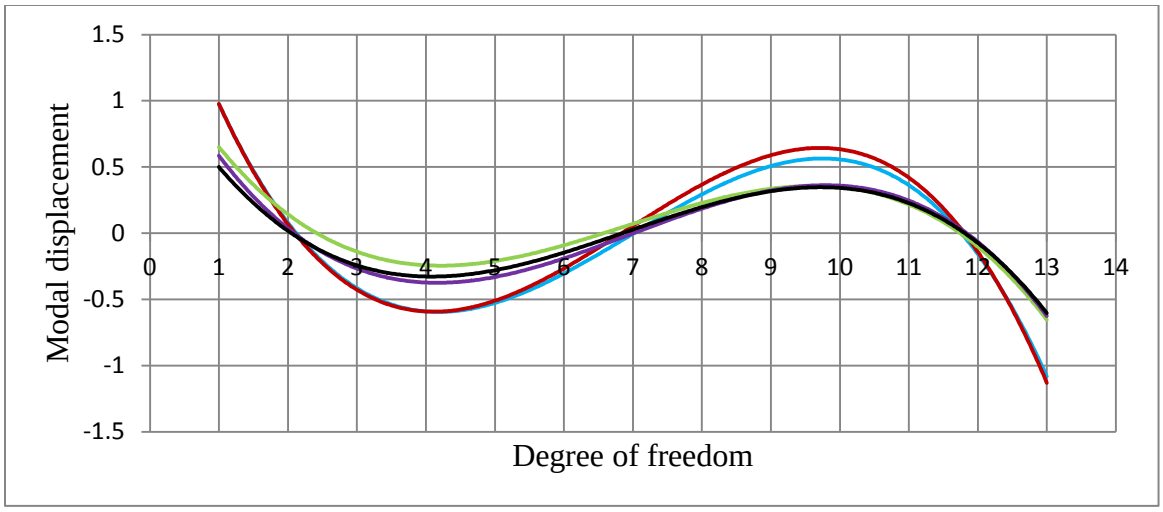

5.8(b): 2nd Mode Shapes

21 shear connectors, 17 shear connectors, 13 shear connectors
9 shear connectors, 7 shear connectors.

Figure 5.8: Undamaged mode shapes

5.4.4 Damage detection using global damage parameters

Damage detection is often achieved by comparing dynamic properties of a system between its initial state and damaged state. Global damage indicators that assess the existence of damage in the system include changes of FRFs, natural frequencies, damping ratio, mode shapes and MAC value.

5.4.4.1 Changes of FRFs

FRFs are very sensitive to any kind of change. When damage occurs in a structure, the amplitudes of the FRFs changes and their frequency peaks shift towards left. Depending on the severity and the type of structural damage new frequency peaks can occur, some peaks can disappear and other peaks stay unchanged. Frequency peaks of different modes behave differently depending on the location of the damage site. Some modes are very sensitive to a specific damage location. For example if damage is located at a node point of a given mode. In this research, the 2nd bending mode was found to be very sensitive to

damage on shear connectors than other modes. Figure 5.9 shows overlaid ODS FRF for undamaged versus damaged state of each composite beam. The number of shear connectors damaged for each beam is as shown in Table 5.3. The ODS FRFs were scaled to compensate for deviations in the impact force. From the results, it can be seen that the FRF peaks for all traces on each beam shift to the left indicating a drop of the natural frequencies. Similar trend is observed on all amplitudes of the FRFs between undamaged and damaged state.

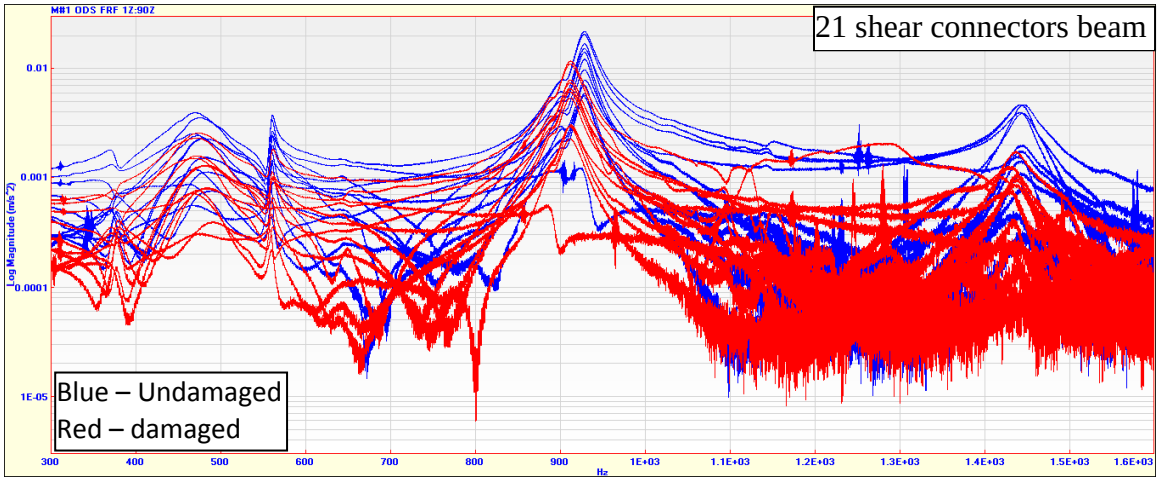

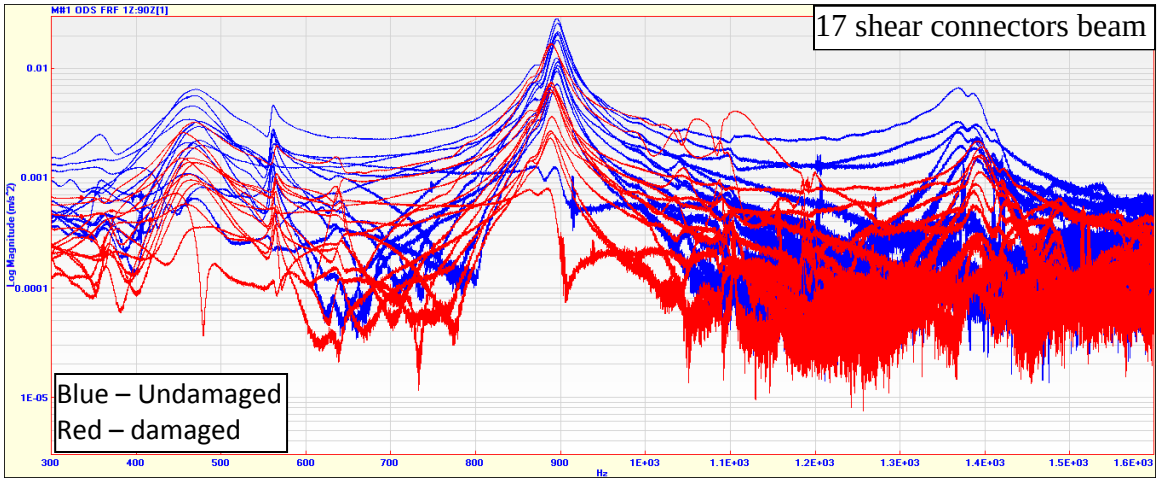

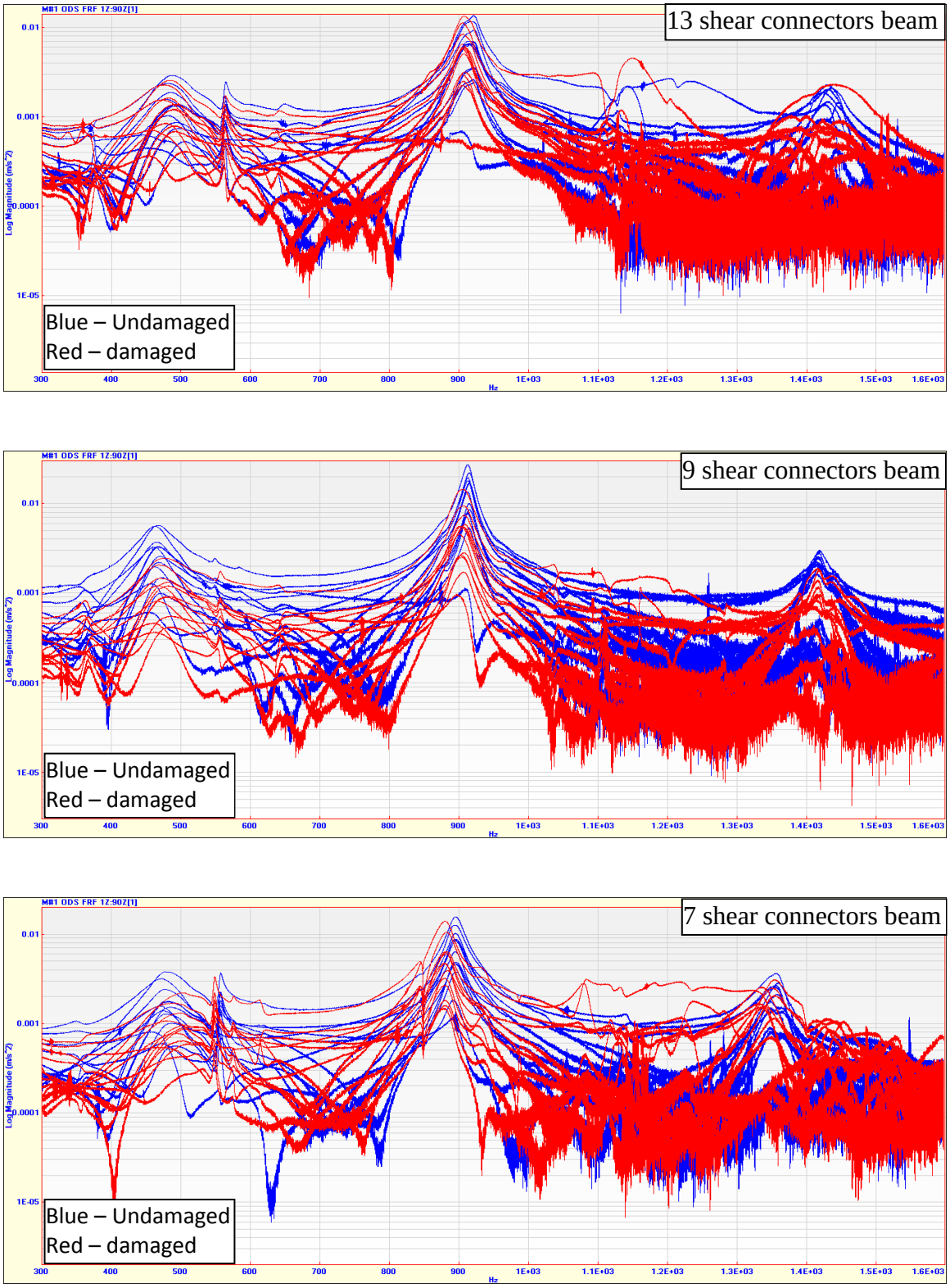

Figure 5.9: Overlaid ODS FRF for undamaged versus damaged beam

5.4.4.2 Natural frequencies

Theoretically, Damage causes the natural frequencies of a structure to drop. The natural frequencies of the first three bending modes of vibration of each beam before and after damage obtained from the experimental results are shown in Tables 5.3. UB stand for undamaged beam and DB stand for damaged beam. As explained before, the natural frequencies of the 3rd modes were roughly estimated from the FRFs graphs. Percentage changes of natural frequencies also shown in the Table and numbers of shear connectors damaged on both sides of the beam are shown in the bracket for each beam. From the results it is evident that the presence of damage in beams causes a decrease in the natural frequencies. This decrease in frequencies reveals a gradual decrease in the global stiffness of the structure resulting from damaged shear connectors.

Table 5.3: Experimental natural frequencies

Beam	Number of shear connectors		Bending Modes		
			1st	2nd	3rd
A	21 (6 damaged both side)	UBA	480	929	1440
		DBA	478	912	1420
		% change	0.42	1.83	1.39
B4	17 (4 damaged both side)	UB4	467	895	1390
		DB4	464	888	1380
		% change	0.64	0.78	0.72
B3	13 (3 damaged both side)	UB3	483	919	1430
		DB3	481	907	1420
		% change	0.41	1.31	0.70
B2	9 (2 damaged both side)	UB2	464	914	1420
		DB2	463	905	1410
		% change	0.22	0.98	0.70
B1	7 (2 damaged both side)	UB1	460	898	1360
		DB1	459	887	1350
		% change	0.22	1.22	0.74

5.4.4.3 Damping of the system

Damping is another dynamic characteristic that change due to damage. Theoretically, the damping ratio of a system should increase as damage increases. Table 5.4 shows the damping ratio (in percentage) of each beam obtained from the experimental results before and after damage. Percentage changes after damage are also shown in the Table. Results shows inconsistent trend between undamaged and damaged beam. Studies conducted by Sibanda et al, 2008; Yong *et al*, 2007 and Wahab and De Roech, 1999 observed similar inconsistent and they concluded that unlike for natural frequencies a reasonably consistent trend could not be established for damping ratios before and after damage. The reason for such inconsistency is that damping is difficult to evaluate accurately due to measurement errors and uncertainties.

Table 5.4: Experimental damping ratios

Beam	Number of shear connectors		Bending Modes	
			1st	2nd
A	21 (6 damaged both side)	UBA	8.16	1.25
		DBA	8.61	1.47
		% change	-5.51	-17.6
B4	17 (4 damaged both side)	UB4	6.60	1.16
		DB4	4.30	1.23
		% change	34.85	-6.03
B3	13 (3 damaged both side)	UB3	9.72	1.96
		DB3	8.27	1.86
		% change	14.92	5.1
B2	9 (2 damaged both side)	UB2	7.45	1.47
		DB2	9.81	2.04
		% change	-31.68	-38.78
B1	7 (2 damaged both side)	UB1	12.2	1.83
		DB1	12.1	1.85
		% change	0.82	-1.09

5.4.4.4 Change of Mode shapes

Local damage will cause changes to the mode shapes in the vicinity of the damage. Failure in composite action resulting from damaged shear connectors was expected to be detected as shift of amplitudes of mode shapes at damaged locations. Figure 5.10 and Figure 5.11 shows the scaled mode shapes plotted for undamaged and damaged state of each beam with solid line indicating undamaged beam and dashed lines after damage. The mode data from the undamaged structure was used for scaling modes of damaged systems and normalized by dividing the values recorded at each data point by the maximum value recorded for the mode shape in question, so that the peak value becomes +/-1. All the considered mode shapes showed good sensitivity to the damage where all damaged modes deviated from the undamaged modes toward the damage location.

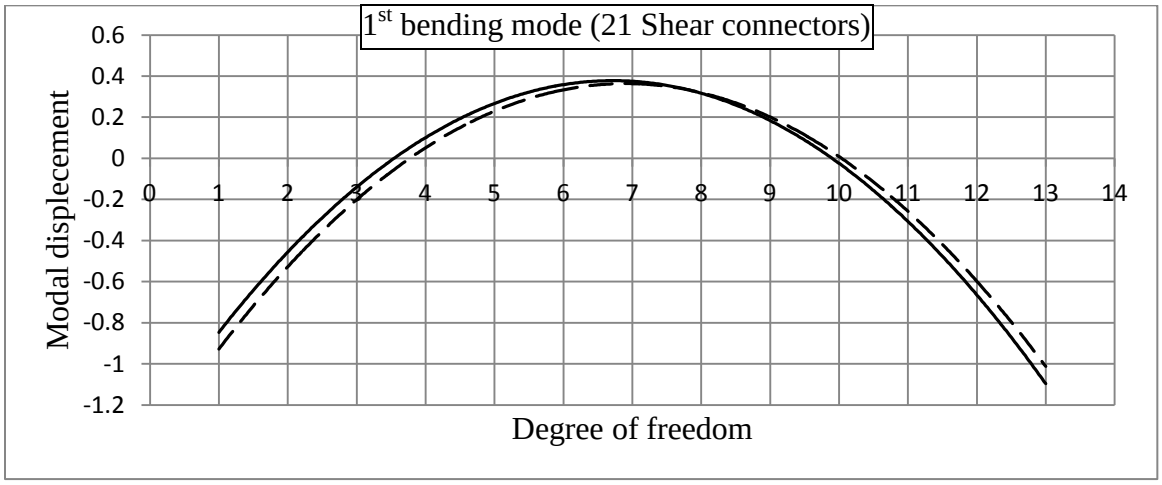

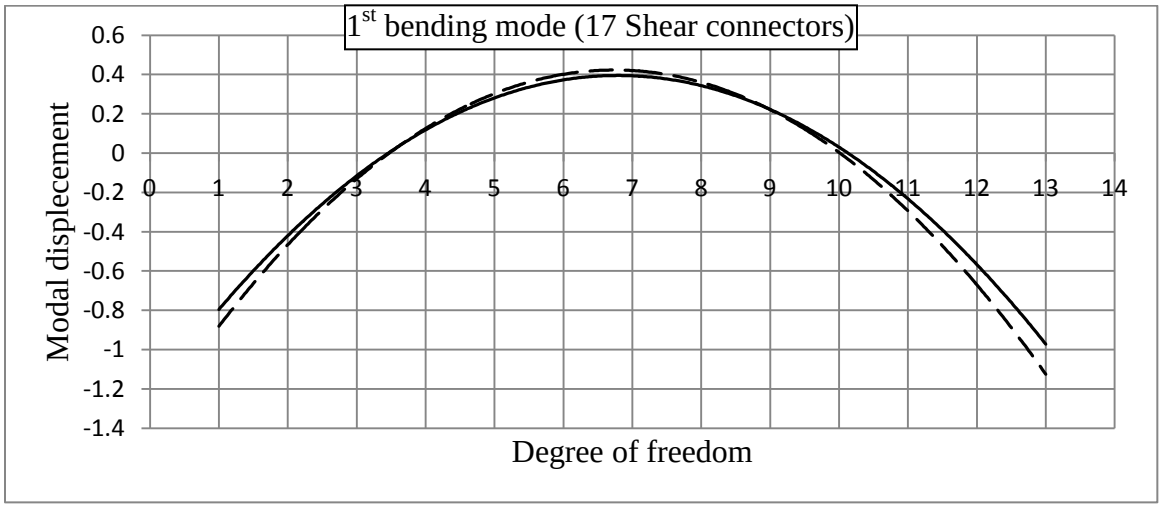

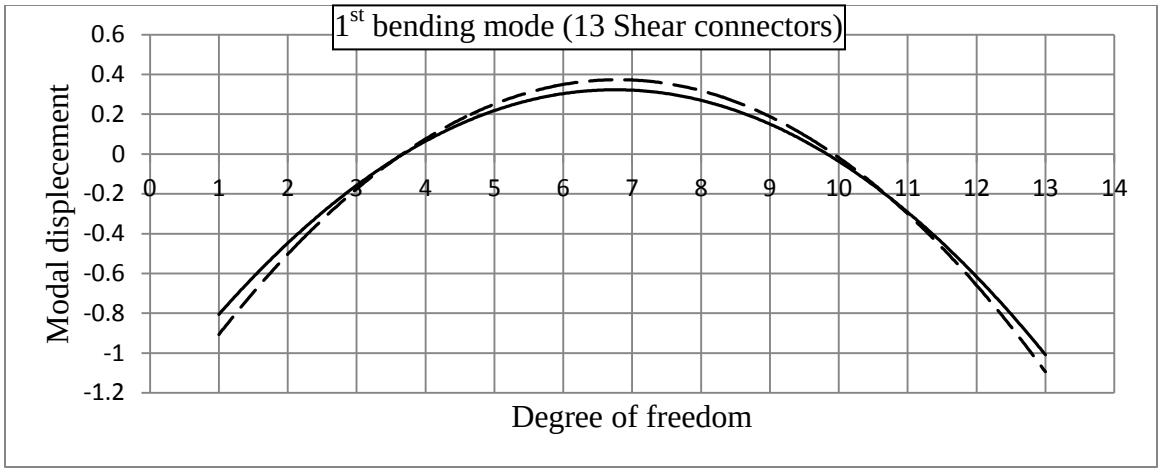

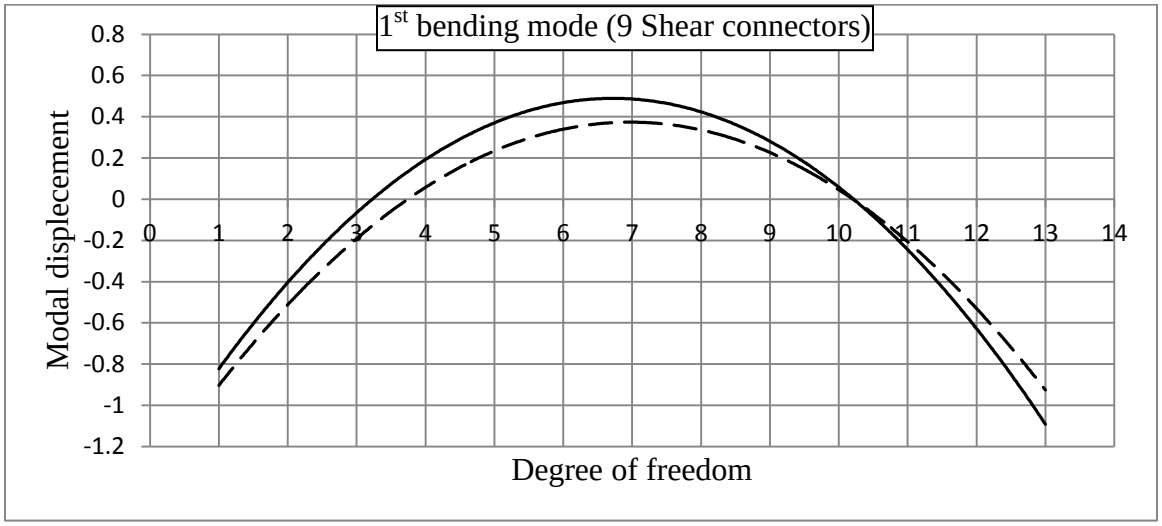

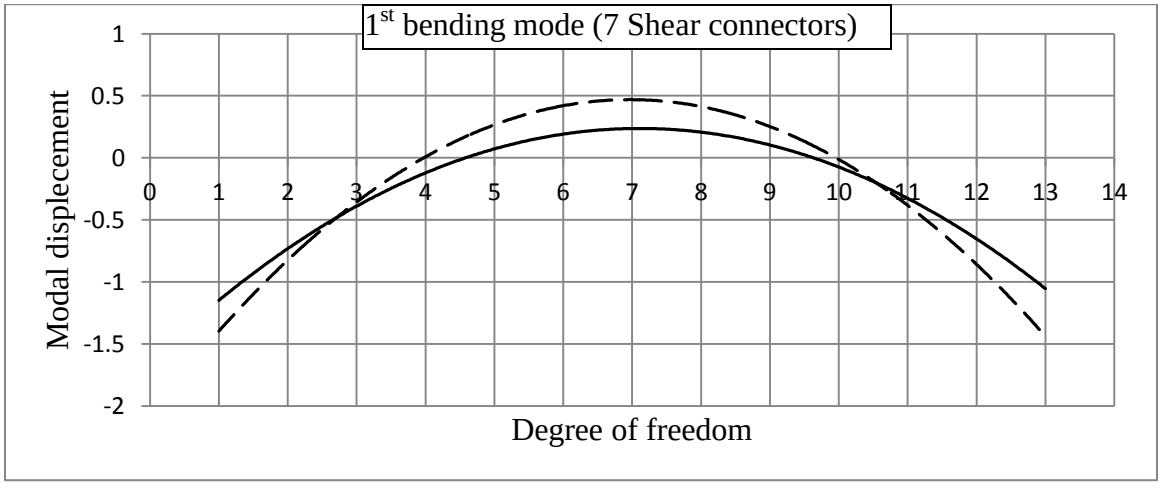

Figure 5.10: 1st bending mode shapes between undamaged and damaged beam

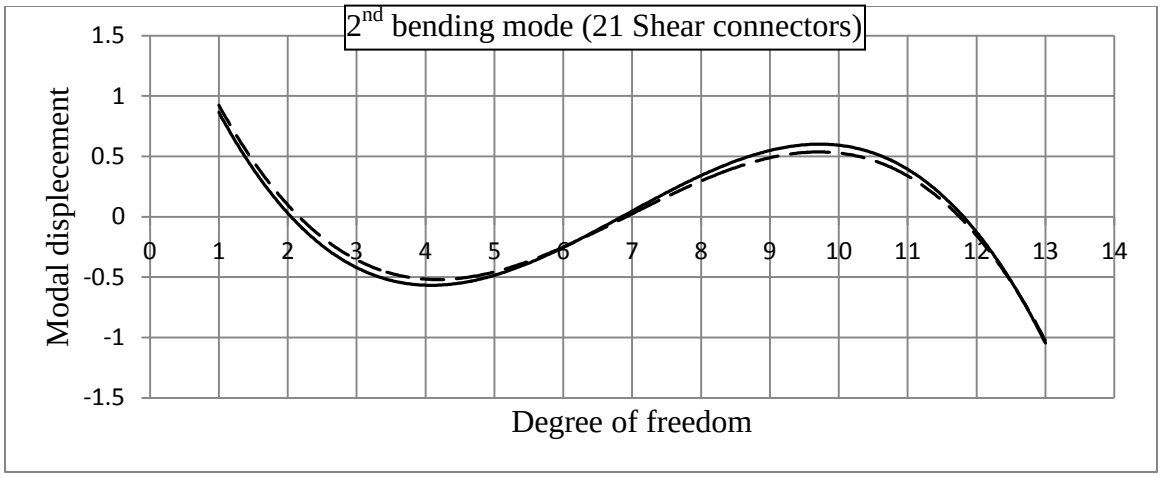
2nd bending mode (21 Shear connectors)
Modal displecement
1.5
1
0.5
0
-0.5
-1
-1.5
0 1 2 3 4 5 6 7 8 9 10 11 12 13 14
Degree of freedom

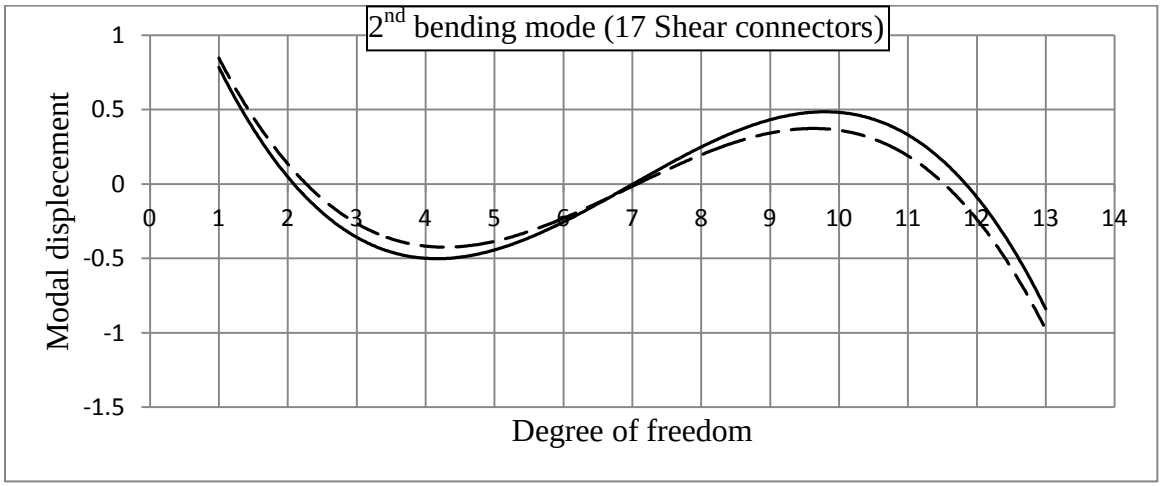
2nd bending mode (17 Shear connectors)
Modal displecement
1
0.5
0
-0.5
-1
-1.5
0 1 2 3 4 5 6 7 8 9 10 11 12 13 14
Degree of freedom

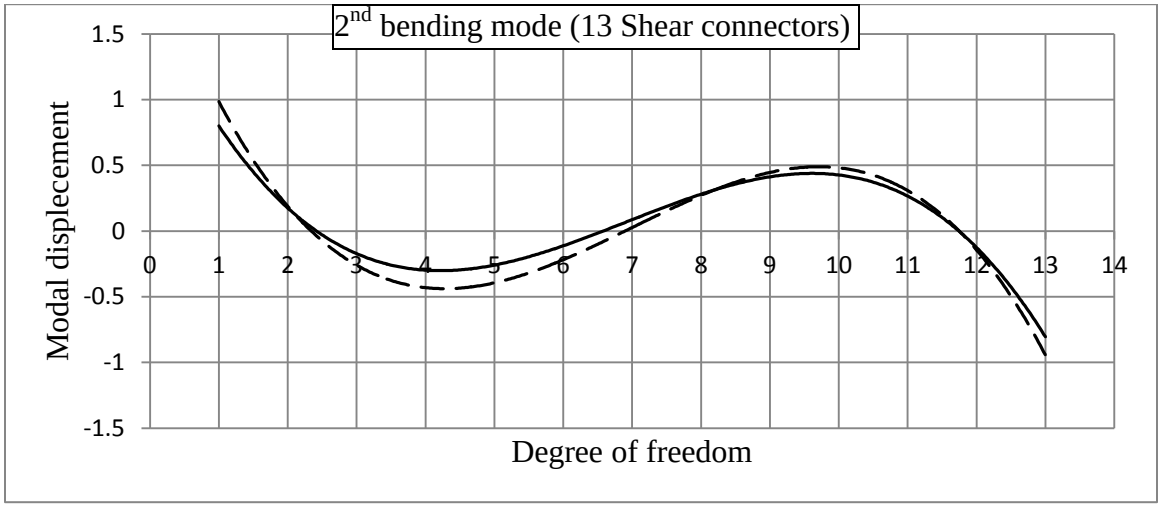
2nd bending mode (13 Shear connectors)
Modal displecement
1.5
1
0.5
0
-0.5
-1
-1.5
0 1 2 3 4 5 6 7 8 9 10 11 12 13 14
Degree of freedom

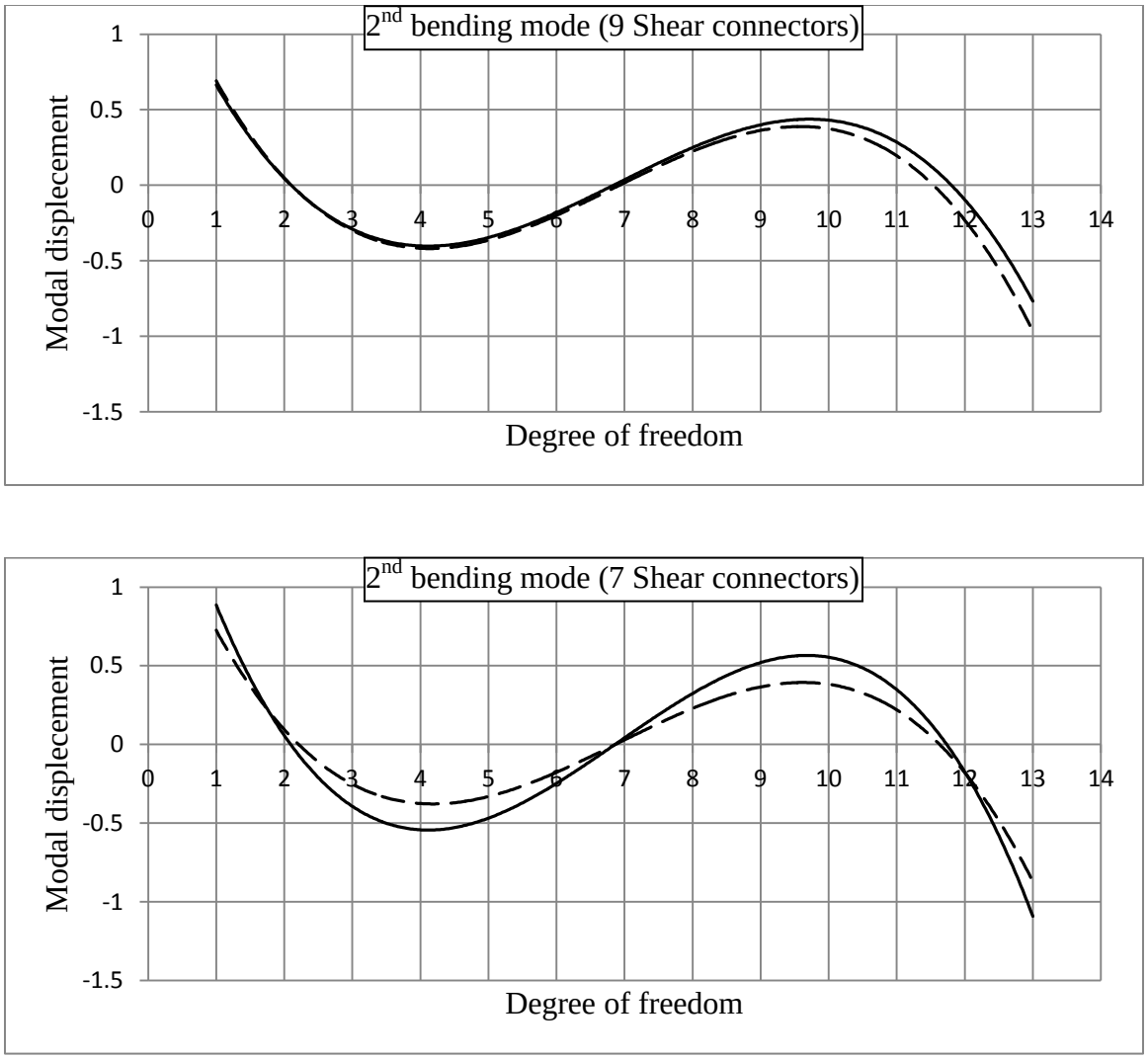

Figure 5.11: 2nd bending mode shapes between undamaged and damaged beam

5.4.4.5 Modal Assurance Criteria (MAC)

Monitoring of mode shape changes is a useful approach for damage detection. MAC makes uses of the orthogonal properties of the mode shape to correlate two modes. MAC values close to zero show that the mode shapes are dissimilar whereas values close to one show that the modes are similar. MAC values between modes of undamaged and damaged state are shown in Table 5.5. The results shows that MAC value for all beams between undamaged and damaged state is greater than 0.9. From the definition of MAC these modes between undamaged and damaged beam are similar, but since the values are

less than 1, this means there is no perfect correlation between undamaged and damaged mode shapes.

Table 5.5: MAC values between undamaged and damaged bending mode shapes

Beam	Number of shear connectors	Bending Modes	
		1^{st}	2^{nd}
A	21	0.97	0.95
B4	17	0.98	0.90
B3	13	0.98	0.96
B2	9	0.97	0.93
B1	7	0.98	0.95

5.4.5 Damage localization

Damages in structures can be localized by modal-based algorithms. These algorithms make use of mode shape data to localize damage within the structure (Pandey, *et al.*, 1991). The algorithms that are used in this study include COMAC, change in flexibility method, change in curvature and change in strain energy method.

5.4.5.1 Coordinate Modal Assurance Criterion (COMAC) values

COMAC values for each beam were calculated using equation 2.12c as described in section 2.12. Only first and second bending modes are used to calculate the COMAC values for each degree of freedom. Usually a bad correlation of mode shapes results in a low COMAC value indicating possible damage around that location. Figure 5.12 present the results for each beam. As it can be seen from the results, COMAC values are less than 0.9 at points near the support especially at sensor location (or degree of freedom) 3 and 11. This shows that the COMAC values are sensitive to damage. However, COMAC values at some other few locations where damage was not introduced are also less than 0.9 and some other location where there is damage are above 0.9. For example for a beam with ‘13’ and ‘7’ shear connectors at sensor location 6 where damage is not present.

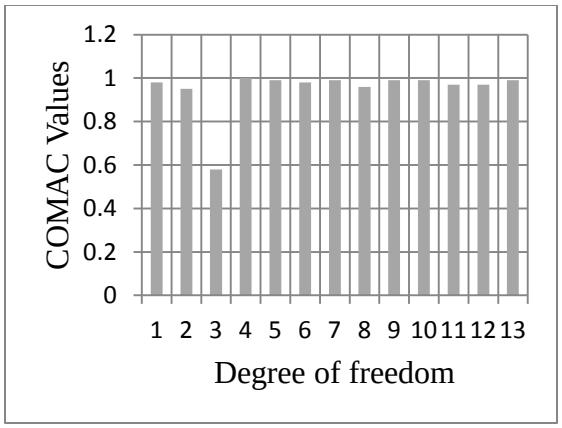

5.12(a): 21 shear connectors

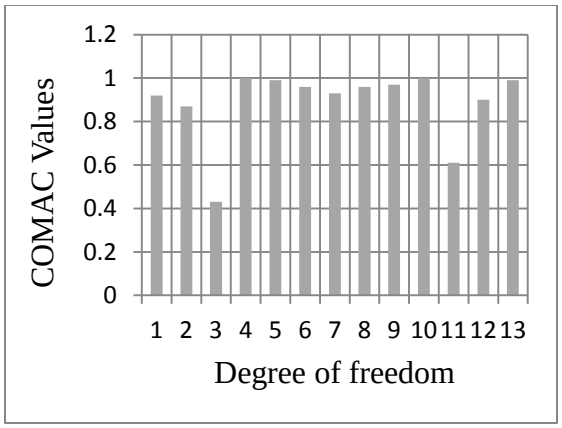

5.12(b): 17 shear connectors

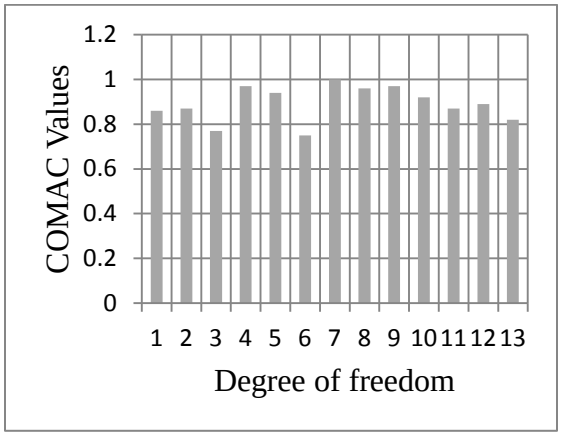

5.12(c): 13 shear connectors

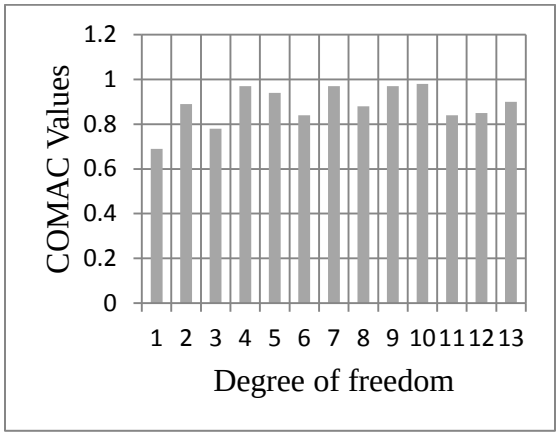

5.12(d): 9 shear connectors

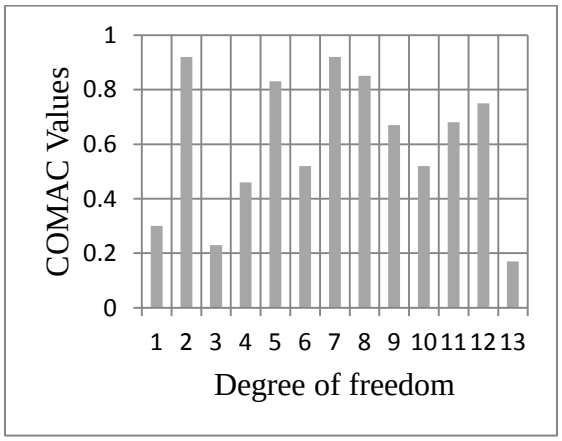

5.12(e): 7 shear connectors

Figure 5.12: COMAC value between undamaged and damaged beam

5.4.5.2 Change in flexibility method

Dynamically measured flexibility matrix which is just the inverse of the stiffness matrix is a useful tool for damage location. The measured flexibility matrix is estimated from the mass-normalized mode shapes and frequencies. Theoretically, damage increases the flexibility of the structure. The 1st and 2nd mode shapes and associated natural frequencies obtained from the experimental results were used to calculate change in flexibility using equation 2.12r and 2.12s. The plots of flexibility change along the beam for all composite beam models are shown in Figure 5.13. In all cases the positive peaks value indicate the location of damage in the beams. From the observations it is evident that the change in flexibility method is able to locate the region along the beam with damaged shear connectors. Again some false identification of damaged location is also observed especially for a beam with '21' and '9' shear connectors, but this might be caused by measurement errors and/or noise contamination in the signals. Again the graph for '21' shear connectors indicates that there is no damage at sensor location 11, 12 and 13; this correlate well with the results of change of mode shape and COMAC. The only reason maybe shear connectors at this location to some unexpected problem were not damaged as expected. This confirms that with minimum measurement errors and noise on the measured data, the change in flexibility method can be used to detect and locate the segment with damaged shear connectors in concrete composite bridges.

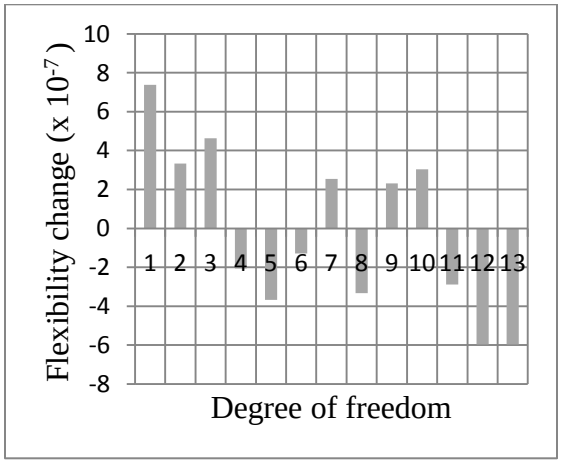

5.13(a): 21 shear connectors

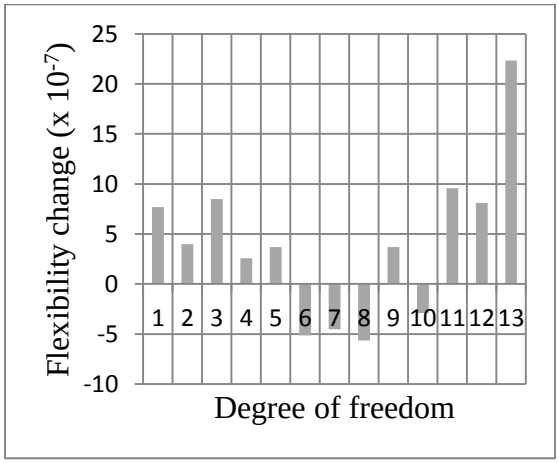

5.13(b): 17 shear connectors

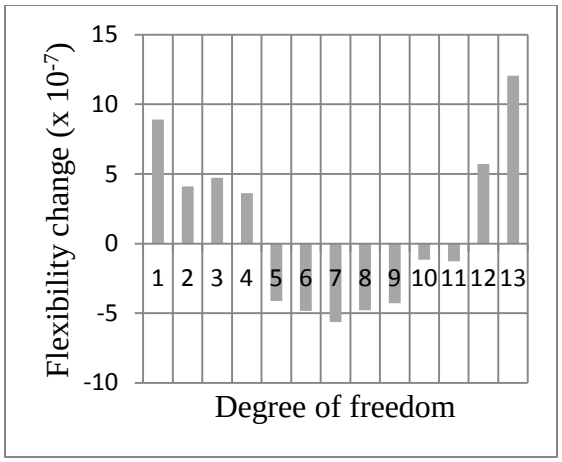

5.13(c): 13 shear connectors

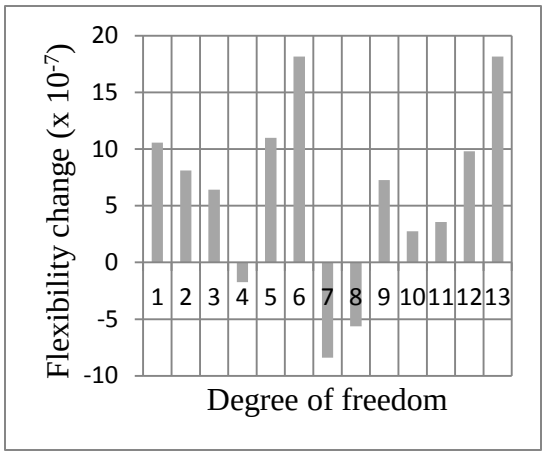

5.13(d): 9 shear connectors

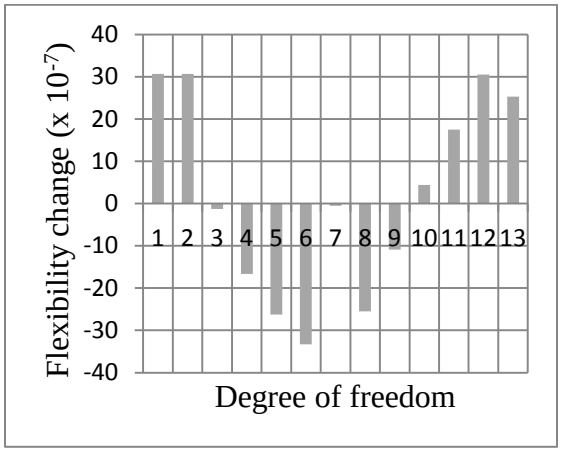

5.12(e): 7 shear connectors

Figure 5.13: Flexibility change between undamaged and damaged beam

5.4.5.3 Change in curvature method

Curvature of the mode shapes for the beams in its undamaged and damaged conditions were estimated numerically from the displacement mode shapes using central difference differentiation schemes. The algorithm (equation 2.12i) was used to compute the curvatures of the 1st and 2nd mode shapes and plotted as shown in Figure 5.14 and 5.15. The idea of this method is that reduction of flexural stiffness of a structure in correspondence with the damaged regions result to increase of the amplitude of curvature at those regions and so can be used to detect and locate damage.

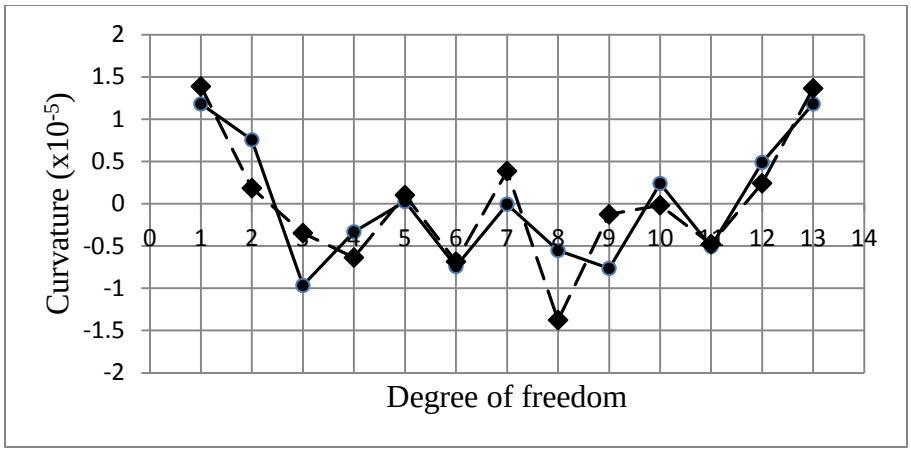

5.14(a): 21 shear connectors

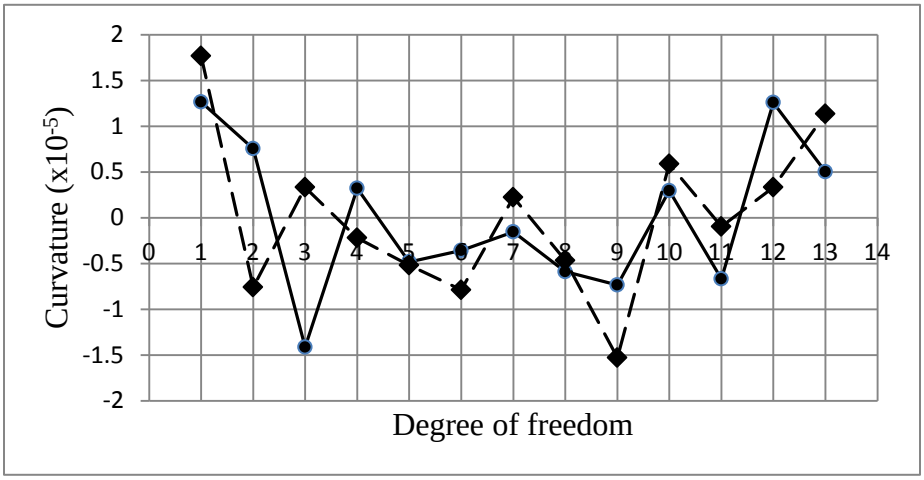

5.14(b): 17 shear connectors

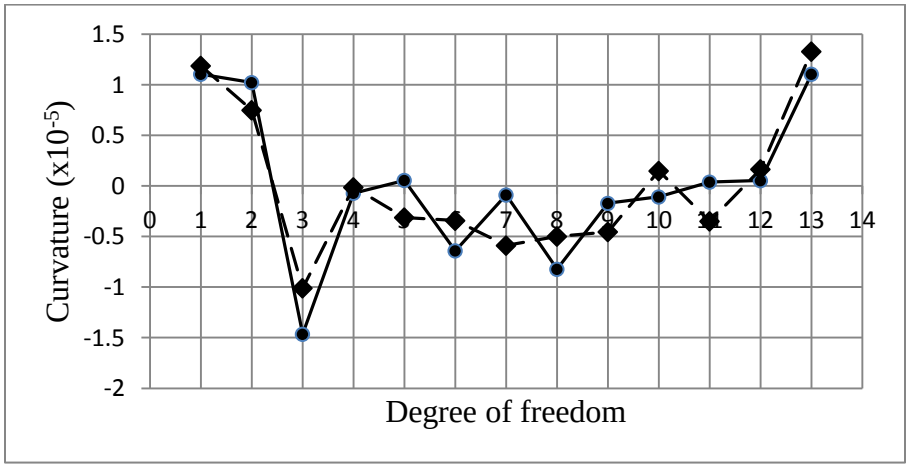

5.14(c): 13 shear connectors

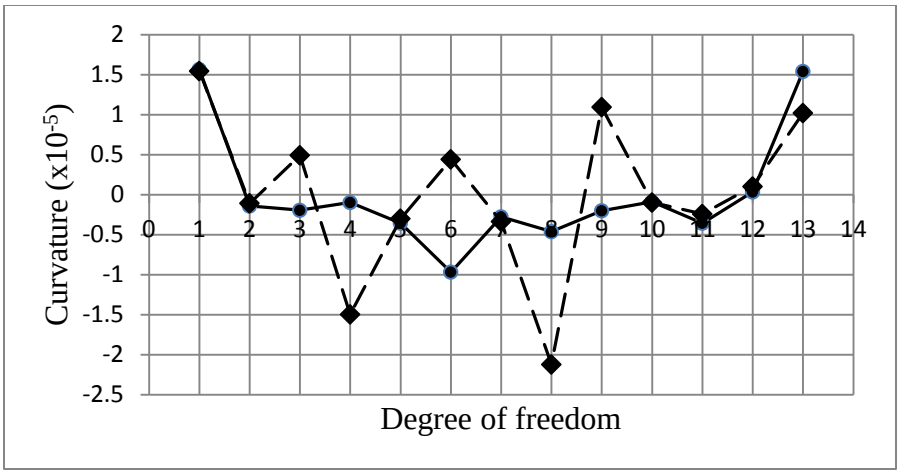

5.14(d): 9 shear connectors

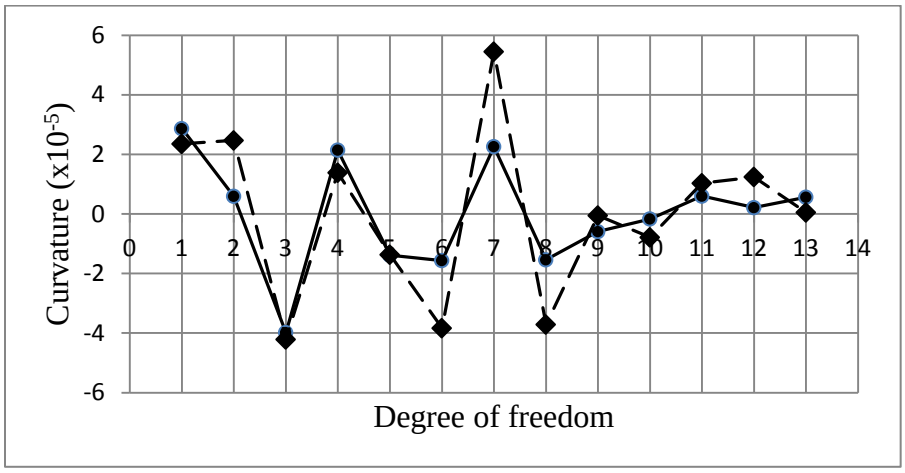

5.14(e): 7 shear connectors

Figure 5.14: Modal curvature plots for 1st bending mode

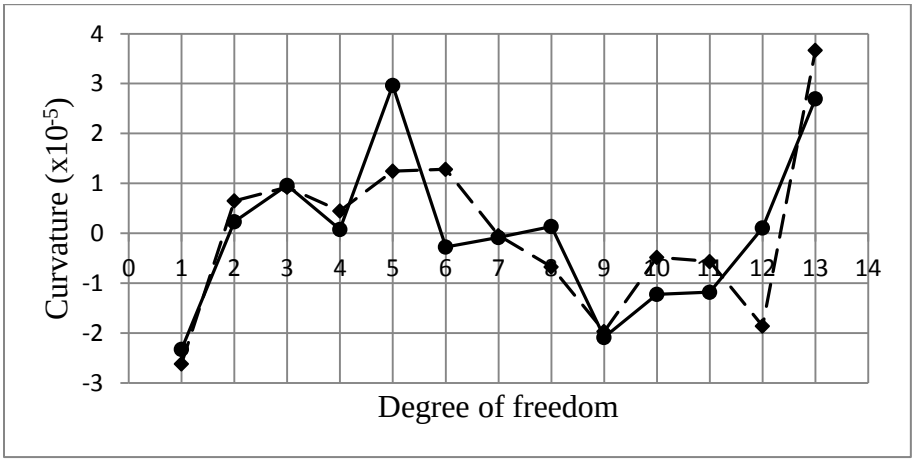

5.15(a): 21 shear connectors

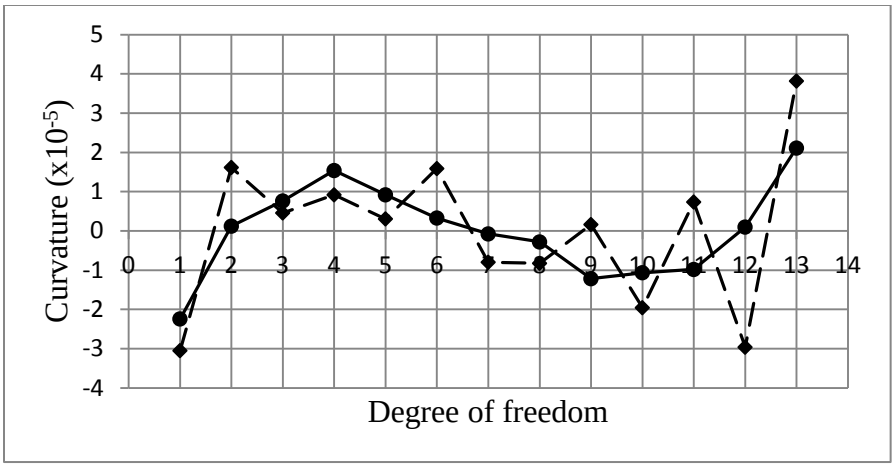

5.15(b): 17 shear connectors

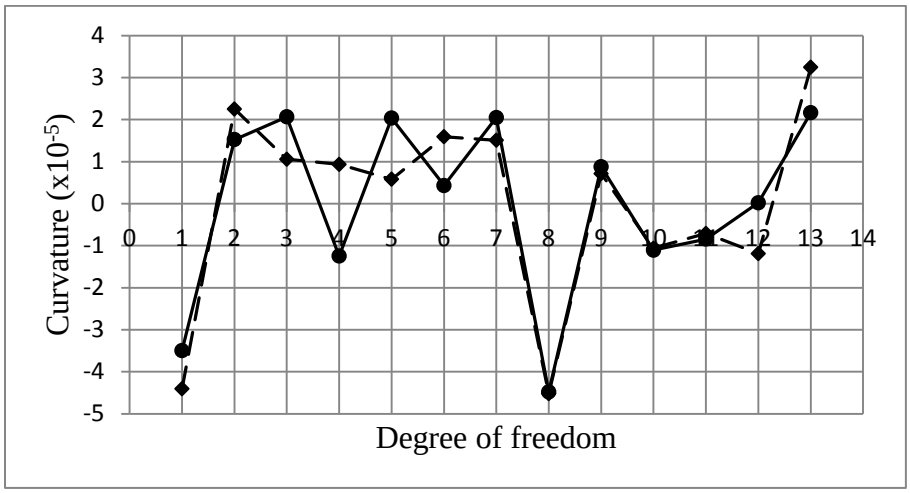

5.15(c): 13 shear connectors

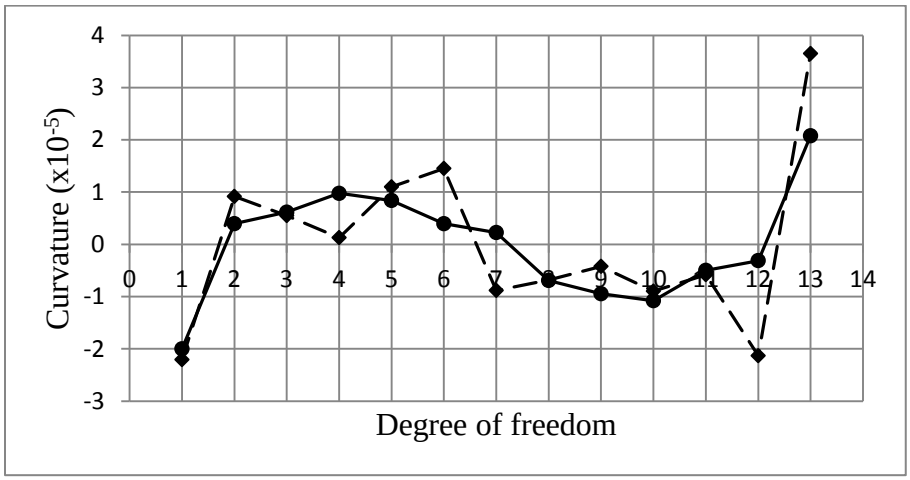

5.15(d): 9 shear connectors

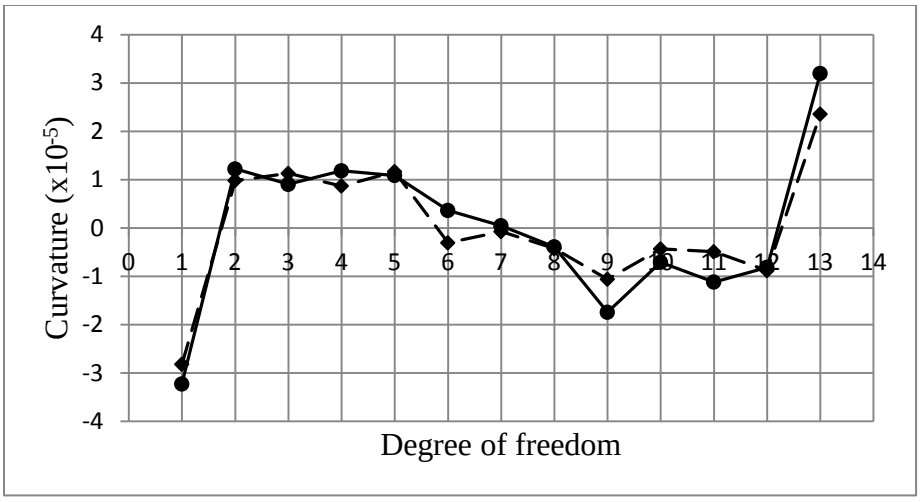

5.15(e): 7 shear connectors

Figure 5.15: Modal curvature plots for 2nd bending mode

As can be seen on curvature plots for both 1st and 2nd mode shape, the shift of curvature is almost everywhere along the length of the beam even at locations where damage is not present. This makes it very difficult to interpret locations where damaged shear connectors are present.

In order to eliminate this misleading information, the Curvature Damage Indicator (CDI) which combines the results for all modes (absolute sum) was computed at each degree of freedom using equation (2.12j) and plotted as shown in Figure 5.16. Improved results can be seen from the plots. Higher damaged indicators are observed at locations where damaged shear connectors are present. However, there is a number of false damage identification at locations where shear connectors were not damaged and lower values at locations where damaged shear connectors are present. This means that it is possible to locate regions with damaged shear connectors in concrete composite bridges using CDI values, but enough number of modes needs to be combined in order to minimize or eliminate possible measurements and noise errors. The number of modes to be considered will obviously depends on the size of the structure.

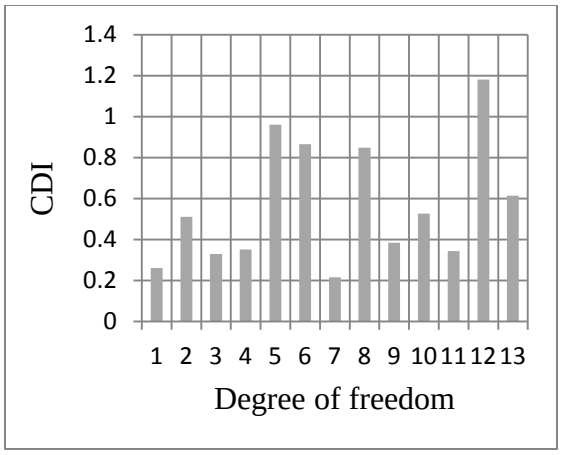

5.16(a): 21 shear connectors

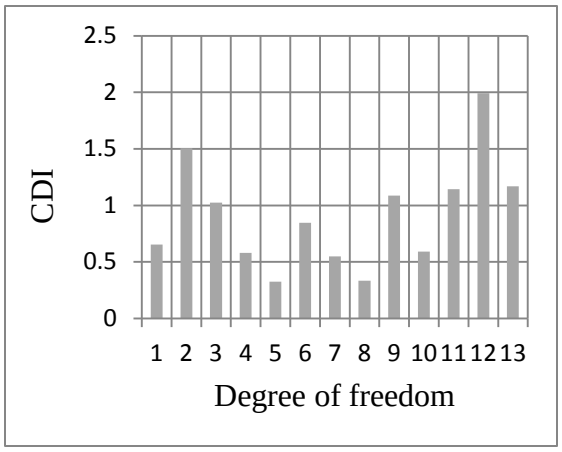

5.16(b): 17 shear connectors

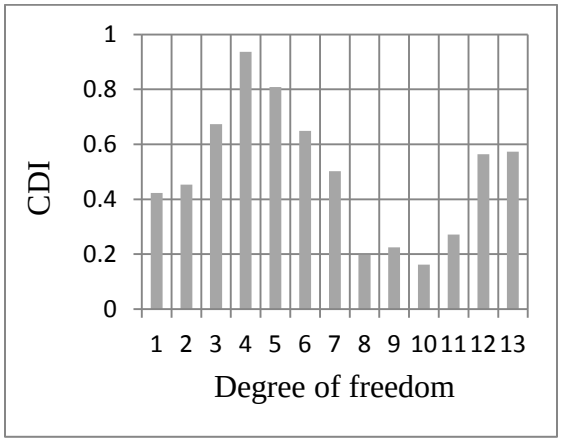

5.16(c): 13 shear connectors

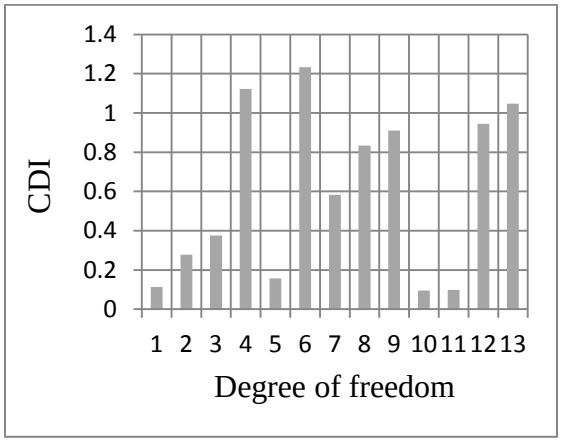

5.16(d): 9 shear connectors

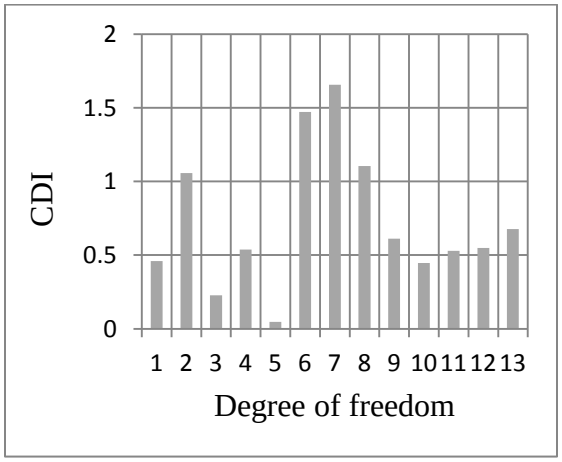

5.16(e): 7 shear connectors

Figure 5.16: Curvature damage indicator plots

5.4.5.4 Change in strain energy method

Only 1st and 2nd mode shape and their corresponding mode shape curvatures obtained from section 5.4.5.3 were used to calculate modal strain energy Normalized Damage Indicator (NDI) on each composite beam model using equation (2.12.1h). Figure 5.17 shows plots of a total sum of NDI obtained from modal displacements of 1st and 2nd bending mode shape for each beam. A location is defined as damaged when the NDI is greater than two (i.e. Zj>2) which corresponds to a hypothesis testing with 95% confidence level (Rivelos, *et al.*, 2010). From the plotted results, some regions with damaged shear connectors are correctly identified in all composite beam models. Again some false damage locations are observed, example at location 7 of '21' shear connectors beam where NDI is greater than 2 but damage is not present. Surprisingly, location 12 of the '21' shears connectors beam shows existence of damage which was not detected by other methods. From these results, it is evident that the strain energy method can also be used to detect and locate a region with damaged shear connectors in concrete composite bridge.

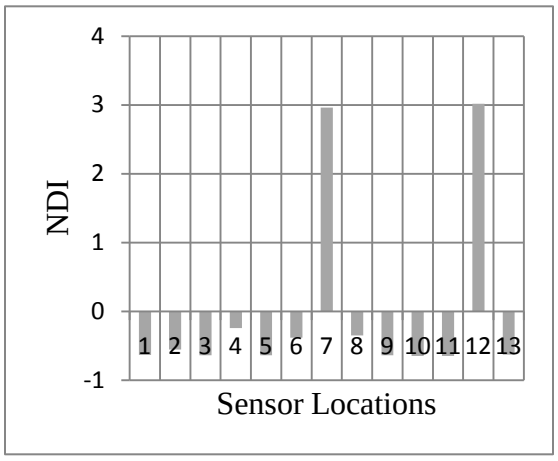

5.17(a): 21 shear connectors

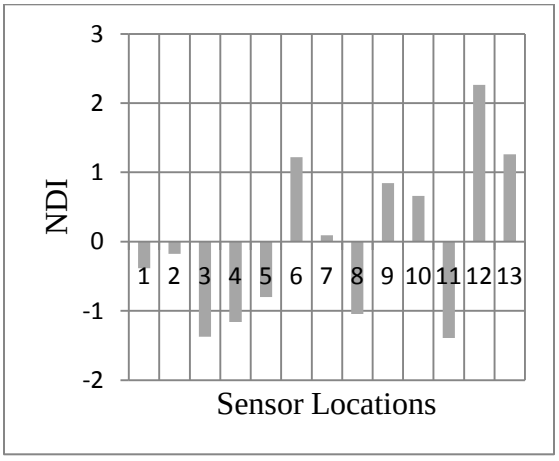

5.17(b): 17 shear connectors

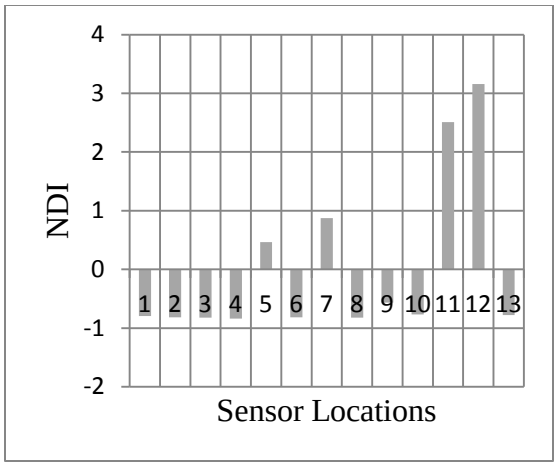

5.17(c): 13 shear connectors

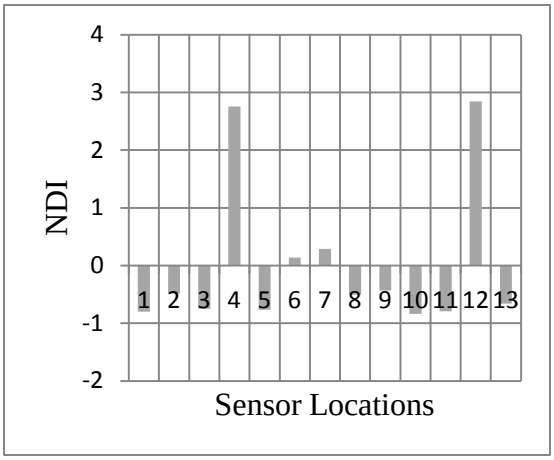

5.17(d): 9 shear connectors

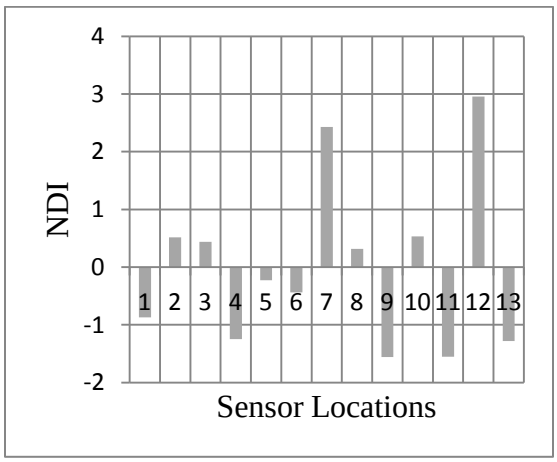

5.17(e): 7 shear connectors

Figure 5.17: Normalized damaged index plots

5.5 Summary

This chapter presented the results of the experimental push-off test and the results of dynamic tests obtained from five experimental concrete composite beam models each with different number and spacing of shear connectors as described in section 4.2.

The results of push-off test shows that the capacity of the shear connectors were reduced by average of 1.5kN at each shear connector cross-section after accelerating corrosion to 15% mass loss. This was done to understand by how much the shear connectors used in

experimental composite beams will be damaged after accelerating corrosion to 15% mass loss. The shear connectors in the experimental composite beams were also damaged by the same amount.

The modal tests were successfully executed and from the modal analysis results it was observed that the modal parameters and FRFs were different for each beam in an expected trend. This is due to the fact that degree of composite action between prestressed concrete beam and concrete slab depends on the number of shear connectors. The following are the summary of observations:

- By comparing all beams before shear connectors were damaged, the results shows that a beam with large number of shears connectors produce high frequencies and high amplitudes of FRFs compared to the one with less number of shear connectors. This was expected on the fact that the stiffness of the concrete composite beam increase as the number of shear connectors increases and stiffness is direct proportional to natural frequency. The FRFs peaks and natural frequencies of the 2^{nd} and 3^{rd} mode showed high sensitivity on the number of shear connectors. The FRFs peaks and natural frequencies of the 1^{st} mode did not show good trend. The only reason for this unexpected result might be due to construction problems (i.e. compaction) especially for '17' and '21' shear connectors beam because of less spacing between the shear connectors. On the other hand, damping ratio showed inconsistent results. The reason for such inconsistency is that damping is difficult to evaluate accurately due to measurement errors and uncertainties.

- After the shear connectors were damaged all beams showed similar results. In the FRFs, the frequency peaks shifted to the left and the peaks amplitudes changed, indicating the existence of damage. The natural frequencies generally dropped. The 1^{st} flexural natural frequencies experienced minimum or almost no changes compared to 2^{nd} and 3^{rd} flexural natural frequencies. Changes in the mode shapes were also observed. MAC values obtained for all beam are between 0.9 and 1, this means the mode shapes are similar but there is no perfect correlation.

- In an attempt to locate regions with damaged shear connectors. The COMAC, change of flexibility method, change of curvature and strain energy method were used. All these methods showed positive and negative results. Using only the modal displacements of the 1^{st} and 2^{nd} bending mode shape, the change of flexibility method showed minimum negative results compared to other methods in locating regions with damaged shear connectors. This might be because this method includes the influence of both the mode shapes and natural frequencies.

CHAPTER 6

CONCLUSIONS AND RECOMMENDATIONS

6.1 Summary and Conclusions

Concrete composite bridges consisting of pre-cast prestressed beams and a cast *in-situ* slab are one of the most common types of bridges in service worldwide for short to medium spans. The use of pre-cast beams results in cost savings as it reduce the need for formwork during construction and shorter construction period can be achieved, thus minimizing the impact on the environment. In this kind of bridges the slab is connected to the beams using shear connectors.

Most bridge management systems still rely on visual inspections for condition assessment, this technique depends mostly on the decisions of the bridge inspectors. Therefore, even for similar bridge conditions, a large variation in the results obtained can be expected. By using this technique, damage in inaccessible parts of the structure such as shear connectors in concrete composite bridges will remain undetected until it is expensive to repair or catastrophic failure occurs. However, there are some localized non-destructive techniques that can be applied for detecting damaged shear connectors in bridges. These include ultrasonic techniques, radar method, impact testing, magnetic based methods and proof load tests. Nevertheless, these techniques are limited to small areas, time consuming, can only detect damage on or near the surface of the structure and require prior knowledge of the damaged location.

The main objective of this work was to investigate experimentally the effectiveness of dynamics-based techniques in assessing the condition of shear connectors in concrete composite bridges based on measurements taken from the surface of the deck slab. In this research, shear links of 8mm bars extended from beam to the slab were used to stimulate shear connectors in real bridges. The experimental work involved building five concrete composite beam models each with different number of shear connectors ranging from number of shear connectors which provide nearly full composite action (CASE A) to

other four cases which provide partial composite action (CASE B1 to B4). The number of shear connectors obtained in the design for full composite action (CASE A) was 21 spaced at 92mm apart. For partial composite action, the number of shear connectors was 17 spaced at 115mm (CASE B4), 13 spaced at 155mm (CASE B3), 9 spaced at 230mm (CASE B2) and 7 spaced at 310mm (CASE B1). The average concrete compressive strength for the slabs was 30MPa and that of the beams (i.e. web) was 50MPa.

The testing procedure consisted of measuring the dynamic properties in both the undamaged and damaged experimental models. Damage was introduced by accelerating corrosion to a group of shear connectors near the supports in each composite beam model. The specimens were damaged by accelerating corrosion to 15% mass loss of the shear connectors using Faraday's equation. Dynamic test was then repeated for each beam to detect the artificial damage of shear connectors by investigating changes of the dynamic properties such as frequencies, mode shapes, damping ratios and frequency response functions. The location 'near the supports' was chosen because shear connectors in these locations are vulnerable to corrosion in real bridges. In addition push-off test was conducted in order to determine the capacity of the shear connectors in undamaged and damaged state. The results of push-off test shows that the capacity of the shear connectors were reduced by average of 1.5kN at each shear connector cross-section or 3kN for each shear connector after accelerating corrosion to 15% mass loss.

The modal tests were successfully executed and from the modal analysis results it was observed that a beam with large number of shear connectors produce high frequencies and high amplitudes of FRFs compared to the one with less number of shear connectors. This result was expected due to the fact that the stiffness of the composite beam which depends on the degree of composite action increase as the number of shear connectors increases and stiffness is direct proportional to natural frequency. The FRFs peaks and natural frequencies of the 2^{nd} and 3^{rd} mode showed high sensitivity on the number of shear connectors. The FRFs peaks and natural frequencies of the 1^{st} mode did not show good trend, the only reason for this unexpected result might be due to construction problems (i.e. compaction) especially for '17' and '21' shear connectors composite beam

because of small spacing between the shear connectors. On the other hand, damping ratio showed inconsistent results. The reason for such inconsistency like other researchers concluded is that damping is difficult to evaluate accurately due to measurement errors and uncertainties.

After the shear connectors were damaged all beams showed similar results. In the FRFs, the frequency peaks shifted to the left and the peaks amplitudes changed, indicating the existence of damage. The natural frequencies generally dropped. The 1st flexural natural frequencies experienced minimum or almost no changes compared to 2nd and 3rd flexural natural frequencies. Changes in the mode shapes were also observed. MAC values obtained for all beam are between 0.9 and 1, this means the mode shapes are similar but there is no perfect correlation.

In an attempt to locate regions with damaged shear connectors, the COMAC, change of flexibility, change of curvature and strain energy method were used. All these methods showed positive and negative results. Using only the modal displacements of the 1st and 2nd bending mode shape, the change of flexibility method showed minimum negative results compared to other methods in locating regions with damaged shear connectors. This might be because this method includes the influence of both the mode shapes and natural frequencies.

Overall, it can be concluded that dynamics-based techniques can be used to assess the conditions of shear connectors in concrete composite bridges consisting of pre-cast prestressed beams and a cast *in-situ* slab by only taking vibration measurements from the surface of the accessible deck slab. As there are some discrepancies in the methods used to detect and locate regions with damaged shear connectors, a combination of some methods may provide the optimum chance of accurate damage detection and localization. In testing real structures, it is suggested that sensors should be well distributed to get a rough estimate on the existence and location of damage and then additional test should be carried out with densely distributed sensors on the suspected damage zone in order to get more accurate results.

6.2 Recommendations

This research focused on the use of dynamics-based techniques is assessing the condition of shear connectors in concrete composite bridges consisting of pre-cast prestressed beams and a cast *in-situ* slab based on the vibration measurements taken from the surface of the accessible deck slab. Further research is recommended to make these techniques easily applicable in real composite bridges. The purpose of this section is therefore to focus on the issues that should be addressed by future researchers to make use of these techniques as a practical tool for detection and localization of regions with damaged shear connectors in concrete composite bridges.

First of all, mode shape plays an important role in damage detection and localization. Since the number and spacing of sensors are critical to getting accurate mode shapes, it is recommended that studies on sensitivity of number or spacing between sensors to number or spacing between shear connectors in concrete composite bridges be carried out. This will help minimize errors that might be caused by inaccurate modal displacements of mode shapes.

Secondly, the effect of prestressing force on the dynamic performance of structures is still not well understood. The limited amounts of literature available are for structures that are not composite. Since concrete composite bridges consist of pre-cast prestressed beams and a cast *in-situ* slab, it is recommended that studies on the effect of prestressing force on dynamic performance of concrete composite bridges be carried out. In addition, studies should consider different pretressing force, different number of prestressing bars and different length of the beam.

Thirdly, the methods used in this research to localize regions with damaged shear connectors are the COMAC, change of flexibility method, change of curvature and strain energy method. All these methods showed positive and negative results. Some modifications need to be done in these methods so that it is be possible to clarify if the changes in parameters are due to actual damage and not other factors such as errors from measurements or noise. In addition, studies need to be done to come up with guidelines

for determining number of vibration mode shapes that are enough to be involved in these algorithms for damage detection and localization.

Fourthly, in this research FRFs was found to be a good indicator of degree of composite action between beam and slab with regard to the number of shear connectors and existence of damaged shear connectors on each beam model. FRFs are direct measurement and have advantage over modal data as they contain information about all the modes the structure possesses and not only that for the frequency range measurement. It is recommended that studies need to be done on how to localize regions with damaged shear connectors using FRFs.

Fifthly, in localization of damage in real bridges, it will be only possible to localize damaged regions of the structure. A challenge will be on how to say damage is on concrete (i.e. Crack), normal reinforcement or shear connectors at that same region throughout the section of the structure. Studies need to be done on how to differentiate damages that are on shear connectors versus damage that are on other part of structure at the same section using vibration measurements.

Finally, it is also very important to investigate the effects of loss in composite action on the load carrying capacity of the concrete composite bridges. This will help in determining the stage when regions with damaged shear connectors need to be repaired or other measures are taken before it is expensive to repair or catastrophic failure of the bridge occurs.

.

REFERENCES

Abdul Razak, H. & Choi, F. C., 2001. The effect of corrosion on the natural frequency and modal damping of reinforced concrete beams. *Engineering Structures*, 23(9), pp. 1126-1133.

Abendroth, R. E., Klaiber, F. W. & Shafer, M. W., 1995. Diaphragm effectiveness in prestressed-concrete girder bridges. *Structural Engineering*, 121(9), pp. 1362-1369.

Al-Darzi, S. Y. K. & Chen, A., 2006. Conceptual design and analysis of steel-concrete composite bridges: State of Art. *Steel Structures*, Volume 6, pp. 393-407.

Alvandi, A. & Cremona, C., 2006. Assessment of vibration-based damage identification techniques. *Sound and Vibration*, Volume 292, pp. 179-202.

Aribert, J. M., 1993. *Application of a numerical model for composite beams with partial shear connection.* Reston, Va., 742757, Proc., Engrg. Found. Con! on Composite Constuction in Steel and Concrete 11, ASCE.

Barroso, L. R. & Rodriguez, R., 2004. Damage detection utilizing the damage index method to a benchmark structure. *Engineering Mechanics ASCE*, Volume 130, pp. 142-151.

BS, 1994_2_2005. *Eurocode 4 - Design of composite and concrete structures ; Part 2: General rules snd rules for bridges.* s.l.:British standard.

Cai, S. C. S. & Avent, R. R., 2008. *Assessing the Needs for Intermediate Diaphragms in Prestressed Concrete Bridges*, Baton Rouge, LA 70808: Report No. FHWA/LA.06/420 ; Conducted for Louisiana Department of Transportation and Development Louisiana Transportation Research Center ; Available online: http://www.ltrc.lsu.edu/pdf/2008/FR_420.pdf.

Carbone, V. I., Mancini, G. & Tondolo, F., 2008. Structural behavior with reinforcement corrosion. *Tailor Made Concrete Structures - Walraven & Stoelhorst*, Volume Taylor & Fransis Group, London, ISBN 978-0-415-47535-8.

Chao, S.-H., Naaman, A. E. & Parra-Montesinos, G. J., 2009. Bond behaviour of reinforcing bars in tensile strain-hardening fiber-reinforced cement composites. *ACI Structural*, 106(6).

Ching, J. & Beck, J. L., 2004. Bayesian analysis of the Phase II IASC-ASCE structural health monitoring experimental benchmark data. *Engineeering Mechanics*, 130(10), pp. 233-1244.

Chopra, A. K., 1995. *Dynamics of Structures, Theory and application to Earthquake Engineering.* New Jersey: Prentice Hall .

Clough, R. W. & Penzien, J., 1993. *Dynamics of Structures.* New York: McGraw-Hill.

Dackermann, U., 2010. *Vibration-based damage identification methods for civil engineering structures using artificial neural networks,* s.l.: PhD Thesis, University of Technology Sydney. Available online (21 June 2012).

Dilena, M. & Morassi, A., 2003. A Damage Analysis of Steel-Concrete Composite Beams Via Dynamic Methods: Part II. Analytical Models and Damage Detection. *Vibration and Control,* Volume 9, pp. 529-565.

Dilena, M. & Morassi, A., 2008. Vibrations of steel–concrete composite beams with partially degraded connection and applications to damage detection. *Sound and Vibration,* Volume 320, p. 101–124.

Doebling, S. W., Farrar, C. R., Prime, M. B. & Shevitz, D. W., 1996. *Damage Identification and Health Monitoring of Structural and Mechanical Systems from Changes in their Vibration Characteristics: A Literature Review,* s.l.: Research Rep. No. LA-13070-MS, ESA-EA, Los Alamos National Laboratory, N.M..

Doubling, S. W., Farrar, C. R. & Prime, M. B., 1998. Summary review of vibration-based damage identification methods. *Shock and Vibration Digest,* 30(2), pp. 91-105.

Dutta, A. & Talukdar, S., 2004. Damage detection in bridges using accurate modal parameters. *Finite Element Analysis and Design,* Volume 40, p. 287 – 304.

Estes, A. C. & Frangopol, D. M., 2003. Updating bridge reliability on bridge management system using visual inspection results. *Bridge Engineering,* 8(6), p. 374 – 382.

Ewins, D. J., 2000. *Modal Testing: theory, practice and application.* 2 ed. London, England.: s.n.

Ewins, D. J., 2001. Modal Analysis, Experimental. In: D. Ewins, S. S. Rao & S. Braun, eds. *Encyclopedia of Vibration.* London: Academic Press.

Farrar, C. R. & Jauregui, D. A., 1997. Comparative study of damage identification algorithms applied to a bridge. 1 Experiment. *Smart Material Structures,* Volume 7, p. 704–719.

Frangopol, D. M., Lin, K.-Y. & Estes, A. C., 1997. Reliability of reinforced concrete gieders under corrosion attack. *Structural Engineering,* 123(3), pp. 286-297.

Friswell, M. I. & Mottershead, J. E., 1995. *Finite element model updating in structural dynamics.* Netherlands: Kluwer Academic Publishers.

Gajanan, M. S., 1979. *Handbook of Composite Construction Engineering.* 1 ed. London: Melborne.

Gattulli, V. & Chiaramonte, L., 2005. Condition assessment by visual inspection for bridge management system. *Computer-Aided Civil and Infrastructure Engineering,* Volume 20, pp. 95-107.

Gene, F., Sirca, J. & Hojjat, A., 2005. Cost optimization of prestressed concrete bridges. *Structural Engineering,* 131(3), p. 380–388.

Girhammar, U. A. & Pan, D., 1993. Dynamic analysis of composite members with interlayer slip. *Solids and Structures,* 30(6), pp. 797-823.

Girhammar, U. A., Pan, D. H. & Gustafsson, A., 2009. Exact dynamic analysis of composite beams with partial interaction. *Mechanical Sciences,* Volume 51, pp. 565-582.

Gutkowski, R. et al., 2008. Laboratory tests of composite wood–concrete beams. *Construction and Building Materials,* Volume 22, p. 1059–1066.

Humar, J., Bagchi, A. & Xu, H., 2006. Performance of Vibration-based Techniques for the identification of Structure Damage. *SAGE Publication,* 5(3), pp. 215-227.

Huth, O., Maeck, J., Kilic, N. & Motavalli, M., 2005. Damage identification using modal data: experience in presressed concrete bridge. *Structural Engineering,* 131(12), pp. 1898-1910.

Johnson, R. P., 1994. *Composite structures of steel and concrete.* 2 ed. vol.1. Oxford, UK: Blackwell Scientific Publication, Ltd.

Johnson, R. P. & May, I. M., 1975. Partial-interaction design of composite beams. *The Structure Engineering, London, U.K,* 53(8), pp. 305-311.

Kim, J. T., Ryu, Y. S., Cho, H. M. & Stubbs, N., 2002. Damage Identification in beam type structures: frequency-based method vs mode-shape-based method. *Engineering Structures,* 25(1), p. 57–67.

Kim, J. T. & Stubbs, N., 2003. Crack detection in beam-type structures using frequency data. *Sound and Vibration,* 259(1), pp. 145-160.

Koch, S. & Roberts-Wollmann, C. L., 2008. *Design Recommendations for the Optimized Continuity Diaphragm for Prestressed Concrete Bulb-T Beams,* s.l.: Report No FHWA/VTRC 09-CR1; done under contract for the Virginia Department of Transportation, Virginia Transportation Research Council; Availble online: http://www.virginiadot.org/vtrc/main/online_reports/pdf/09-cr1.pdf.

Kumar, A., 1998. *Composite concrete bridge superstructure.* 1 ed. s.l.:British Cement Association.

Li, H., Li, D. & Song, G., 2004. Recent applications of fiber optic sensors to health. *Engineering Structures,* 26(11), pp. 1647-1657.

Lioyd, R. M. & Wright, H. D., 1990. Shear connection between composite slabs and steel beams. *Constructional Steel Res,* Volume 15, pp. 255-285.

Li, Y. Y., 2010. Hypersensitivity of strain-based indicators for structural damage identification: a review. *Mechanical Systems and Signal Processing,* Volume 24, pp. 653-664.

Maia, N. M. M. & Silva, J. M. M., 1997. *Theoretical and experimental modal analysis.* Great Britain: Research Studies Press Ltd.

McCann, D. M. & Forde, M. C., 2001. Review of non-destructive methods in the assessment of concrete and masonry structures. *NDT & International,* Volume 34, pp. 71-84.

Nigel, R. H., 2003. *Prestressed concrete bridges, Design and Construction.* 1 ed. London: Thomas Telford.

Oehlers, D. J., Nguyen, N. T., Ahmed, M. & Bradford, M. A., 1997. Partial Interaction in Composite Steel and Concrete Beams with Full Shear Connection. *Constructional Steel Research,* Volume 41, pp. 235-248.

Pandey, A. K. & Biswas, M., 1994. Damage detection in structures using changes in flexibility. *Sound and Vibration,* 169(1), pp. 3-17.

Pandey, A. K., Biswas, M. & Samman, M. M., 1991. Damage detection from changes in curvature mode shapes. *Sound and Vibration,* 145(2), pp. 321-332.

Parkash, S., Goel, R. & Kumar, R., 2006. Fatigue performance of prestressed concrete bridges: State-of-the art. *Advances in Bridge Engineering,* 24(25), p. 479–486.

Queiroz, F. D., Vallasco, P. S. & Nethercot, D. A., 2006. Finite element modeling of composite beams with full and partial shear connection. *Construction Steel Research,* 63(4), pp. 505-521.

Racliffe, C. P., 1997. Damage detection using a modified Laplacian Operator on mode shape data. *Sound and Vibration,* 204(3), pp. 505-517.

Richardson, M. & Schwarz, B., 2003. Modal parameter estimation from operating data. *Sound and Vibration.*

Riveros, C. A., Garcia, E. F. & Builes, M. A., 2010. A numerical approach for fault detection in beam-like structures using modal strain energy. *Revista EIA, ISSN 1794-1237 Número 13,* pp. 171-184.

Ryall, M. J., Parke, G. A. R. & Harding, J. E., 2003. *Manual of Bridge Engineering.* London: Thomas Tedford Publishing.

Salane, H. J. & Baldwin, J. W., 1990. Identification of modal properties of bridges. *Structural Engineering,* 116(7).

Sazonov, E. & Klinkhachorn, P., 2005. Optimal spatial sampling interval for damage detection by curvature or strain energy mode shapes. *Sound and Vibration,* Volume 285, pp. 783-801.

Seracino, R., Lee, C. T., Lim, T. C. & Lim, J. Y., 2004. Partial interaction stresses in continuous composite beams under serviceability loads. *Construction Steel Research,* Volume 60, p. 1525–1523.

Shih, Y. C., Tsuei, Y., Allemang, R. & Brown, D., 1989. Complex mode indicator function and its application to spatial domain parameter estimation. *Mechanical Systems and Signal Processing,* 2(4), pp. 367-377.

Sibanda, B., Moyo, P. & Beushausen, H., 2008. Vibration based assessment of shear connectors in concrete composite bridges. *Concrete Repair, Rehabilitation and Retrofitting II – Alexander et al (eds) © 2009 Taylor & Francis Group, London, ISBN 978-0-415-46850-3.*

Silva, J. M. M., 2001. Measurement techniques. In: D. Ewins, S. S. Rao & S. Braun, eds. *Encyclopedia of Vibration.* London: Academic Press.

Stratford, T. J. & Burgoyne, C. J., 1999. Lateral Stability of long precast concrete beams. Proceedings of the Institution of Civil Engineers. *Structures and Buildings,* Volume 124, p. 169 – 180.

Stubbs, N. & Kim, J. T., 1994. *Field verification of a nondestructive damage localization and severity estimation algorithm,* s.l.: Texas A&M University report for New Mexico State University.

Tamberg, K. G., 1968. *Aspects of torsion in concrete structure design, In Torsion of.* 1 ed. Michigan, USA: ACI Publications.

Vinson, J. R. & Sierakowski, R. L., 1990. *The behavior of structures composed of composite materials.* s.l.:Mechanics of structural systems.

Wahab, M. A. & De Roeck, ,. G., 1999. Damage detection in bridges using modal curvatures: Application to a real damage scenario. *Sound and Vibration,* 2(227), p. 217–235.

Wai, S. H., 2009. *Damage assessment in structures using vibration characteristics" PhD Thesis, Queensland University of Technology,* s.l.: Available online: http://eprints.qut.edu.au/30319/1/Hoi_Shih_Thesis.pdf.

Wang, Y. C., 1998. Deflection of Steel-Concrete Composite Beams with Partial Shear Interaction. *Structural Engineering,* 124(10), pp. ©ASCE, ISSN 0733-9445/98/0010-1159-1165..

Wirtu, L. B., Nicholas, H. & Massoud, S., 2011. Comparative study of broadband damage localization methods applied to test data. *Ocean Engineering,* Volume 38, p. 329–340.

Yaoting, Z. & Ruige, L., 2007. Natural Frequency of Full-Prestressed Concrete Beam. *ISSN 1006-4982,* 13(5), pp. 354-359.

Yong, X., Hong, H. & Deeks, A. J., 2006. Dynamic assessment of shear connectors in slab-girder bridges. *Engineering Structures,* Volume 29, p. 1475–1486.

Zivanovic, S., Pavic, A. & Reynolds, P., 2007. Finite element modeling and updating of a lively footbridge: the complete process. *Sound and Vibration,* Volume 301, pp. 126-145.

APPENDICES

APPENDIX 1

Compressive Cube Strength (28days) for Beam (target is 50MPa) W/C =0.45

Cube ID	Mass (g)			Cube Density (Kg/m^3)			Mean density (Kg/m^3)		
	1	2	3	1	2	3	1	2	3
Cube 1	2460	2480	2500	2460	2480	2500	2465	2481.7	2491.7
Cube 2	2465	2490	2485	2465	2490	2485			
Cube 3	2470	2475	2490	2470	2475	2490			
Total Average	2479.4			2479.4			2479.5		

Cube ID	f_{cu} (MPa)			Mean f_{cu} (MPa)			Standard deviation		
	1	**2**	**3**	**1**	**2**	**3**	**1**	**2**	**3**
Cube 1	51.2	54.5	54.8	52.5	53.9	54.5	1.2	1	0.9
Cube 2	53.5	54.4	55.2						
Cube 3	52.7	52.8	53.4						
Total Average				53.6			1		

Compressive Cube Strength (28days) for Slab (target is 30MPa) W/C =0.7

Cube ID	Mass (g)			Cube Density (Kg/m^3)			Mean density (Kg/m^3)		
	1	**2**	**3**	**1**	**2**	**3**	**1**	**2**	**3**
Cube 1	2435	2450	2410	2435	2450	2410	2430	2441.7	2408.3
Cube 2	2425	2440	2410	2425	2440	2410			
Cube 3	2430	2435	2405	2430	2435	2405			
Total Average	2426.7			2426.7			2426.7		

Cube ID	**f_{cu} (MPa)**			**Mean f_{cu} (MPa)**			**Standard deviation**		
	1	**2**	**3**	**1**	**2**	**3**	**1**	**2**	**3**
Cube 1	30.2	32.7	32.8	31.4	32.2	33.3	1.1	1.2	0.5
Cube 2	31.8	33.1	33.8						
Cube 3	32.2	30.8	33.4						
Total Average				32.3			0.9		

APPENDIX 2: DESIGN CALCULATIONS FOR EXPERIMENTAL BEAM

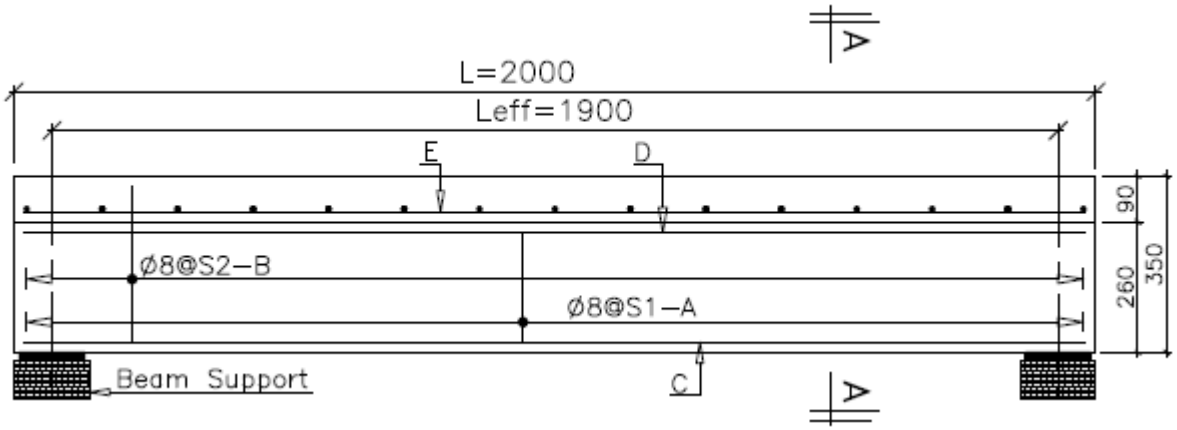

Longitudinal section of a beam

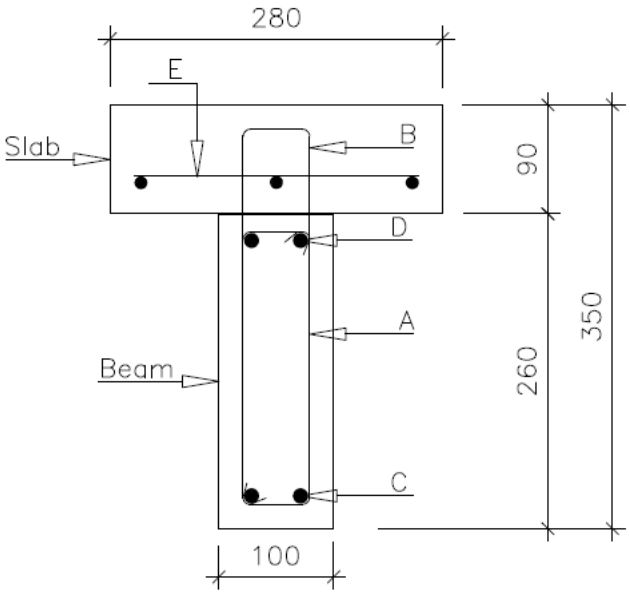

Section A-A

KEY

A – Shear Links (8mm diameter bars) for the beam.

B – Shear connectors (8mm diameter bars) extended from the beam to the slab.

C – Beam bottom reinforcement (10mm)

D – Beam top reinforcement (10mm)

E – A mesh of 10mm as slab reinforcement.

Compressive strength of slab (f_{cu}) $= 30$MPa

Modulus of Elasticity for slab concrete (E_{sc}) $= 28$GPa (TMH7 part 3; Table 3)

Compressive strength of beam (f_{cu}) $= 50$MPa

Modulus of Elasticity for beam concrete (E_{bc}) $= 34$GPa (TMH7 part 3; Table 3)

Characteristic yield strength of reinforcement $(f_y) = 450$MPa

Modulus of Elasticity for reinforcing steel (E_s) $= 200$GPa (TMH7 part 3; 2.3.2.2)

8.1 STRESSES FOR NON-COMPOSITE ACTION – BEAM ONLY

- **Position of neutral axis for the beam** (y_b)

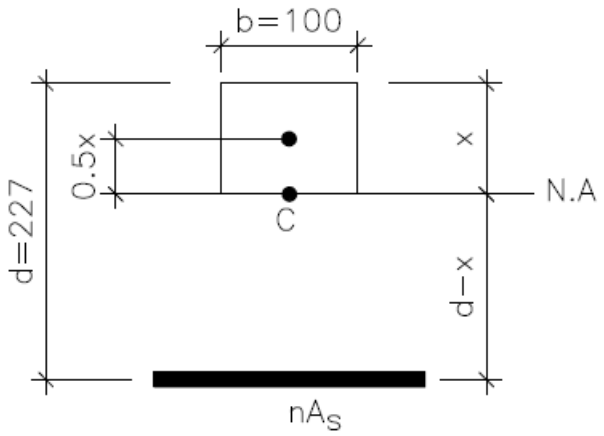

$$n = \frac{\text{Modulus of Elasticity for steel}}{\text{Modulus of Elasticity for beam concrete}} = \frac{E_s}{E_{bc}} = \frac{200}{34} \approx 5.88$$

For neutral axis; $\quad 0.5bx^2 + nA_sx - nA_sd = 0$

and $A_s = 157.1\text{mm}^2$ (2T10)

$$0.5 \cdot 100 \cdot x^2 + 5.88 \cdot 157.1x - 5.88 \cdot 157.1 \cdot 227 = 0$$

$$x^2 + 18.5x - 4193.8 = 0$$

$$x = \frac{-18.5 \pm \sqrt{18.5^2 + 4 \cdot 4193.8}}{2} = \frac{-18.5 + 130.8}{2} \approx 56.2\text{mm from the top}$$

Therefore, the position of neutral axis(y_b) from the bottom is 260 – 56.2 =203.8mm

- **Ultimate moment resistance for the beam only**(M_{ub})

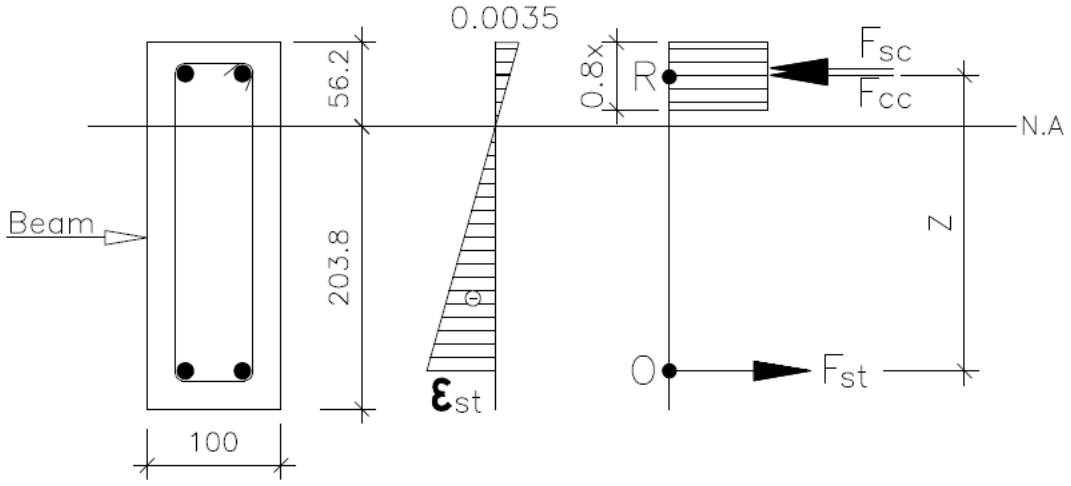

$$\text{Concrete cover (c)} = 20\text{mm} \;; \quad d' = 20 + 8 + 0.5(10) = 33\text{mm}$$

$$d = 260 - d' = 227\text{mm} \;; \quad A'_s = 157.1\text{mm}^2 \text{ (2T10)}$$

$$z = d - 0.5(0.8x) = 227 - 0.5 \cdot (0.8 \cdot 56.2) \approx 204.5\text{mm}$$

$$F_{cc} = \frac{0.67 f_{cu}}{\gamma_c} b(0.8x) = \frac{0.67 \cdot 50}{1.5} \cdot 100 \cdot (0.8 \cdot 56.2) = 100410.7\text{N}$$

$$F_{sc} = F_{st} = 0.87 f_y A_s = 0.87 \cdot 450 \cdot 157.1 = 61504.65\text{N}$$

- Take Moment about point O (for compression)

$$M_{ub} = F_{cc} z + F_{sc} \cdot (d - d') \;; \quad 10\text{mm} = \text{diameter of steel}$$

$$= 100410.7 \cdot 204.5 + 61504.65 \cdot (227 - 33)$$

$$= 32465890.3\text{Nmm} \approx 32.5\text{KNm}$$

- Take Moment about point R (for Tension)

$$M_{ub} = F_{st} z + F_{sc} \cdot (0.8x - d')$$

$$= 61504.65 \cdot 204.5 + 61504.65 \cdot (0.8 \cdot 56.2 - 33)$$

$$= 13313296.5 \approx 13.3\text{KNm} < 32.5\text{KNm} \;; \quad \therefore \; M_{ub} = 13.3\text{KNm}$$

- **Maximum concentrated load (P) that can be applied at the centre of the beam**

  - Self weight of the slab = $26 \cdot 0.09 \cdot 0.28 \approx 0.6552\text{KN/m}$
  - Self weight of the beam = $26 \cdot 0.26 \cdot 0.1 \approx 0.676\text{KN/m}$

$$\text{Total self weight of concrete(D)} \approx 1.33\text{KN/m}$$

  - Considering SLS

Maximum bending moment that can be caused by the dead load (M_D)

$$M_{Db} = \frac{DL^2}{8} = \frac{1.33 \cdot 1.8^2}{8} = 0.54\text{KNm}$$

$$M_{ub} = M_D + M_L$$

Where M_L is the Maximum bending moment that can be caused by the live load (P)

$$M_L = M_{ub} - M_D = 13.3 - 0.54 = 12.76\text{KNm}$$

$$M_L = \frac{PL}{4} \rightarrow P = \frac{4 \cdot M_L}{L} = \frac{4 \cdot 12.76}{1.8} \approx 28.4\text{KN}$$

$$\text{Thus,} \quad P = 28.4\text{KN}$$

- **Normal stress(σ) in the beam**

$$\text{Moment of inertia (I)} = \frac{bh^3}{12} + A_c(y_b - 0.5h)^2 + A_s y_b^2 + A_s(x - d')^2$$

$$= \frac{100 \cdot 260^3}{12} + (260 \cdot 100)(203.8 - 0.5 \cdot 260)^2 + 157.1 \cdot 203.8^2 + 157.1 \cdot (56.2 - 33)^2$$

$$I = 294683724.7\text{mm}^4$$

$$\sigma_b = -\frac{M_{ub} y_b}{I} = -\frac{13.3 \cdot 10^6 \cdot 203.8}{294683724.7} = -9.2\text{MPa}$$

$$\sigma_t = \frac{M_{ub} x}{I} = \frac{13.3 \cdot 10^6 \cdot 56.2}{294683724.7} = 2.54\text{MPa}$$

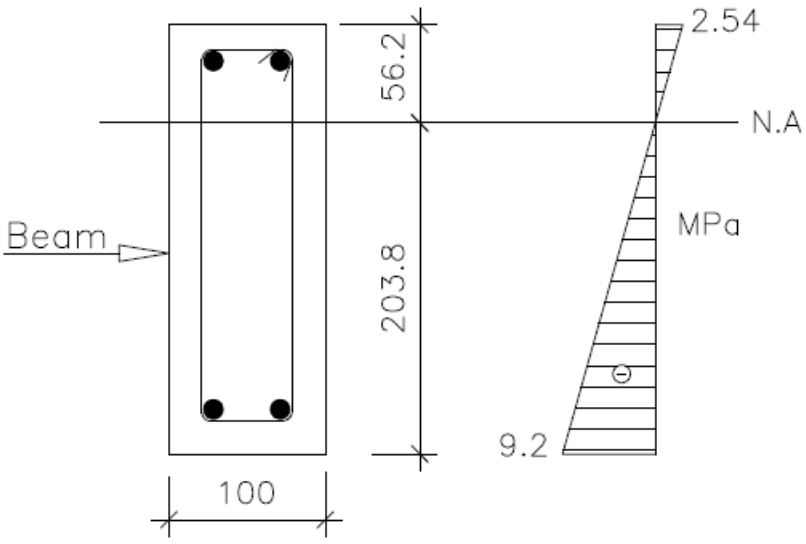

- **Design of Shear reinforcement for beam**

Shear force (V_{Ed}) due to ultimate load $= \frac{1.2 \cdot 1.33 \cdot 1.8}{2} + \frac{1.5 \cdot 28.4}{2} \approx 22.7\text{KN}$

- Crushing strength($V_{Rd,max}$)

  Assume $\theta = 22^{\circ}$ and Ø8mm for links

  $V_{Rd,max} = 0.124 b_w d\left(1 - {}^{f_{cu}}/_{250}\right) f_{cu}$

  $= 0.124 \cdot 100 \cdot 227\left(1 - {}^{40}/_{250}\right)40 = 94577.3\text{N} = 94.6\text{KN}$

  $V_{Rd,max} = 94.6\text{KN} (> V_{Ed} = 22.7\text{KN})$ OK

- Minimum Shear links($V_{Rd,max}$)

$\frac{A_{sw,min}}{s} = \frac{0.08 f_{cu}^{0.5} b_w}{f_y} \rightarrow s \leq \frac{A_{sw.min} f_y}{0.08 f_{cu}^{0.5} b_w} = \frac{100.5 \cdot 450}{0.08 \cdot 40^{0.5} \cdot 100}$; $s = 893.8\text{mm}$

- Shear links required($V_{Rd,max}$)

$$\frac{A_{sw}}{s} = \frac{V_{Ed}}{0.78df_y\cot\theta} \rightarrow s \leq \frac{0.78dA_{sw}f_y\cot\theta}{V_{Ed}} = \frac{0.78 \cdot 227 \cdot 100.5 \cdot 450 \cdot 2.5}{21.72 \cdot 10^3}$$

$$s = 921\text{mm}$$

- Maximum spacing of links

$$s \leq 0.75d = 0.75 \cdot 227 = 170.25\text{mm} \text{ ; take } 150\text{mm}$$

Therefore, provide shear links $\emptyset 8 - 150\ ^{c}/_{c}$

8.2. STRESSES FOR NON-COMPOSITE ACTION – SLAB ONLY

- **Ultimate moment resistance for the slab**(M_{us}) – TMH7 Part 3; 3.3.2.3

$$d = 90 - 20 - 0.5(10) = 65\text{mm}$$

$$M_{us} = 0.15f_{cu}bd^2$$

$$M_u = 0.15 \cdot 30 \cdot 280 \cdot 65^2 = 5323500\text{Nmm} \approx 5.32\text{KNm}$$

or $M_{us} = (0.87f_y)A_sz$

$$A_s = 235.7\text{mm}^2 \text{ (3T10)}$$

$$z = \left[1 - \frac{1.1f_yA_s}{f_{cu}bd}\right]d = \left[1 - \frac{1.1 \cdot 450 \cdot 235.7}{30 \cdot 280 \cdot 65}\right] \cdot 65 = 51.1\text{mm}$$

$$M_{us} = \left(0.87f_y\right)A_sz = (0.87 \cdot 450) \cdot 235.7 \cdot 51.1 \cdot 10^{-6} \approx 4.7 < 5.32\text{KNm}$$

Thus, $M_{us} = 4.7\text{KNm}$

- **Maximum concentrated load (P) that can be applied at the centre of the slab**

  - Self weight of the slab = $26 \cdot 0.09 \cdot 0.28 \approx 0.6552\text{KN/m}$

    $$\text{Total self weight of concrete(D)} \approx 0.6552\text{KN/m}$$

  - Considering SLS

    Maximum bending moment that can be caused by the dead load (M_D)

$$M_D = \frac{DL^2}{8} = \frac{0.6552 \cdot 1.8^2}{8} = 0.27\text{KNm}$$

$$M_u = M_D + M_L$$

Where M_L is the Maximum bending moment that can be caused by the live load (P)

$$M_L = M_u - M_D = 5.32 - 0.27 = 5.05\text{KN/m}$$

$$M_L = \frac{PL}{4} \rightarrow P = \frac{4 \cdot M_L}{L} = \frac{4 \cdot 5.05}{1.8} \approx 11.2\text{KN}$$

$$\text{Thus,} \quad P = 11.2\text{KN}$$

- **Position of neutral axis for the slab** (y_s)

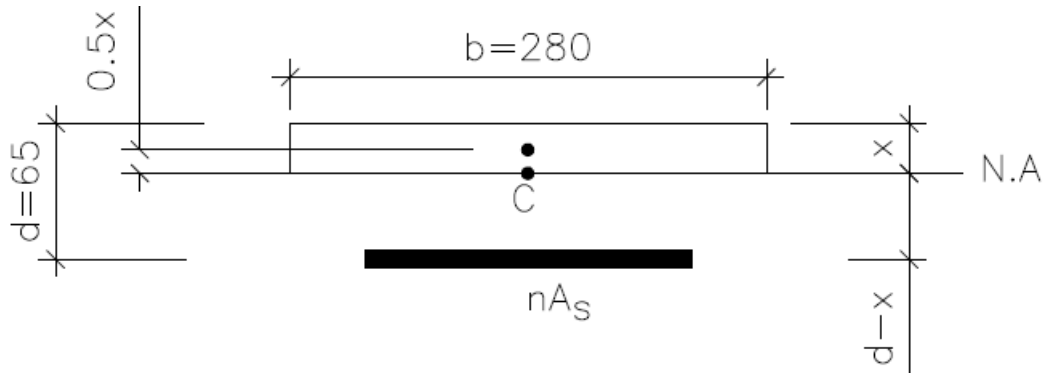

$$n = \frac{\text{Modulus of Elasticity for steel}}{\text{Modulus of Elasticity for slab concrete}} = \frac{E_s}{E_{sc}} = \frac{200}{28} \approx 7.1$$

For neutral axis; $0.5bx^2 + nA_s x - nA_s d = 0$

and $A_s = 235.7\text{mm}^2$ (3T10)

$$0.5 \cdot 280 \cdot x^2 + 7.1 \cdot 235.7x - 7.1 \cdot 235.7 \cdot 65 = 0$$

$$x^2 + 12x - 777 = 0$$

$$x = \frac{-12 \pm \sqrt{12^2 + 4 \cdot 777}}{2} = \frac{-12 + 57}{2} \approx 22.5 \text{ mm from the top}$$

Therefore, the position of neutral axis(y_s) from the bottom is 90 – 22.5 =67.5mm

- **Normal stress(σ) in the slab**

$$\text{Moment of inertia (I)} = \frac{bh^3}{12} + A_c(y_s - 0.5h)^2 + A_s y_s^2$$

$$= \frac{280 \cdot 90^3}{12} + (90 \cdot 280)(67.5 - 0.5 \cdot 90)^2 + 235.7 \cdot 67.5^2$$

$$I = 30841408.13\text{mm}^4$$

$$\sigma_b = -\frac{M_{us} y_b}{I} = -\frac{4.7 \cdot 10^6 \cdot 67.5}{30841408.13} = -10.3\text{MPa}$$

$$\sigma_t = \frac{M_{us} x}{I} = \frac{4.7 \cdot 10^6 \cdot 22.5}{30841408.13} = 3.43\text{MPa}$$

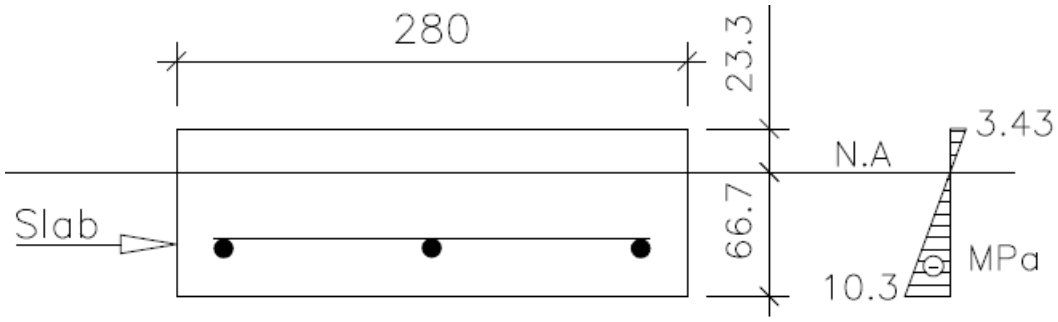

8.3. STRESSES FOR FULL COMPOSITE ACTION

- **Position of neutral axis for the full composite action between beam and slab** (y_c)

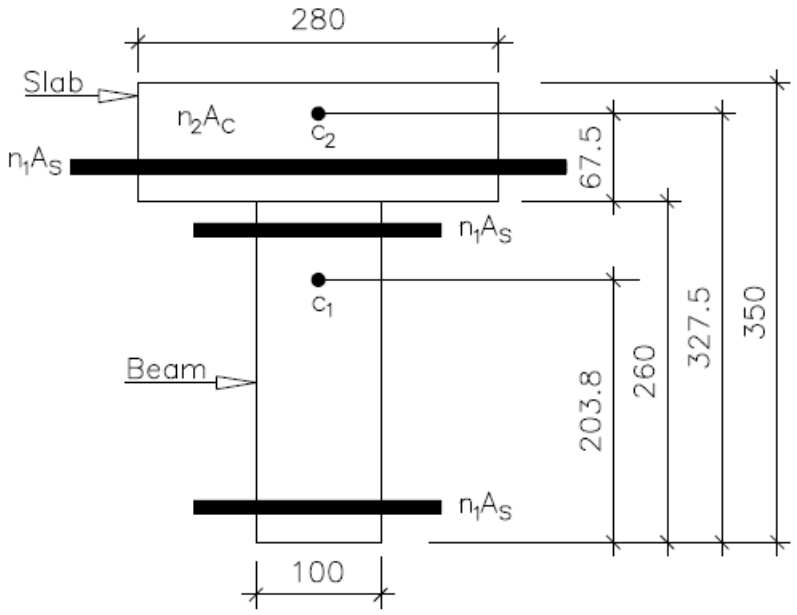

$$n_1 = \frac{E_s}{E_{bc}} = \frac{200}{34} \approx 5.88 \quad \text{and} \quad n_2 = \frac{E_{sc}}{E_{bc}} = \frac{28}{34} \approx 0.82$$

$$A_{bc} = A_c + 2n_1A_s = 260 \cdot 100 + 2 \cdot 5.88 \cdot 157.1 = 27847.5\text{mm}^2$$

$$A_{sc} = n_2A_c + n_1A_s = 0.82 \cdot 90 \cdot 280 + 5.88 \cdot 235.7 = 22050\text{mm}^2$$

Where; A_{bc} = Total area of beam concrete (including area of steel transformed to beam concrete.

A_{sc} = Total area of slab and steel both transformed to beam concrete.

$$y_c = \frac{\sum Ay}{\sum A} = \frac{A_{bc} \cdot y_b + A_{sc} \cdot (h_b + y_s)}{A_{bc} + A_{sc}} = \frac{27847.5 \cdot 203.8 + 22050 \cdot (260 + 67.5)}{27847.5 + 22050}$$

$$= 258.5\text{mm}$$

$$y_c = 258.5\text{mm}$$

- **Ultimate moment resistance of the full composite action** (M_{uc})

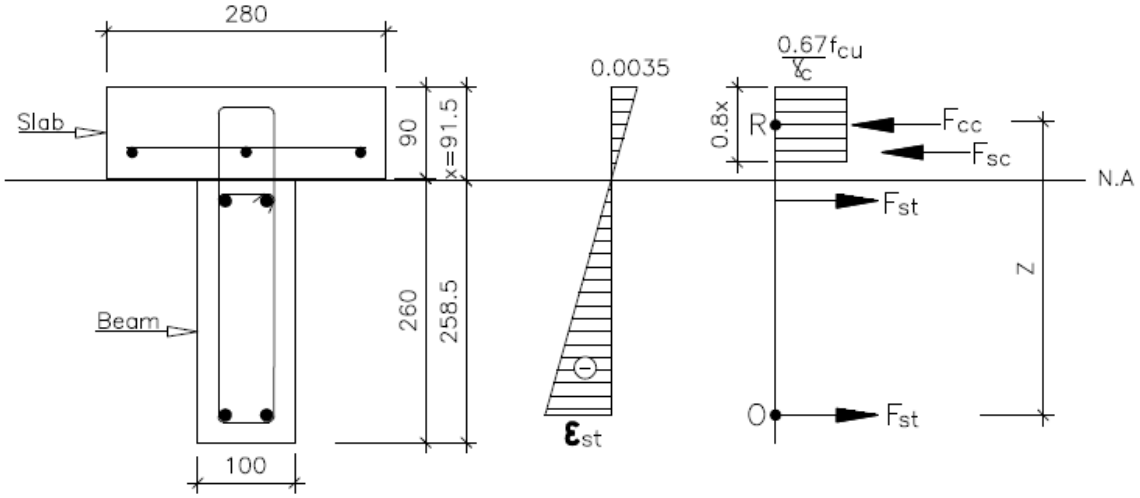

Concrete cover $(c) = 20\text{mm}$; $d = 350 - 20 - 8 - 0.5(10) = 317\text{mm}$

$$z = d - 0.5(0.8x) = 317 - 0.5 \cdot (0.8 \cdot 91.5) = 280.4\text{mm}$$

$$F_{cc} = \frac{0.67f_{cu}}{\gamma_c}\, b(0.8x) = \frac{0.67 \cdot 30}{1.5} \cdot 280 \cdot (0.8 \cdot 91.5) = 274646.4\text{N}$$

$$F_{sc} = 0.87f_yA_s = 0.87 \cdot 450 \cdot 235.7 = 92276.55\text{N}$$

$$F_{st} = 0.87f_yA_s = 0.87 \cdot 450 \cdot 157.1 = 61504.65\text{N}$$

Take Moment about point O (for compression)

$M_{uc} = F_{cc}z + F_{sc} \cdot (260) - F_{st} \cdot (260 - 2c - 10)$; $10\text{mm} = \text{diameter of steel}$

$$= 274646.4 \cdot 280.4 + 92276.55 \cdot (260) - 61504.65 \cdot (260 - 2 \cdot 20 - 10)$$

$$= 88086777.1\text{Nmm} \approx 88.1\text{KNm}$$

Take Moment about point R (for Tension)

$M_{uc} = F_{st}z - F_{sc} \cdot (90 - c - 5 - 0.5 \cdot 0.8x) + F_{st} \cdot (90 + c + 8 + 5 - 0.5 \cdot 0.8x)$

$$= 61504.65 \cdot 280.4 - 92276.55 \cdot (28.4) + 61504.65 \cdot (86.4)$$

$$= 19939251.6\text{Nmm} \approx 20\text{KNm} < 88.1\text{KNm}$$

$$M_{uc} = 20\text{KNm}$$

- **Maximum concentrated load (P) that can be applied at the centre of the beam**

  - Self weight of the slab = $26 \cdot 0.09 \cdot 0.28 \approx 0.6552\text{KN/m}$
  - Self weight of the beam = $26 \cdot 0.26 \cdot 0.1 \approx 0.676\text{KN/m}$

$$\text{Total self weight of concrete(D)} \approx 1.33\text{KN/m}$$

  - Considering SLS

    Maximum bending moment that can be caused by the dead load (M_D)

$$M_D = \frac{DL^2}{8} = \frac{1.33 \cdot 1.8^2}{8} = 0.54\text{KNm}$$

$$M_{uc} = M_D + M_L$$

Where M_L is the Maximum bending moment that can be caused by the live load (P)

$$M_L = M_{uc} - M_D = 20 - 0.54 = 19.46\text{KNm}$$

$$M_L = \frac{PL}{4} \rightarrow P = \frac{4 \cdot M_L}{L} = \frac{4 \cdot 19.46}{1.8} \approx 43.24\text{KN}$$

$$\text{Thus,} \quad P = 43.24\text{KN}$$

- **Normal stresses(σ) in the composite beam**

$$I = \frac{100 \cdot 260^3}{12} + (100 \cdot 260)(128.5)^2 + \frac{280 \cdot 90^3}{12} + (280 \cdot 90)(46.5)^2 + 157.1 \cdot 225.5^2 + 157.1 \cdot 31.5^2 + 235.7 \cdot 26.5^2 = 651662714.3\text{mm}^4$$

$$I = 655593843.8\text{mm}^4$$

$$\sigma_b = -\frac{M_{uc} y_b}{I} = -\frac{20 \cdot 10^6 \cdot 258.5}{655593843.8} = -7.9\text{MPa}$$

$$\sigma_t = \frac{M_{uc} x}{I} = \frac{20 \cdot 10^6 \cdot 91.5}{655593843.8} = 2.8\text{MPa}$$

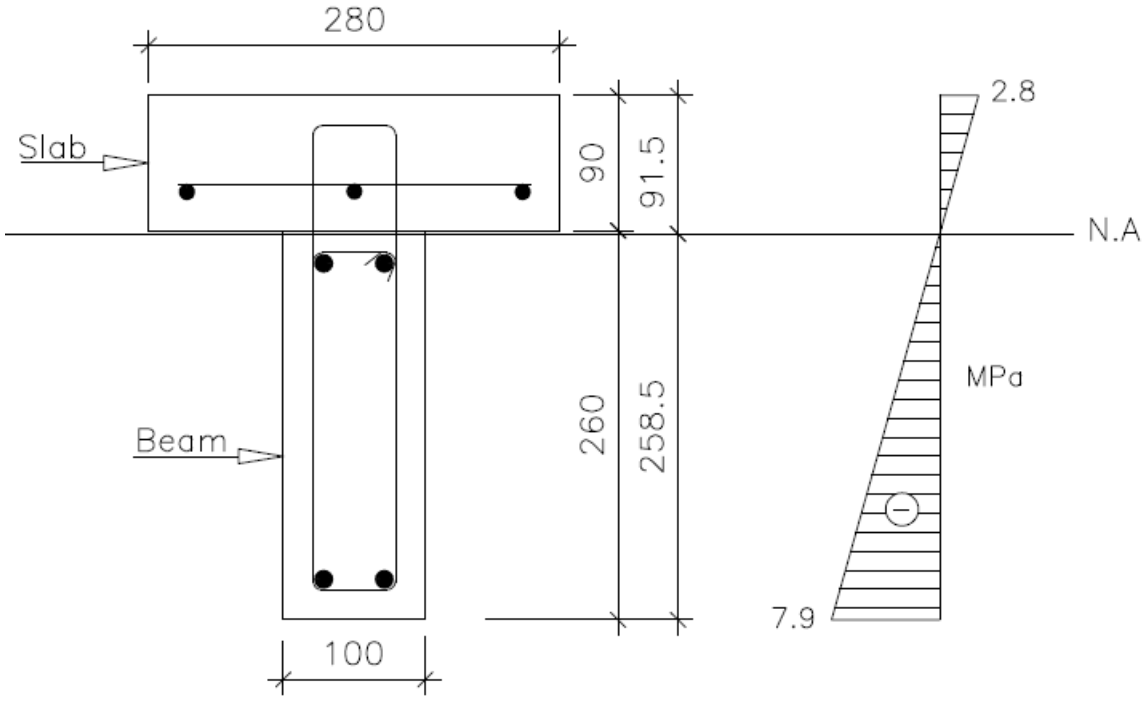

8.4. DESIGN OF PRESTRESSING FORCE AT RELEASE AND TENDONS POSITION

Design for Class 1 member (No tensile stress is allowed in the concrete hence no cracking)

Maximum stress occur on the beam for non-composite action

- Beam properties
  - Section moduli (z) $= \frac{I}{y}$

    $z_b = \frac{I}{y_b} = \frac{294683724.7}{203.8} = 1445945.7\text{mm}^3$

    $z_t = \frac{I}{x} = \frac{294683724.7}{56.2} = 5243482.6\text{mm}^3$
  - Area $(A_c) = 260 \cdot 100 = 26000\text{mm}^2$
  - Tota self weight (beam and slab) $= 1.33\text{KN/m}$

- Loading (Mid-span)
  - $M_{max} = M_{ub} = 13.3\text{KNm}$
  - $M_{min} = M_{Db} = \frac{\gamma_L DL^2}{8} = \frac{1.2 \cdot 1.33 \cdot 1.8^2}{8} = 0.65\text{KNm}$

- Minimum section properties (z)
  - $f_{max} = \frac{f_{cu}}{3} = \frac{40}{3} = 13.3\text{N/mm}^2$ and $f_{min} = 0\text{N/mm}^2$
  - $M_v = M_{max} - M_{min} = 13.3 - 0.65 = 12.65\text{KNm}$

$$z = \frac{M_v}{f_{max} - f_{min}} = \frac{12.65 \cdot 10^6}{13.3 - 0} = 951127.8\text{mm}^3 < z_t \quad \text{OK}$$

- Prestressing bars
  - Diameter $= 7\text{mm} \rightarrow A_{ps} = 38.5\text{mm}^2$
  - Indented/ chevron wires to achieve bonding between the concrete and steel
  - Braking load$(P_b) = 64.3\text{KN}$

Try For;

- Three prestressed bar of diameter 7mm $(38.5mm^2)$
- Placed at $e = -50.2, -150.2$ and $+ 9.8mm$ as shown in the figure below
- Tendon profile: Straight.
- Initial prestressing force $(P_0) = 40KN$ for each bar
- Assume 30% total losses

  Therefore, the force (P')after losses $= P_o - 30\%P_o = 28KN$;

  and Total force $(P'_T) = 3P' = 84KN$

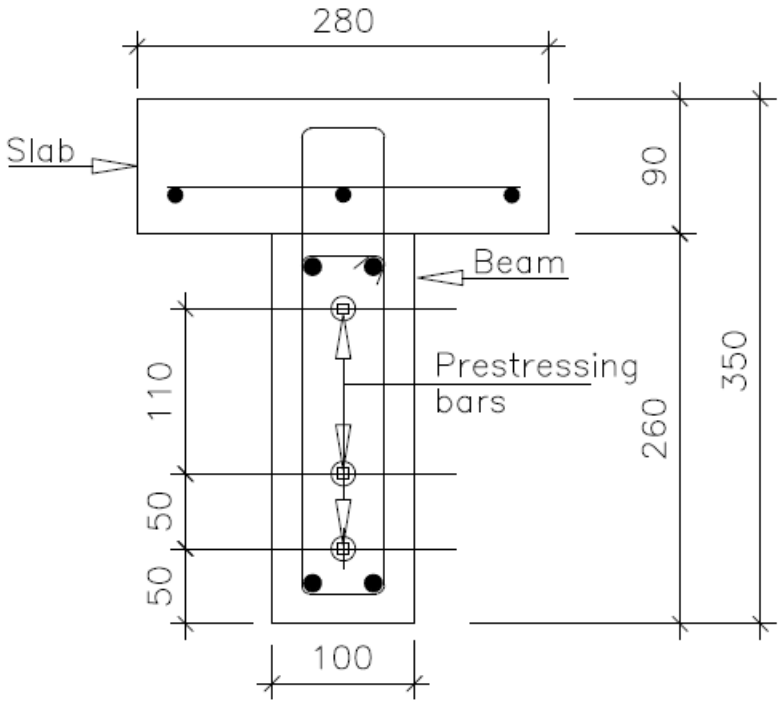

- Prestressing losses (Eurocode 2)

  If the transfer force is P_0 and force after losses is P'

  $P_0 = 75\%P_b = 75\% \cdot 64.3 \approx 48KN$

  then $P' = P_o -$ loss in force(ΔP)

  - Elastic shortening

$$P' = \frac{P_o}{1 + \alpha_e \frac{A_{ps}}{A_c}\left(1 + \frac{e^2 A_c}{I}\right)}; \qquad \alpha_e = \frac{E_{ps}}{E_{cm}} = \frac{205}{35} = 5.86$$

$$P' = \frac{P_o}{1 + 5.86 \cdot \frac{38.5}{24700}\left(1 + \frac{200.2^2 \cdot 24700}{267275331.1}\right)} = 0.96P_0$$

Therefore, $\Delta P = P_o - 0.96P_0 = 0.04P_0 = 4\%P_o = 1.92KN$

- Creep

$$\Delta P = \phi \frac{E_{ps}A_{ps}}{(1.05E_{cm})A_c}\left(1 + e^2 \frac{A_c}{I}\right)P'; \qquad \phi = \text{final creep coefficient}$$

$\phi = 1.8$ (BS EN 1992: 2004, Figure 3.1)

$$\Delta P = 1.8 \cdot \frac{205 \cdot 38.5}{(1.05 \cdot 35) \cdot 24700}\left(1 + 200.2^2 \cdot \frac{24700}{267275331.1}\right)P' = 0.074P'$$

$$\Delta P = 0.074P' = 0.074(0.96P_0) = 0.071P_0 = 7.1\%P_0 = 3.41KN$$

- Shrinkage

Assuming relative humidity of about 80% (coastal town) and $F_{cu} = 40MPa$

From **Table 3.2 of** BS EN 1992:2004
The value of shrinkage is $0.25 \cdot 10^{-3}$

$$\Delta P = \varepsilon_{cs}E_sA_p = 0.25 \cdot 10^{-3} \cdot 205 \cdot 10^3 \cdot 38.5 \cdot 10^{-3} \approx 1.97KN$$

- Relaxation of steel

$$\mu = \frac{\sigma_{pi}}{f_{pk}}$$

Initial prestress $\mu \leq 70\%$ $\left(\text{BS EN } 1992 - 1 - 1, 3.3.2(5)\right)$.

Assuming, we have Class 2: low relaxation strand and $\mu = 68\%$.

Then;

From Table 3.5 of BS EN 1992-1-1: For Class 2 of relaxation with $\mu = 68\%$, the long-term value of loss of prestress$(\Delta\sigma_{rlx})$ due to relaxation of steel is **3.6%** of initial prestress (σ_{pi}).

$$\text{i.e} \quad \Delta P = 3.6\%P_o = 1.73\text{KN}$$

Total losses for one bar $(\Delta P_T) = 1.92 + 3.41 + 1.97 + 1.73 = 9.03\text{KN} \equiv 18.8\%$

30% loss was assumed; This is OK

- **Stresses at Mid-span under** M_{min}

  - 1st CASE: Non-composite action (beam only)

Stress at top: $f_t = \frac{3P'}{A_c} + \frac{M_{min}}{z_t} - P'\left(\frac{e_1 + e_2 - e_3}{z_t}\right)$

$$\rightarrow \frac{3 \cdot 28000}{26000} + \frac{0.54 \cdot 10^6}{5243482.6} - \frac{28000 \cdot (153.8 + 103.8 - 6.2)}{5243482.6}$$

$$= 3.23 + 0.1 - 1.34 = 1.99\text{N/mm}^2 > 0 \quad \textbf{OK}$$

Stress at bottom: $f_b = \frac{3P'}{A_c} - \frac{M_{min}}{z_b} + P'\left(\frac{e_1 + e_2 - e_3}{z_b}\right) \geq 0$

$$\rightarrow \frac{3 \cdot 28000}{26000} - \frac{0.54 \cdot 10^6}{1445945.7} + \frac{28000 \cdot (153.8 + 103.8 - 6.2)}{1445945.7} \geq 0$$

$$= 3.23 - 0.37 + 4.87 = 7.73\text{N/mm}^2 > 0 \quad \textbf{OK}$$

- 2nd CASE: Full-composite action (beam and slab)

  In this case;

  $e_1 = 258.5 - 50 = 208.5\text{mm};\ \ e_2 = 258.5 - 100 = 158.5\text{mm}$ and

  $e_3 = 258.5 - 210 = 48.5\text{mm}$

$$z_b = \frac{I}{y_b} = \frac{655593843.8}{258.5} = 2536146.4\text{mm}^3$$

$$z_t = \frac{I}{x} = \frac{655593843.8}{91.5} = 7164960\text{mm}^3$$

- Area $(A_c) = (260 \cdot 100) + (280 \cdot 90) = 51200\text{mm}^2$

Stress at top: $f_t = \frac{3P'}{A_c} + \frac{M_{min}}{z_t} - P'\left(\frac{e_1 + e_2 + e_3}{z_t}\right)$

$$= \frac{3 \cdot 28000}{51200} + \frac{0.54 \cdot 10^6}{7164960} - \frac{28000 \cdot (208.5 + 158.5 + 48.5)}{7164960}$$

$$= 1.64 + 0.08 - 1.62 = 0.1\text{N/mm}^2 > 0 \quad \textbf{OK}$$

Stress at bottom: $f_b = \frac{2P'}{A_c} - \frac{M_{min}}{z_b} + P'\left(\frac{e_1 + e_2 + e_3}{z_b}\right)$

$$= \frac{3 \cdot 28000}{51200} - \frac{0.54 \cdot 10^6}{2536146.4} + \frac{28000 \cdot (208.5 + 158.5 + 48.5)}{2536146.4}$$

$$= 1.64 - 0.21 + 4.59 = 6\text{N/mm}^2 > 0 \quad \textbf{OK}$$

- **Stresses at ends** $(M = 0)$
  - 1st CASE: Non-composite action (beam only)

Stress at top: $f_t = \frac{3P'}{A_c} - P'\left(\frac{e_1 + e_2 - e_3}{z_t}\right)$

$$\rightarrow \frac{3 \cdot 28000}{26000} - \frac{28000 \cdot (153.8 + 103.8 - 6.2)}{5243482.6}$$

$$= 3.23 - 1.34 = 1.89\text{N/mm}^2 > 0 \quad \textbf{OK}$$

Stress at bottom: $f_b = \frac{3P'}{A_c} + P'\left(\frac{e_1 + e_2 - e_3}{z_b}\right) \geq 0$

$$\rightarrow \frac{3 \cdot 28000}{26000} + \frac{28000 \cdot (153.8 + 103.8 - 6.2)}{1445945.7} \geq 0$$

$$= 3.23 + 4.87 = 8.1\text{N/mm}^2 > 0 \quad \textbf{OK}$$

2nd CASE: Full-composite action (beam and slab)

In this case;

Stress at top: $f_t = \frac{3P'}{A_c} - P'\left(\frac{e_1 + e_2 + e_3}{z_t}\right)$

$$= \frac{3 \cdot 28000}{51200} - \frac{28000 \cdot (208.5 + 158.5 + 48.5)}{7164960}$$

$$= 1.64 - 1.62 = 0.02\text{N/mm}^2 > 0 \quad \textbf{OK}$$

Stress at bottom: $f_b = \frac{2P'}{A_c} + P'\left(\frac{e_1 + e_2 + e_3}{z_b}\right)$

$$= \frac{3 \cdot 28000}{51200} + \frac{28000 \cdot (208.5 + 158.5 + 48.5)}{2536146.4}$$

$$= 1.64 + 4.59 = 6.23\text{N/mm}^2 > 0 \quad \textbf{OK}$$

Stresses for (M_u)

- 1st CASE: Non-composite action (beam only)

Stress at top: $f_t = \frac{3P'}{A_c} + \frac{M_u}{z_t} - P'\left(\frac{e_1 + e_2 - e_3}{z_t}\right)$

$$\rightarrow \frac{3 \cdot 28000}{26000} + \frac{13.3 \cdot 10^6}{5243482.6} - \frac{28000 \cdot (153.8 + 103.8 - 6.2)}{5243482.6}$$

$$= 3.23 + 2.54 - 1.34 = 4.43\text{N/mm}^2$$

Stress at bottom: $f_b = \frac{3P'}{A_c} - \frac{M_u}{z_b} + P'\left(\frac{e_1 + e_2 - e_3}{z_b}\right) \geq 0$

$$\rightarrow \frac{3 \cdot 28000}{26000} - \frac{13.3 \cdot 10^6}{1445945.7} + \frac{28000 \cdot (153.8 + 103.8 - 6.2)}{1445945.7} \geq 0$$

$$= 3.23 - 9.2 + 4.87 = -1.1/\text{mm}^2$$

- 2nd CASE: Full-composite action (beam and slab)

  In this case;

  $e_1 = 257.7 - 50 = 207.7\text{mm}$; $e_2 = 257.7 - 100 = 107.7\text{mm}$ and

  $e_3 = 257.7 - 210 = 47.7\text{mm}$

Stress at top: $f_t = \frac{3P'}{A_c} + \frac{M_u}{z_t} - P'\left(\frac{e_1 + e_2 + e_3}{z_t}\right)$

$$= \frac{3 \cdot 28000}{51200} + \frac{20 \cdot 10^6}{7164960} - \frac{28000 \cdot (208.5 + 158.5 + 48.5)}{7164960}$$

$$= 1.64 + 2.79 - 1.62 = 2.81\text{N/mm}^2$$

Stress at bottom: $f_b = \frac{2P'}{A_c} - \frac{M_u}{z_b} + P'\left(\frac{e_1 + e_2 + e_3}{z_b}\right)$

$$= \frac{3 \cdot 28000}{51200} - \frac{20 \cdot 10^6}{2536146.4} + \frac{28000 \cdot (208.5 + 158.5 + 48.5)}{2536146.4}$$

$$= 1.64 - 7.89 + 4.59 = -1.66\text{N/mm}^2$$

9. DESIGN FOR FULL SHEAR CONNECTION (Full composite action)

$$\text{Shear force (V) due to ultimate load} = \frac{1.2 \cdot 1.29 \cdot 1.9}{2} + \frac{1.5 \cdot 43.24}{2} \approx 34\text{KN}$$

- Shear flow at the interface (V_1)

$$V_1 = \frac{VA_{bc}(y_c - y_b)}{I} = \frac{34 \cdot 10^3 \cdot 27847.5 \cdot (258.5 - 203.8)}{655593843.8} \approx 79\text{N/mm}$$

- Shearing stress at the interface (τ_1)

$$\tau_1 = \frac{V_1}{b} = \frac{79}{100} \approx 0.79\text{N/mm}^2$$

- According to TMH7 part 3; 5.4.2.3

$A_{smin} = 0.15\%A_{cs}$ and $S_{sc} \leq 4h_f$

Where; A_{smin} = Minimum area of fully anchored shear connectors

A_{cs} = Total interface area between beam and slab

S_{sc} = Spacing of shear connectors

h_f = slab thickness

Thus, $A_{smin} = 0.15\%(100 \cdot 2000) = 300\text{mm}^2$

and $S_{sc} \leq 4 \cdot 90 = 360\text{mm}$

Taking Ø8mm shear connectors spaced at $S_{sc} = 100\text{mm}$

Area of one shear connector passing the interface $(A_{sc}) = 2 \cdot 50.3$

$A_{sc} = 100.6\text{mm}^2$

shear flow (V_1) should not exceed the lesser of either

$$k_1 f_{cu} L_s = 0.15 \cdot 50 \cdot 100 = 750\text{N/mm} \quad (f_{cu}\text{of beam})$$

$$V_1 L_s + 0.7\frac{A_s}{S_{sc}} f_y = 0.8 \cdot 100 + 0.7\frac{100.6}{100} \cdot 450 \approx 397\text{N/mm} > 79\text{N/mm}$$ **OK**

- Shearing stress(τ_{sc}) on the connectors at M_u

$$\text{Area of shear connectors per unit length}(q) = \frac{100.6}{100} = 1.006\text{mm}^2/\text{mm}$$

$$\tau_{sc} = \frac{V_1}{q} = \frac{79}{1.006} = 78.5\text{N/mm}^2$$

- Resisitance of shear connectors (P_{Rd}) $---$ **EN 1994 − 2; 6.6.3.1(1)**

Two possibilities: Failure of concrete or shear failure of connectors.

  - Failure of concrete

$$P_{Rd}^1 = \frac{0.29\alpha d^2}{\gamma_v}\sqrt{f_{ck}E_{cm}}\ ;$$

$$\text{Partial factor } (\gamma_v) = 1.25\ ; \quad f_{ck} = \frac{f_{cu}}{0.8} = \frac{30}{0.8} \approx 37.5\text{MPa}$$

$$\text{Diameter of the connector}(d) = 8\text{mm}\ ; \quad \frac{h_{sc}}{d} > 4\ \rightarrow \alpha = 1$$

h_{sc} = overall nominal height of the connector

$$P_{Rd}^1 = \frac{0.29 \cdot 1 \cdot 8^2}{1.25}\sqrt{37.5 \cdot 28 \cdot 10^3} = 15.2\text{KN}$$

  - Shear failure of connector

$$P_{Rd} = \frac{0.8f_u}{\gamma_v} \cdot \left(\frac{\pi d^2}{4}\right) \quad \text{for headed stud connectors}$$

$$\text{Assume for stirrups } P_{Rd}^2 = 0.6\,P_{Rd} \text{ and } f_u = \frac{f_y}{\gamma_s} = \frac{450}{1.15} = 391.3\text{MPa}$$

$$P_{Rd}^2 = 0.6\left[\frac{0.8f_u}{\gamma_v} \cdot \left(\frac{\pi d^2}{4}\right)\right] = 7553\text{N for one leg of shear connector}$$